Summer 9-1-2016

Modeling of Historic Columbia River Flood Impacts Based on Delft 3D Simulations

Lumas Terence Helaire
Portland State University

Modeling of Historic Columbia River Flood Impacts

Based on Delft 3D Simulations

by

Lumas Terence Helaire

A thesis submitted in partial fulfillment of the
requirements for the degree of

Master of Science
in
Civil and Environmental Engineering

Thesis Committee:
Stefan A. Talke, Chair
David A. Jay
Scott A. Wells

Portland State University
2016

Abstract

Natural and anthropogenic processes over the past 150 years have altered the bathymetry of the Lower Columbia River (LCR) and have changed the long wave propagation of tides and floods. Possible causes for the increase in tidal amplitudes (+7% in tidal range in Astoria) are decreases in river discharge, lengthening of the river channel due to the construction of jetties at the mouth, dredging and deepening of the shipping channel, and reduction of the tidal prism due to the filling and diking of tidal wetlands. In this study, changes in the characteristics of long waves are elucidated by developing two hydrodynamic models of the LCR which reflect historical and modern bathymetric conditions and forcing. The historic model simulates late 19th century conditions and is extensively validated using recently recovered tide records along the LCR (e.g., Astoria, 1853-1876) and river stage measurements (e.g., Portland, 1876-1964). Results suggest that water levels in Portland at low river discharge are up to 0.5-1.0m lower than in the past. However, historical water levels during a flood scenario based on the 1880 spring freshet are similar to modern water levels. Since tidal range in the modern scenario is persistently higher at all locations, the flood risk in many locations along the LCR has increased for the same boundary conditions. The results are explained by considering the governing equations of momentum and mass-conservation. At low river flow, greater depth leads to reduced frictional effects, producing amplified tidal range and tidal velocities but a decreased river slope (and lower Portland water levels). At high flow, the modern flood is confined by dikes and the loss of wetlands, which counteracts the effect of decreased friction. Nonetheless, the high friction of the historical wooded floodplain also confined

i

the historical flood path. Hence, historical and modern flood heights are surprisingly similar, though scaling analysis suggests that the historical flood wave was more diffusive.

DEDICATION

This work is dedicated to my mother the late Madeline Lewis Helaire whose courage and wisdom has inspired me.

ACKNOWLEDGEMMENTS

List of Tables

List of Figures

1 Introduction and Setting

This study uses hydrodynamic modeling, tidal analysis and statistical water level analysis to understand the interplay between bathymetry and hydrodynamic processes in the late 19th century Lower Columbia River (LCR). Through modeling scenarios this study will examine how bathymetry and friction affect the transmission and dispersion of flood waves and will investigate how flood waves, tides, and inundation have changed over time. More specifically, this thesis will address the following questions:

1. How has tidal range changed from late 19th century to today and what effect has changing bathymetry had on those changes?

2. How have mean water levels and river slope evolved since the late 19th century?

3. Has the response of the LCR changed for a spring freshet with a 6 month duration?

The study begins with a description of the Lower Columbia River (LCR) and estuary. This is followed by model development for both a historical and modern bathymetry. The study concludes with an analysis of simulations and interpretation of the results.

The Columbia is the largest river on the Pacific Coast of North America and drains an area of 660,480 km^2. The LCR, with an area of 46,650 km^2, is the tidal-fluvial section of the Columbia River downstream of Bonneville Dam (Figures 1-1 & 1-2). Several smaller tributaries discharge into the LCR, including the Cowlitz River, Sandy River, Lewis River and Willamette River. The largest tributary, the Willamette River, enters the

Columbia River at river kilometer (rkm) 163 just downstream of Vancouver, WA. Together, the Willamette and Columbia River provide 90% of the discharge that flows into the ocean [*Naik & Jay*, 2011; *Orem*, 1968]. With an average discharge of ~7500 CMS [m^3s^{-1}], the Columbia River is the largest river on the Pacific Coast of North America [*Naik & Jay*, 2005]. The Columbia River discharge at The Dalles, located ~100 km upstream of Bonneville Dam, accounts for 75% of the flow that reaches the mouth of the river. Daily river flow has been measured at or near The Dalles (Figure 1.1) since June 1878 by the United States Geological Survey (USGS)

[http://waterdata.usgs.gov/usa/nwis/uv?14105700].

Figure 1-1: The Columbia River basin. The interior basin is east of the The Dalles. Taken from [Naik & Jay, 2011]
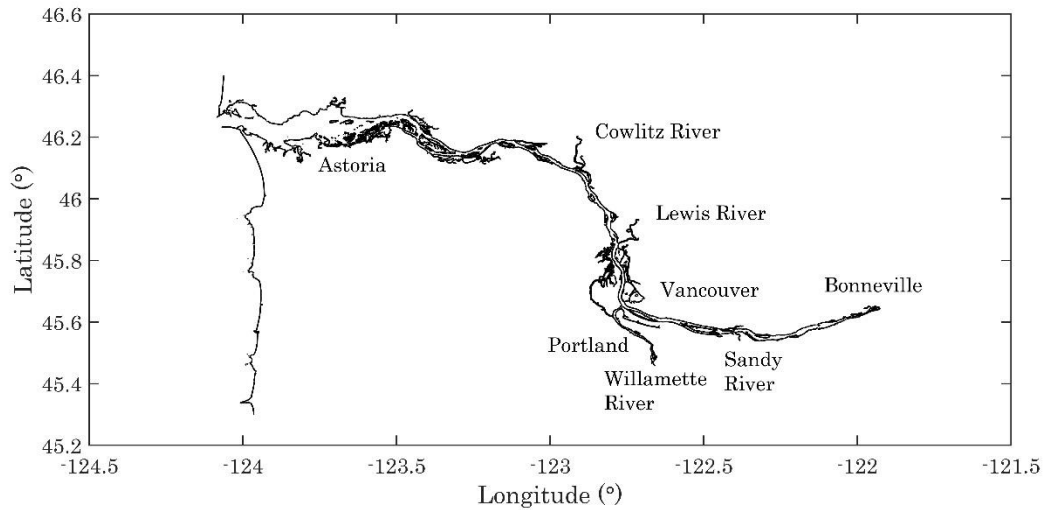
Figure 1-2: The present-day shoreline of the LCR. The LCR extends from Bonneville, OR to the mouth of the river. The Willamette River is modeled from Oregon City to the confluence with the Columbia River.

The discharge of the Columbia River is seasonally variable. The largest flows occur during the spring freshet in May/June, caused by snowmelt in the interior basin of the Columbia River. For example, the hydrograph for the LCR at Bonneville in 2011(e.g. Figure 1-3) shows elevated flow during the May to early July period. Much lower flows are observed during the winter except for intermittent winter and spring events such as the short 11,000 CMS event in April 2011. The LCR is characterized by a dry period from approximately July to October.

Though the 2011 hydrograph was the largest since 1997, it is small by historical standards; 18 of the 22 spring freshets between 1879 and 1900 were larger in magnitude. The construction of dams along the Columbia River (beginning in the late 1930's) altered the natural hydrologic cycle, reducing the magnitude of spring freshets by 40% and

increasing base flow during low flow periods [*Bottom et al.,* 2005, *Jay & Naik,* 2005; 2010].

The Willamette River discharge in 2011 was characterized by several brief flow events in the first half of the year. A spring-freshet in the March/April time period was punctuated by several flow events, and followed by a steady drop in discharge from May to November (Figure 1-4). The magnitude of Willamette River flows is considerably less than the Columbia River, on average, but occasional floods (like February 1996) have produced substantial flows of up to 14 kCMS.
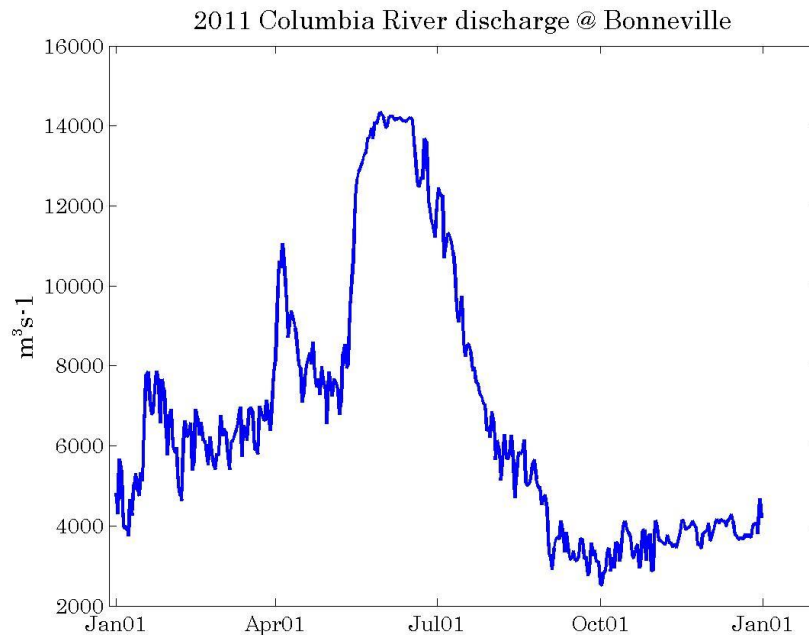
Figure 1-3: 2011 Columbia River daily discharge at Bonneville (rkm 234). Discharge in June 2011 is maintained between 14,000 – 15, 000 CMS by the reservoir system upstream of Bonneville Dam.
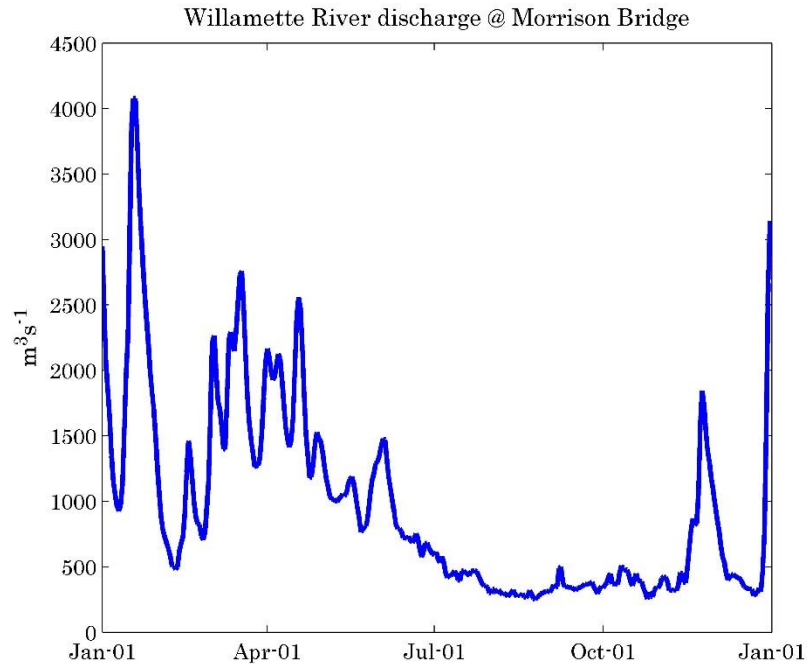
Figure 1-4: Willamette River daily discharge at Morrison Street Bridge (rkm – 20.6).

While the upper portion of the LCR is mainly dominated by river discharge, the Columbia River in Vancouver can have a tidal range as high as 1m under low discharge conditions. Tides in the Columbia River are mixed-semidiurnal, with an M_2 amplitude maximum of 0.95m at Tongue Point (rkm 25), and a K_1 amplitude of 0.4m [tidesandcurrents.noaa.gov] (Figure 1.5). Three regimes exist in the LCR in terms of tidal and fluvial potential energy: a tidally dominated lower estuary downstream of rkm 21: a fluvial region above rkm- 56; and an intermediate cross-over region between rkm 21 and rkm 56 [*Jay et al.*, 1990].
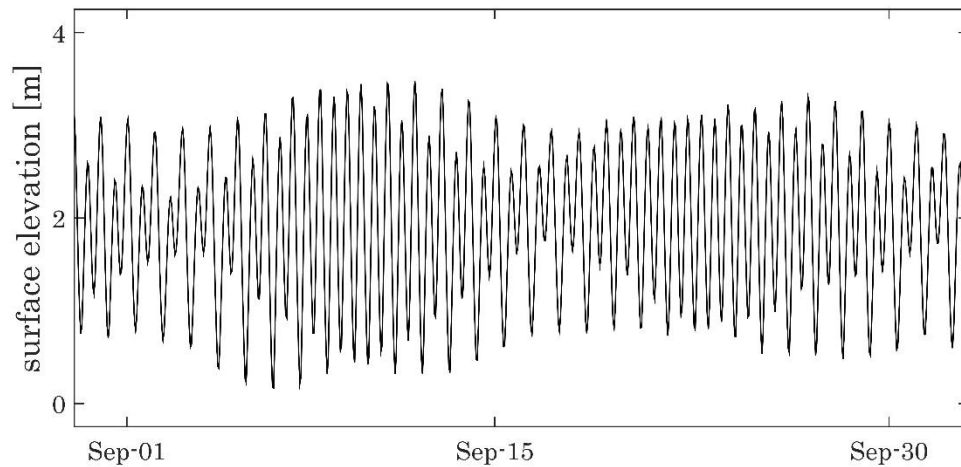
Figure 1-5: water surface elevation of the Columbia River at Astoria, OR, (rkm 30) during September, 2010.

The LCR is considered to be a convergent estuary [*Lanzoni & Seminara*, 1998]; and the channel width deceases upstream in an approximately exponential manner (Equation 1.1 & Figures 1-6, 1-7), with an e-folding length of L_b = 135 km. Although the estuary and lower tidal river are convergent, especially from rkm 30 to 100, it has a near constant width of 1 km from rkm 100 to the end of tidal influence at rkm 230.

$$B = B_0 e^{\frac{-x}{L_b}}:$$ (*Equation 1.1*)

B = half width of the estuary
B_0 = half width of the estuary at the entrance
x = along channel distance
L_b = convergence length
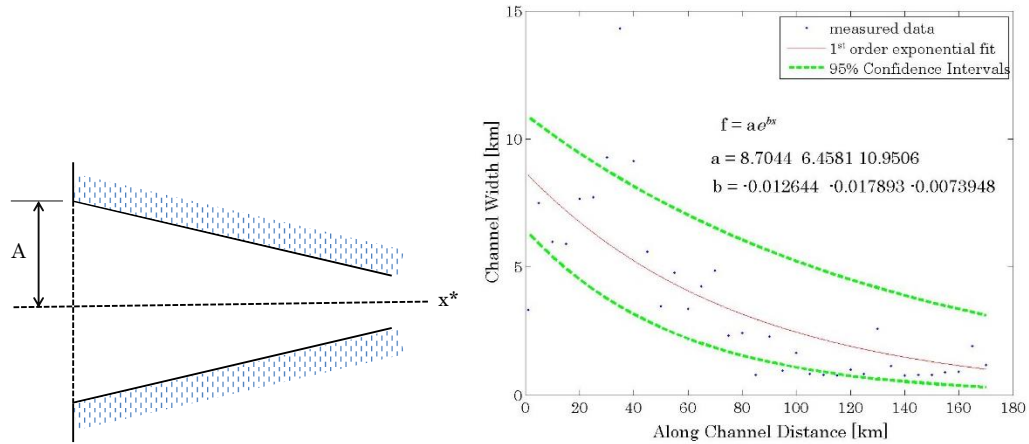
Figure 1-6: (left) conceptual drawing of a convergent estuary (right) Channel width versus along channel distance in the Lower Columbia River. Coefficients are given as fit, 95% confidence intervals on the upper and lower bound. Data used in this figure is described in section 4.2.

Large scale changes have occurred over the past 150 years in the LCR including a 15% decrease in the tidal prism and net accumulation of 68×10^6 m^3 of sediment in the estuary. *Sherwood et al.,* [1990] concluded that the single greatest agent of change to the estuarine morphology has been the system's response to the construction of permeable pile dikes and jetties, especially jetties at the entrance to the Columbia River. Aside from jetty and dike installation, extensive dredging of the river channel and the disposal of dredged material significantly altered the morphology of both the estuary and the tidal river further upstream.

The physical changes that can occur due to dredging are twofold. First, dredging artificially deepens the river channel; according to the theory of tidal propagation, the amplitude of a tidal wave is inversely proportional to the channel depth *h,* and channel width *b,* as $b^{-1/2}h^{-1/4}$ (Green's Law) [*Green,* 1837] in a channel without friction. However, *Chernetsky et al.* [2010] and *de Jonge et al.* [2014] have shown that in the Ems estuary,

deepening of the river channel increased tidal range beyond the Green's law prediction. In *Ianello* [1979], *Jay* [1990], and *Friedrichs & Aubrey* [1994], scaling of the momentum equation shows that at first order the effective friction is inversely proportional to the depth in a tidal channel. Conceptually, as a channel becomes deeper, the effective friction associated with the channel decreases. Thus, despite Green's Law, deepening a channel can lead to larger tides. Resonance effects can also play a prominent effect (*Chernetsky et al.* [2010]).

Second, much of the dredged material uncovered during channel dredging was dumped in intertidal areas, in some cases turning intertidal areas to supratidal areas [*Thomas,* 1983; *Sherwood et al.,* 1990]. Because tidal flats do not convey much momentum, the loss of wetland and tidal flats implies a shift to a channel dominated system with lower friction. According to Green's Law as modified by [*Jay,* 1991], tidal amplitude varies with $b^{-1/4}b_T^{-1/4}h^{-1/4}$, where b is the width of the channel conveying momentum and b_T is the total width of the channel including tidal flats that do not convey momentum. By this scaling, a reduction in b_T should also increase the amplitude of tides.

Previous analysis of Columbia River water levels at Vancouver (rkm 169) (Figure 1-1), indicates that mean water levels (MWL) have dropped between 0.3-1.5 m since 1902, depending on the river discharge [*Jay et al.*, 2011]. This study concluded that the reduced water levels are due to a reduction in overall total bed roughness, channelization of the flow into a deeper, narrower channel, and a reduction in sand supply.

Improved understanding of how changing bathymetry has affected water levels, tides, and flood waves is necessary due to the flood history in the LCR. Spring freshet

8

floods in 1862, 1876, 1880, 1894 and 1948, along with winter floods in 1861, 1881, 1890, 1923, 1943, 1955, 1964 and 1996 have caused major and sometimes catastrophic property damage. A substantial number of fatalities occurred in the Vanport (1948) flood, and likely others. The frequency of extreme flood events on the LCR, and the potential for property damage and loss of life underscores the need to understand the response of the system to changes in bathymetry.

In light of the changing state of the LCR, some effort has been made to develop predictive numerical models. To understand changing morphology, *Elias et al.*, [2012] used the Delft3D modeling system to develop a coupled hydrodynamic and wave model for the Mouth of the Columbia River. Similarly, the Center for Coastal Margin Observation & Prediction (CMOP) has developed a predictive model of the Columbia River estuary for the purpose of monitoring and scientific research [*Kärnä & Baptista,* 2015; *Kärnä et al.,* 2016].

Recently, the Wetland Ecosystem Team (WET) at the University of Washington digitized a series of hydrographic surveys in the LCR conducted between 1867 and 1901 [*Burke*, 2005]. The surveys span from the mouth of the Columbia to Rooster Rock, above Vancouver. The surveys also include a portion of the Willamette River in Portland. The dataset contains digitized bathymetry of the river channel and a georeferenced map of the surrounding floodplain. This dataset was compiled into a digital elevation model (DEM). A comprehensive bathymetry dataset also exists for the modern bathymetry [*USACE*, 2010]. The modern DEM stretches from the mouth of the Columbia River to Bonneville in the upper reaches of the LCR. This dataset also includes the Willamette River from the

9

Willamette Falls in Oregon City to the confluence with the Columbia River, with a resolution of 0.5m.

To investigate changes over the past century, we use the historical DEM and recently recovered 19th century data to create a historic hydrodynamic model of the LCR. Several historical discharge and tidal records are available for use as inputs in to the model [*Talke & Jay,* 2013*; Jay & Naik,* 2011]. A long series of hourly tide data at Astoria from 1853-1876 has been recovered [*Talke & Jay,* 2013], as well as tide logs from 13 stations in the LCR from September – October 1877. Daily water level readings from the Willamette River in Portland are available from the City of Portland archives, the U.S. Army Signal Corps archives [https://www.ncdc.noaa.gov/EdadsV2], and the Weather Bureau archives [*US Weather Bureau*, 2012]. The final dataset necessary for developing a hydrodynamic model of the historical Columbia River are discharge records for the Columbia River and Willamette River. Discharge records for the Columbia River at The Dalles from 1878 to the present are available on a USGS website [http://waterdata.usgs.gov/usa/nwis/uv?14105700]. Discharge from the Willamette River at Morrison Street Bridge in Portland since 1878 is estimated from the water level at upstream gauges, though instrumented flow records at that station did not begin until the 1970's.

A comprehensive tidal record is also used for modern analysis. Hourly water level records are available since 2002 for 8 LCR stations. These tide stations stretch from Hammond, OR, near the mouth of the river, to Vancouver, WA in the fluvial river and at Morrison Street Bridge.

2   Literature Review of Modeling Tidal Rivers

The goal of the study is to use hydrodynamic models to analyze how long term changes to the bathymetry of the LCR, such as dredging, filling of tidal wetlands and installation of pile dikes, affect tidal and flood wave propagation. While flood waves in estuaries are rarely studied, a rich literature in tidal dynamics provides insights into the physical processes that affect shallow water waves, i.e., waves with a wavelength that is large relative to the depth and usually long relative to the estuary. We first review some case studies of systems that have changed with respect to tidal and sediment dynamics because of physical changes to the system.

The first important work in the analysis of long wave propagation in a channel was *Green* [1837]. *Green* developed a solution to long wave propagation where tidal elevation and transport are proportional to the width and depth of the channel (Equations 2.1 & 2.2).

$$\zeta \cong b^{-\frac{1}{2}} h^{-\frac{1}{4}}$$

(*Equation 2.1*)

$$Q \cong b^{+\frac{1}{2}} h^{+\frac{1}{4}}$$

(*Equation 2.2*)

ζ = tidal long-wave elevation [L]
Q = tidal transport [$L^3 T^{-1}$]
b = channel width [L]
h = channel depth [L]

Green [1837] neglected friction and assumed a slowly varying topography. According to *Jay* [1991], most subsequent treatments of wave propagation implicitly referenced Green and assumed weak topographic variation. *Ippen* [1966] accounted for exponentially varying width but neglected frictional effects. However, in many cases

friction is significant and topography can greatly affect wave propagation [*Jay,* 1991; *Friedrichs & Aubrey,* 1994; *Lanzoni & Seminara,* 1998]. The consequence is that channels with large strong friction and/or topography variations show large deviations from Green's Law (Equations 2.1 & 2.2). Essentially, tidal propagation represents a balance between topographic funneling (convergence) that tends to amplify the incoming tide while friction tends to dampen the incoming tide.

Jay [1991] applies a perturbation analysis to the cross-sectionally integrated continuity and along-channel momentum equations, and includes finite amplitude effects, river flow and tidal flats that store water but do not convey momentum. The author derived two solutions by solving the wave equation. The standard solution has nearly constant coefficients when the effects of topographic convergence and acceleration dominate over frictional damping in determining the wave number. The critical solution has nearly constant coefficients when friction controls the wave number because convergence and acceleration are nearly in balance. A modified form of the standard equation applies to the case of strong convergence, in which convergence is much larger than acceleration. In all cases the behavior of the solution is determined to the first order by two non-dimensional parameters – the ratio of bed stress to acceleration and the ratio of topographic convergence/divergence to acceleration. An important result of *Jay* [1991] is that a long wave incident on a convergent channel may have any elevation-transport wave between 0 and 90°, even in the absence of a reflected wave.

Friedrichs & Aubrey [1994] also analyzed the effects of tidal propagation in strongly convergent channels. The authors scaled the continuity and momentum equations.

The scaling used was appropriate to shallow, strongly convergent channels such as the Thames and Tamar in the United Kingdom and the Delaware in the United States. The authors found that gradients in tidal discharge are dominated at first order by gradients in cross-sectional area. In the momentum equation, the effect of local and convective acceleration are negligible at first order. The only two remaining terms in the momentum equation to the first order are then pressure and friction. The resulting governing equations for wave elevation became a first-order wave equation as opposed to the classic second-order wave equation. The resulting wave has characteristics of both a progressive wave and a standing wave, though a true standing wave only occurs in the absence of friction. In this solution, friction also acts to modify the wave by causing a phase shift. The phase shift increases upstream, and an increase in friction causes the wave to slow down.

Lanzoni & Seminara, [1998] considered four limiting cases defined by relative intensity of dissipation versus local inertia in the momentum equation and the role of channel convergence in the mass balance. The authors scaled 23 tidal estuaries around the world and classified them based on the level of convergence (strong/weak) and the level of frictional dissipation (strong/weak). The authors found that the Columbia River is strongly convergent and strongly dissipative. In this case the effect of friction increasingly counteracts the amplification effect of convergence.

The previous three papers show that factors such as depth, convergence, the area of tidal flats, and bed friction are important to tidal processes. *Chernetsky et al.* [2010] developed a two dimensional semi-analytical model to examine how changes in depth and friction affect the tidal and sediment dynamics within the Ems estuary, Germany. The

study showed that deepening the controlling depth from 4.5 m to 7 m between 1980 and 2005 changed the tidal amplitude and tidal asymmetry. The model calibration indicates that bed roughness decreased between 1980 and 2005. In 1980 the amplitude of the M_2 tide reached a maximum at the entrance of the estuary and progressively dampened as it progressed upstream. In 2005 the M_2 tide was slightly larger at the entrance than in 1980; unlike 1980, the amplitude now increases as the tide progress upstream, and the system is now closer to resonance. The phase difference between the horizontal velocity and the amplitude is closer to 90º, and the tidal range increased by 1.5m to 3.8m in the upstream reaches of the estuary between 1980 and 2005.

One way to evaluate the changes in tidal characteristics is to determine changes to the overtides, which are frictionally generated harmonics of the astronomical tides. In the Ems estuary, the velocity magnitude of both the internally generated and externally generated M_4 have increased throughout the estuary [*Chernetsky et al.* 2010]. The character of the M_4 velocity phase therefore evolved over time. In 1980 the modelled phase increased rapidly from -250º to -100º. In 2005 the phase remains close to -100º. The relative phase between the M_2 tide and its first overtide, the M_4, $\phi_{u_{M_4}} - 2\phi_{u_{M_2}}$, determines flood or ebb dominance [*Aubrey & Speer*, 1985]. A relative phase between -90º and 90° is usually associated with a flood dominant estuary; i.e., an estuary with strong flood currents, otherwise, the estuary is ebb dominant. In 1980, the Ems estuary was flood dominant only in the most landward 30 km, conversely in 2005 the entire estuary was flood dominant. Changes in tidal asymmetry, flood or ebb dominance, also create changes in the tidal residual (tidally averaged) transport. Gravitational circulation was also observed to

increase; combined with the altered settling lag effects, such as the changes in tidal dynamics caused the estuarine turbidity maximum to shift upstream and sediment trapping to occur over a larger area.

de Jonge et al. [2014] used the model of *Chernetsky et al.* [2010] to explore the connection between channel deepening and Suspended Particulate Matter (SPM) concentrations. The authors used archival bathymetry and tidal records to model five time periods from 1965 to 2005 in the Ems estuary. Successive channel deepening projects resulted in tidal changes and a landward shift of the SPM trapping location. The Ems estuary study shows that bathymetry alterations could cause long-term changes in tidal and sediment dynamics. In light of the changes to the LCR, it is likely that the alterations in bathymetry of the 150 years has affected tides and morphodynamics. While we do not directly model sediment transport, we do investigate how tidal dynamics and flood dynamics have shifted as a result of channeling deepening and isolation of the floodplain.

To analyze altered flood wave dynamics, we will follow the approach of *Moussa et al.* [1996], who studied river waves in the Loire River, France. The authors developed a scaling of the 1-D Saint Venant equation using the Froude number and a term related to the period of the input hydrograph. The scaling is used to determine the nature of the flood wave (kinematic, diffusive, steady dynamic and gravity wave). A significant part of this project is to understand the effect of changing land cover on the bed roughness as it applies to flood waves. Historical maps and topography provide a qualitative overview of the land cover in the late 19th century. *Arcement et al.* [1989] published a USGS guide for

determining a roughness coefficient for vegetated floodplains. This parameterization is used on the numerical modeling simulations described in the Chapter 5.

3   Background

3.1   Flow Equation in Computational Model

The Delft3D hydrodynamic modeling software is used to create a numerical simulation of historical conditions. Additionally, an existing modern model of the LCR [*Elias et al.*, 2012] was modified and improved, allowing inter-comparison of system changes. The following section is a brief overview of the modeling software and some of the simplifying assumptions used in the flow equations. This section is divided in to three parts. The first section describes the Navier-Stokes equation used on the computational grid. The second section provides a brief overview of the turbulences closure methods used. Finally, a third section describes how the bathymetry and hydrology of the historical Lower Columbia River is implemented on the Delft3D model.

The following are assumptions made by Delft3D that are important for the 2D barotropic model [*Deltares*, 2010]:

- The depth is assumed to be much smaller than the horizontal length scales (shallow water assumption)
- The model is depth averaged so the immediate effect of buoyancy is not considered
- A Cartesian frame of reference is applied, Earth's Curvature is not taken into account
- Quadratic bed stress formulation with a free slip boundary is assumed
- The governing equations are Reynolds averaged
- First order closure
- A logarithmic law of the wall is assumed
- Eddy viscosity is isotropic
- There is no flux of matter from the bed or the water surface

In the depth averaged continuity and momentum equations, the following variables are defined below:

17

C	Chézy roughness coefficient
c	mass concentration [ML^{-3}]
D_H	total horizontal diffusion coefficient [L^2T^{-1}]
f_u	Coriolis parameter in the x-direction [T^{-1}]
f_v	Coriolis parameter in the y-direction [T^{-1}]
H	total water depth [L]
M_x	source or sink of momentum flux in x-direction [MLT^{-1}]
M_y	source or sink of momentum flux in y-direction [MLT^{-1}]
P_x	Gradient of hydrostatic pressure in the x-direction [$ML^{-2}T^{-2}$]
P_y	Gradient of hydrostatic pressure in the y-direction [$ML^{-2}T^{-2}$]
Q	global source or sink per unit area (discharge/unit area) [LT^{-1}]
q_{in}	local source per unit volume [T^{-1}]
q_{out}	local sink per unit volume [LT^{-1}]
S	source or sinks of salinity [ppt]
t	time [T]
$\hat{U}$	velocity of water discharged in the x-direction [LT^{-1}]
u	flow velocity in the x -direction [LT^{-1}]
$\hat{V}$	velocity of water discharged in the y-direction [LT^{-1}]
v	flow velocity in the y - direction [LT^{-1}]
w	flow velocity in the z- direction [LT^{-1}]
ρ_0	reference density of water [ML^{-3}]
τ_b	bed stress [$ML^{-1}T^{-2}$]
ν_H^{back}	background eddy viscosity [L^2T^{-1}]
σ	Prandtl-Schmidt number
ζ	water level above datum [L]

The depth-averaged continuity equation is given by:

$$\frac{\partial \zeta}{\partial t} + \frac{\partial U}{\partial x} + \frac{\partial v}{\partial y} = Q \qquad \qquad (Equation\ 3.1.1)$$

$$Q = H \int_{-1}^{0} (q_{in} - q_{out})\, dz \qquad \qquad (Equation\ 3.1.2)$$

The physical meaning of Equation 3.1.1 is that the discharge per unit area is balanced by the temporal changes in the surface elevation and spatial gradients in discharge per unit area within the control volume. The discharge term Q, is the net influx of fluid per unit area within the control volume.

The momentum equations in the x and y directions are given in equations 3.1.3 and 3.1.4.

18

$$\frac{\partial u}{\partial t} + \frac{u\partial u}{\partial x} + \frac{v\partial u}{\partial y} + \frac{w\partial u}{\partial z} - f_v = -\frac{P_x}{\rho_0} + F_x + M_x \qquad (Equation\ 3.1.3)$$

$$\frac{\partial v}{\partial t} + \frac{u\partial v}{\partial x} + \frac{v\partial v}{\partial y} + \frac{w\partial v}{\partial z} + f_u = -\frac{P_y}{\rho_0} + F_y + M_y \qquad (Equation\ 3.1.4)$$

$$M_x = q_{in}(\hat{U} - u) \qquad (Equation\ 3.1.5)$$

$$M_y = q_{in}(\hat{V} - v) \qquad (Equation\ 3.1.5)$$

The momentum sources and sinks (M_x and M_y) are generated from the discharge of water or the withdrawal of water from the system.

To solve the momentum equation, several boundaries conditions need to be defined. We assume an impermeable bed and water surface. The resulting kinematic boundary conditions are given in equations 3.1.6 and 3.1.7.

$$w|_{surface} = 0 \qquad (Equation\ 3.1.6)$$

$$w|_{bed} = 0 \qquad (Equation\ 3.1.7)$$

At the bed, we also specify that be stress is given by:

$$\tau_b = g\rho\,\bar{U}\,|\bar{U}|/C^2 \qquad (Equation\ 3.1.8)$$

The arrow over the velocity term indicates a depth average quantity. The *C* is the Chézy roughness coefficient. The roughness parameterization is discussed in Chapter 5.

The conservation of salt is defined in a manner analogous to the momentum equation. The horizontal eddy diffusivity is set to the default value of 10 m^2s^{-1}. The barotropic model has constant properties throughout the water column. Turbulent energy is assumed to be transported laterally, although in an actual system there is some vertical transport of turbulent energy.

$$\frac{\partial c}{\partial t} + \frac{\partial uc}{\partial x} + \frac{\partial vc}{\partial y} + \frac{\partial wc}{\partial z} = \left\{ \frac{\partial}{\partial x}\left(D_H \frac{\partial c}{\partial x} \right) + \frac{\partial}{\partial y}\left(D_H \frac{\partial c}{\partial y} \right) \right\} + S$$

<div align="right">(Equation 3.1.9)</div>

$$S = (q_{in}c_{in} - q_{out}c) \qquad\qquad \text{(\emph{Equation 3.1.10})}$$

$$D_H = \frac{\nu_H}{\sigma} \qquad\qquad \text{(\emph{Equation 3.1.11})}$$

The only scalar included in this model is salt. The incoming tides are set to a salinity of 31.5 ‰ at a temperature of 20°C. Fresh water in the river channel and from the discharge boundaries do not have salinity. It should be noted a 3-D baroclinic model is required to correctly model salinity intrusion. Since we are focused here on the fluvial domain, salinity intrusion is beyond the scope of this thesis.

3.2 Classic Harmonic Analysis

Analysis of the tidal signal is required for evaluation of the tide data and calibration of the hydrodynamic model. For a good calibration, the simulated water level should be similar in elevation and should have similar tidal amplitudes and phases as the real data. Tides are usually represented as the sum of sine waves with different amplitudes and frequencies.

A single tidal constituent can be considered to be a cosine wave with an amplitude, frequency and a phase shift (Equation 3.2.1) where A is the amplitude, ω is the frequency in radians and φ is the phase with respect to G.M.T.

$$Y = A\cos(\omega t + \varphi) \qquad\qquad \text{(\emph{Equation 3.2.1})}$$

$$Y = A\cos(\omega t)\cos\varphi + A\sin(\omega t)\sin\varphi \qquad\qquad \text{(\emph{Equation 3.2.2})}$$

The sum of cosines formula can be used to obtain Equation 3.2.2. By defining the following new constants,

$$A_1 = A \cos \varphi \qquad (Equation\ 3.2.3)$$

$$B_1 = A \sin \varphi \qquad (Equation\ 3.2.4)$$

$$\frac{B_1}{A_1} = \tan \varphi \qquad (Equation\ 3.2.5)$$

we can next rewrite Equation 3.2.2 as a linear equation that can be solved by least squares analysis for unknowns K, A_1 and B_1.

$$K + A_1 \cos(\omega t) + B_1 \sin(\omega t) = Y \qquad (Equation\ 3.2.6)$$

$$K + A_1 X_1 + B_1 X_2 = Y \qquad (Equation\ 3.2.7)$$

More generally the tide is composed of multiple constituents. In a tidally influenced system the measured water level at a given time is composed of a mean water level and fluctuations due to tidal forcing (Equation 3.2.8).

$$h_i = c_0 + \sum_{k=1}^{n} \left(a_k \cos(2\pi \theta_k t_i + \phi_i) \right) + error \qquad (Equation\ 3.2.8)$$

In Equation 3.2.1 h_i is the measured water level, c_0 is the mean water level, $a_{1..n}$ are unknown amplitudes, $\phi_{1...n}$ are phases and $\theta_{1...n}$ are tidal constituent frequencies from astronomical forcing or frictionally induced overtides.

The equations are solved simultaneously for amplitudes and phases of multiple constituents. Nodal corrections are applied to account for variations in the constituent amplitudes over time and the phase angle is referenced to Greenwich Mean Time (GMT). Hundreds of tidal constituents have been defined but harmonic analysis is usually limited

21

by the length of the record [*Foreman*, 1977; *Jay & Leffler*, 2009]. The five largest tidal constituents in the Columbia River are the M_2, S_2, N_2, K_1 and O_1 constituents. The M_2 constituent (12.421 hours) is the principal lunar semidiurnal (twice-daily). It is caused by the gravitational attraction the moon on the earth. The orbit of the earth around the moon is elliptical and because of this the amplitude of the M_2 tide is modulated over an anomalistic month (27.5545 days), the amount time between successive lunar perigees (farthest point from the earth). The resulting modulation in the M_2 tide gives rise to the N_2 (lunar elliptical) tidal constituent (12.658 hours). The S_2 constituent (12.000 hours) is the principal solar and is caused by the gravitational attraction of the sun on the earth. The declination of the moon's orbit around the earth with respect to the equator changes from north to south over the course of a tropical month (27.322 days). This declination generates two diurnal constituents, K_1 (23.93 hours) and O_1 (25.82 hours).

In the development of the Historic Model, multiple tide records are available. The choice of harmonic analysis parameters depends on the record. The length of time needed to separate two constituents is dictated by Rayleigh's criterion,

$$|\sigma_2 - \sigma_1| \geq \frac{C_1}{T} \qquad (\textit{Equation 3.2.9})$$

which states that to resolve two frequencies, their difference must be as least as large as the inverse length of the data record. In the previous equation, σ_1 and σ_2 are the frequencies of two neighboring tidal constituents, T is the length of record needed resolve these two constituents, and C_1 is the Rayleigh criterion; C_1 is O(1). Lowering the Rayleigh criterion from unity reduces the required length of record. The minimum length of record used for

this study 15 days. This is sufficiently long enough to resolve the M_2 constituent (12.4206 hours), N_2 constituent (12.6583 hours) and S_2 constituent (12.0000 hours), Q_1 constituent (26.86385 hours), O_1 constituent (25.8193 hours) and K_1 constituent (23.9344 hours) [*Parker*, 2007]. Although the K_2 constituent (11.9672 hours) and P_1 (24.0659 hours) tides are significant in terms of forcing, the tidal records are not long enough to resolve those two constituents. A tidal record of 12 months is required to separate the K_2 and M_2 constituents, likewise for the P_1 and S_1 (24.000 hours) constituents

The R_T_Tide program is used for evaluation of the tidal amplitudes and constituents [*Leffler and Jay*, 2009; *Pawlowicz et al.,* 2002]. The R_T_Tide program fits the surface elevation to a list of known tidal frequencies, and improves upon classic harmonic analysis by statistically down-weighing the effect of outliers, by using a robust regression analysis [*Holland & Welsch,* 1977]

3.3 Tidal-Fluvial Interactions

The Lower Columbia is mesotidal and periodically has large river flow. These two factors interact nonlinearly to produce quite variable system behavior [*Giese & Jay*, 1989]. In order to understand how the system functions it is important to understand how the tidal and river flows interact.

Equations for Riverine Tides

The St. Venant equations describe the cross-sectionally integrated conservation of mass and momentum. Several simplifying assumptions are made in the 1-D St. Venant equations;

23

1. Molecular viscosity is assumed to be negligible

2. The Boussinesq and hydrostatic approximations are applied, i.e., variations in density are ignored except when they are multiplied by the acceleration due to gravity g, and vertical accelerations are assumed negligible

3. Lateral and vertical variations are unimportant so the flow can be sectionally integrated

4. The Coriolis force is neglected

These assumptions lead to the following equations, commonly known as the St. Venant equations,

$$\frac{\partial Q}{\partial t} + \frac{\partial}{\partial x}\left(\frac{Q^2}{A}\right) + gA\frac{\partial \zeta}{\partial x} + bT = 0,$$ (*Equation 3.3.1*)

| local acceleration | convective acceleration | pressure force | friction force |

$$\frac{\partial Q}{\partial x} + b\frac{\partial \zeta}{\partial t} = 0,$$ (*Equation 3.3.2*)

| Outflow through control volume | change in mass in control volume |

$$T_b = c_D U|U|,$$ (*Equation 3.3.3*)

where:

A = cross-sectional area of the channel [L^3]

b = channel width [L]

C = wave celerity [LT^{-1}]

c_D = drag coefficient

g = acceleration due to gravity [L^{2}T^{-2}]

h = channel depth [L]
Q = discharge per unit length [L^{2}T^{-1}]

T = bed stress divided by water density [L^{2}T^{-2}]

$t =$ time [T]

$u =$ river velocity [LT⁻¹]

$x =$ along channel distance [L]

$\zeta =$ elevation of the tide static water level [L]

$\omega =$ frequency of oscillating wave [T⁻¹]

The tidal and river velocities combine nonlinearly to produce greater bed stress and energy dissipation than would exist if they were analyzed separately. During the flood tide, tidal and river flows oppose each other, reducing the resultant velocity. During ebb tide, the river and tide are flowing in the same direction so that the river and tide interact positively with each other, producing an asymmetric stress tidal cycle (Equation 3.3.3).

The tide in a deep basin is commonly described as an inviscid wave. In this case the friction caused by the interaction with bed is not significant in the total force balance (Equation 3.3.1). However, friction becomes significant in a shallow river. The effects of friction can be assessed using idealized solutions of Equations 3.3.1 and 3.3.2. The following derivation is a simplification of the analytical perturbation model of *Jay* [1991]. First, the along channel variation in cross section is assumed to be zero so the second term in equation 3.3.1 is eliminated. To enable an analytical solution, the friction term is linearized. After simplification, Equations 3.3.1 – 3.3.3 can be written as the following:

$$T_b = \frac{\tau_b}{\rho} \qquad \text{(\textit{Equation 3.3.4})}$$

$$T_b = Ru = \frac{R}{h}Q \qquad \text{(\textit{Equation 3.3.5})}$$

$$\frac{\partial Q}{\partial t} + gh\frac{\partial \zeta}{\partial x} + \frac{R}{h}Q = 0 \qquad \text{(\textit{Equation 3.3.6})}$$

$$\frac{\partial Q}{\partial x} + \frac{\partial \zeta}{\partial t} = 0 \qquad\qquad (\textit{Equation 3.3.7})$$

where:

$T_b = [\text{L}^2\text{T}^{-2}]$

$R = [\text{LT}^{-1}]$

Equations 3.3.6 and 3.3.7 can be solved by forming a wave equation using the following procedure

- Take the partial derivative with respect x of Equation 3.3.6

- Take the partial derivative with respect t of Equation 3.3.7

- Substitute to eliminate $\frac{\partial^2 Q}{\partial x \partial t}$ from both equations

- Use the continuity equation (Equation 3.3.7) to eliminate $\frac{\partial Q}{\partial x}$

- Assume ζ is a harmonic wave oscillating with a frequency of ω

This procedure leads to a new set of equations:

$$\frac{\partial^2 Q}{\partial x \partial t} + gh\frac{\partial^2 \zeta}{\partial x^2} + \frac{R}{h}\frac{\partial Q}{\partial x} = 0 \qquad\qquad (\textit{Equation 3.3.8})$$

$$\frac{\partial^2 Q}{\partial x \partial t} + \frac{\partial^2 \zeta}{\partial t^2} = 0 \qquad\qquad (\textit{Equation 3.3.9})$$

$$\zeta(x,t) = Re\left(M(x)e^{i\omega t}\right) \qquad\qquad (\textit{Equation 3.3.10})$$

Combining equations 3.3.8 and 3.3.9 and substituting for ζ yields the following:

$$\left(ghM'' - (i\omega)^2 - \frac{iR\omega}{h}M\right)e^{i\omega t} = 0 \qquad\qquad (\textit{Equation 3.3.11})$$

$$M' = \frac{dM}{dx} \qquad\qquad (\textit{Equation 3.3.12})$$

$$M'' = \frac{d^2 M}{dx^2} \qquad\qquad (\textit{Equation 3.3.13})$$

$$M'' + \frac{\omega^2}{gh}\left(1 - \frac{ir}{\omega}\right)M = 0 \qquad\qquad (\textit{Equation 3.3.14})$$

The solution for Equation 3.3.14 can be given in terms of a complex wave number q (Equation 3.3.15). The complex wave number has a real part k, related to wave propagation, and a complex part p, which is defined as the damping modulus.

$$q = \frac{\omega}{\sqrt{gh}}\left(1 - \frac{ir}{\omega}\right)^{1/2} = k + ip \qquad\qquad (\textit{Equation 3.3.15})$$

$$\zeta(x,t) = Re(M(x)e^{i\omega t}) \qquad\qquad (\textit{Equation 3.3.16})$$

$$\zeta = Re((Ae^{iq} + Be^{-iq})e^{i\omega t}) \qquad\qquad (\textit{Equation 3.3.17})$$

In the presence of friction the wave will have aspects of an incident wave (A) and a reflected wave (B).

This result is extremely simplified because depth and width are assumed to be constant and the river channel is assumed to be rectangular. The LCR system is much more complex, but this analysis can begin to explain observed spatial changes in the tides. In particular, as shown in Figure 1-6, the LCR approaches a constant width channel in the fluvial regime (upstream of rkm 100). In the Columbia River, the frictional damping in Equations 3.3.15 and 3.3.16 means that the tide will gradually diminish as it propagates through a river channel.

Modifications to the Wave Equations Due to Friction and Convergence

In estuaries where the width changes with upriver distance, the estuary can be convergent or divergent. In an overall sense the Columbia River is convergent below rkm

100 but there are regions where the estuary is straight or divergent (Figure 1.6). The following derivation of the wave equation [*Jay*, 2012] takes into account friction and lengthwise changes in the width of the estuary. In this case the channel width b, is assumed to vary exponentially along channel.

$$b(x) = b_0 e^{-\gamma x} \qquad (Equation\ 3.3.18)$$

In Equation 3.3.18 γ is positive for convergent estuaries and negative for divergent estuaries. Equations 3.3.19 and 3.3.20 are the momentum and continuity equations with a width, $b(x)$, varying exponentially with along channel distance. The combination of these two equations gives a wave equation for a width convergent channel, e.g. Equation 3.3.21.

$$\frac{\partial Q}{\partial t} + ghb(x)\frac{\partial \zeta}{\partial x} + rQ = 0 \qquad (Equation\ 3.3.19)$$

$$\frac{\partial Q}{\partial x} + b(x)\frac{\partial \zeta}{\partial t} \qquad (Equation\ 3.3.20)$$

$$M'' - \gamma M' + \frac{\omega^2}{gh}(1 - \frac{ir}{\omega})M = 0 \qquad (Equation\ 3.3.21)$$

The surface elevation, ζ, is assumed to be a harmonic and the same solution procedure from the previous section is applied to solve Equations 3.3.19 and 3.3.20. Simplification of Equation 3.3.21 leads to a characteristic equation with two roots (Equations 3.3.22 & 3.3.23),

$$D^2 - \gamma D + \frac{\omega^2}{gh}(1 - \frac{ir}{\omega}) = 0 \qquad (Equation\ 3.3.22)$$

$$D_{1,2} = \frac{\gamma}{2} \pm \frac{1}{2}\left(\frac{\gamma}{2} + \frac{4\omega^2}{gh}\left(1 - \frac{ir}{\omega}\right)\right)^{1/2} = \frac{\gamma}{2} \pm \frac{i}{2}\left(\frac{4\omega^2}{gh} - \gamma^2 - \frac{i4\omega}{gh}\right)^{1/2} \quad (Equation\ 3.3.23)$$

Equation 3.3.23 can be written rewritten in terms of complex wave number q

$$D_{1,2} = \frac{\gamma}{2} \pm iq \qquad \text{(Equation 3.3.24)}$$

$$q = \frac{\omega}{\sqrt{gh}}\left(1 - \frac{\gamma^2 gh}{4\omega^2} - \frac{ir}{\omega}\right)^{1/2} = k + ip \qquad \text{(Equation 3.3.25)}$$

The surface elevation ζ is the real part of M from Equation 3.3.21

$$\zeta(x,t) = Re\left(M(x)e^{i\omega t}\right) = e^{\frac{\gamma x}{2}}Re\left[\left(Ae^{iqx} + Be^{-iqx}\right)e^{i\omega t}\right] \quad \text{(Equation 3.3.26)}$$

This result is similar to Equation 3.3.17 for a wave with friction except that a) the wave number q now consists of a balance between acceleration, convergence and friction, b) the effects of convergence and divergence are now accounted for by the term $e^{\gamma x/2}$. Propagation of the tide in the Columbia River will not be solved explicitly in this manner, but the effects of friction and convergence can be observed as the tide propagates upriver.

Nonlinear Tidal Analysis

Godin [1984] analyzed the modification of the tides from river discharge in the St. Lawrence River, St. John River and Fraser River. The author noted that during periods of high discharge the incoming wave is damped and the timing is modified. Godin divided the river into three zones, upstream, intermediate and downstream. The regions are delineated by the relative magnitude of the tidal and river currents. In the downstream region the tidal current is considerably larger than the river current; in the upstream region currents do not reverse and the river currents are larger than the tidal current. In the intermediate region, the river and tidal currents are of the same magnitude. Godin showed that river discharge reduced friction during the flood and high water. During ebb and low water, tides were more strongly damped because the current and tides both flowed

29

downstream. In the downstream region the timing of high water is shifted forward (earlier in time) and low water is delayed. Conversely, the upstream region has increased discharge which reduces the tidal range; here, the timing of low water is shifted forward and the timing of high water is delayed. Godin was able to develop a simple regression model to predict the modification of the tide using the tidal admittance, i.e., the ratio between the tidal amplitude at the mouth and at an upstream location.

Mofthakhari et al. [2013] analyzed the long tidal record at San Francisco Bay. The authors developed a method of estimating the discharge into the San Francisco Bay by analyzing the modification of the tidal signal produced by river discharge from the Sacramento Delta. Based on tidal theory, the method compares tidal properties at a river-influenced gauge with a reference estimate (or station). The reference station can be the astronomical potential or a tidal property at a coastal station that is minimally influenced by discharge. The ratio of tidal property at the reference station and the upstream is called the tidal property ratio (TP_R).

$$TP_R = \frac{TP_X}{TP_{REF}}$$
(*Equation 3.3.27*)

The tidal property ratio and the river discharge (Q_R) are related as follows,

$$Q_R \approx \alpha + \beta TP_R^\gamma$$
(*Equation 3.3.28*)

In equation 3.3.28 α, β and γ are coefficients developed from the available data. The authors were able to hindcast the discharge into the San Francisco Bay between 1858 and 1929 by examining how the ratio of the tidal potential (TP_{REF}) and the measured tides at

San Francisco (*TP$_X$*). Tides in the Columbia River are similarly influenced by river flow [*Moftakhari et al.*, 2016].

3.4   Flood Routing

Equations similar to the tidal equations (Eqn 3.4.1 to 3.4.4) are used to interpret and understand the propagation of flood waves in rivers. The following assumptions are usually made:

- The molecular viscosity is negligible

- Flow is 1-D (width and depth averaged)

- The hydrostatic approximation is applied

- Lateral and vertical variations are unimportant so the flow can be sectionally integrated

- The only body force acting on the fluid is gravity, Coriolis forces are neglected

Further, in the fluvial tidal river, changes in surface elevation are dominated by changes in riverine discharge. An understanding of flood routing is therefore helpful in calibrating and interpreting model results.

With these assumptions, the full one-dimensional St. Venant equations are given in equation 3.4.1 [*Cunge et al.*, 1980]

$$\frac{1}{g}\frac{\partial u}{\partial t} \; + \; \frac{u}{g}\frac{\partial u}{\partial x} \; + \; \frac{\partial h}{\partial x} \; = \; S_O \; - \; S_f \qquad (\textit{Equation 3.4.1})$$

dynamic wave   *dynamic quasi-steady wave*   *diffusive wave*   *kinematic wave*

31

where:

t time scale [L]
g acceleration due to gravity [LT^{-2}]
h elevation above mean surface elevation [L]
x along stream direction
S_O surface slope
S_f friction slope
R_h hydraulic radius (A/P) channel cross sectional area/wetted perimeter [L]

The equation can be reduced to four cases depending on the magnitude of the length and time scales. Equation 3.4.1 is considered the Unsteady-Uniform Equation. Neglecting the dynamic wave contribution yields the Steady-Nonuniform Equation (Equation 3.4.2),

$$\frac{u}{g}\frac{\partial u}{\partial x} + \frac{\partial h}{\partial x} = S_O - S_f. \qquad (\textit{Equation 3.4.2})$$

Elimination of the dynamic quasi-steady waves produces the diffusional or noninertial equation (Equation 3.4.3),

$$\frac{\partial h}{\partial x} = S_O - S_f. \qquad (\textit{Equation 3.4.3})$$

Finally, a kinematic wave occurs when the surface slope is approximately equal to the surface bed slope (Equation 3.4.4),

$$S_O = S_f. \qquad (\textit{Equation 3.4.4})$$

In this thesis, a scaling analysis of model results is used to determine the magnitude of each term of the full one-dimensional Saint Venant equations. These equations will be used to determine which terms are important. The scaling will also be used to determine how the nature of the floods in the LCR changed over the past 150 years.

32

4 Model Development

4.1 Archival Water Level and Flow Records

19th Columbia River Tides

Hydrographic records of river flow, water levels, tides and bathymetry are indispensable for developing and calibrating the Historic Model. Table 4.1 lists the water level and flow records used in this study.

Table 4-1: 19th century hydrology data. CR – Columbia River, WR – Willamette River, MSB-Morrison Street Bridge, Portland

Station	River	Location	Type	Dates
1 Fort Stevens, OR	CR	2.6	high/low tide	Jul 15 – Sep 15, 1868
1 Astoria, OR	CR	24	hourly water level	1870 – 1876
1 Cathlamet, WA	CR	60	high/low tide	Sep 12 – Oct 15, 1877
1 Oak Point, WA	CR	87	high/low tide	Sep 12 – Oct 15, 1877
1 Rainier, OR	CR	108	high low tide	Sep 12 – Oct 15, 1877
1 Vancouver, WA	CR	165	high/low tide	Sep 12 – Oct 15, 1877
1 Warrendale, OR	CR	228	30-60 min, 18-20 hrs/day	Sep 12 – Oct 15, 1877
2 MSB	WR	12.8	daily water level	Jan 1876 - Jun 1878
3,4 MSB	WR	12.8	daily water level	1879 – 1898
2 Albany, OR	WR	190	daily water level	Jun 1877 – Jun 1878
5 Albany, OR	Willamette	190	daily discharge	1878 – 1888
6 The Dalles, OR	Columbia	305	daily discharge	1878-present

1. digitized tide logs [*USC&GS*, 1877] 2. Discharge estimates [*USACE*, 1881-1915] 3 daily water level available at EV2 database 4. [*USWB*, 1879-1898] 5. [*USWB*, 1878-1888] 6. [*Henshaw & Dean, 1915*]

Three types of 19th century hydrographic records were recently recovered for the Lower Columbia River in the US National Archives (College Park, MD) and at NOAA (Silver Spring, MD):

- hourly tide data from Astoria from 1870-76

- daily high/low tide logs from 11 stations throughout the Lower Columbia River from June-October 1877 covering 221 km of the river (Figure 4-1)

- daily water level records of the Willamette River at Portland since 1879 (Table 4-1 & Figure 4-1) [*USWB*, 1879-1898]

High/Low tide logs consist of water levels measured at 10-20 minute intervals for 1-2 hours around high and low tide. Analysis of the tidal data helps us to understand the upriver propagation of the tide and are used to help calibrate model parameters such as channel floodplain roughness.

Figure 4-1: Location of 19th century tide logs used in calibration of Historic Model [Google, 2015]

The tide data described in Table 4-1 are close enough in time that tidal constituents from the various locations can be assumed to be from the same period (Figure 4-2). Since the 1877 tidal record in Astoria is relatively short (14 days), we substitute data from a low flow period in 1874 (Jul 31 – Aug 31) to obtain the harmonic constituents used in our spatial calibration. The amplitudes of the six largest tidal constituents from July 31 – August 31, 1874 are shown in Table 4-2 for Astoria. Additionally, a tidal record from Fort Stevens in 1868 is used to obtain harmonic constituents close to the mouth of the river.
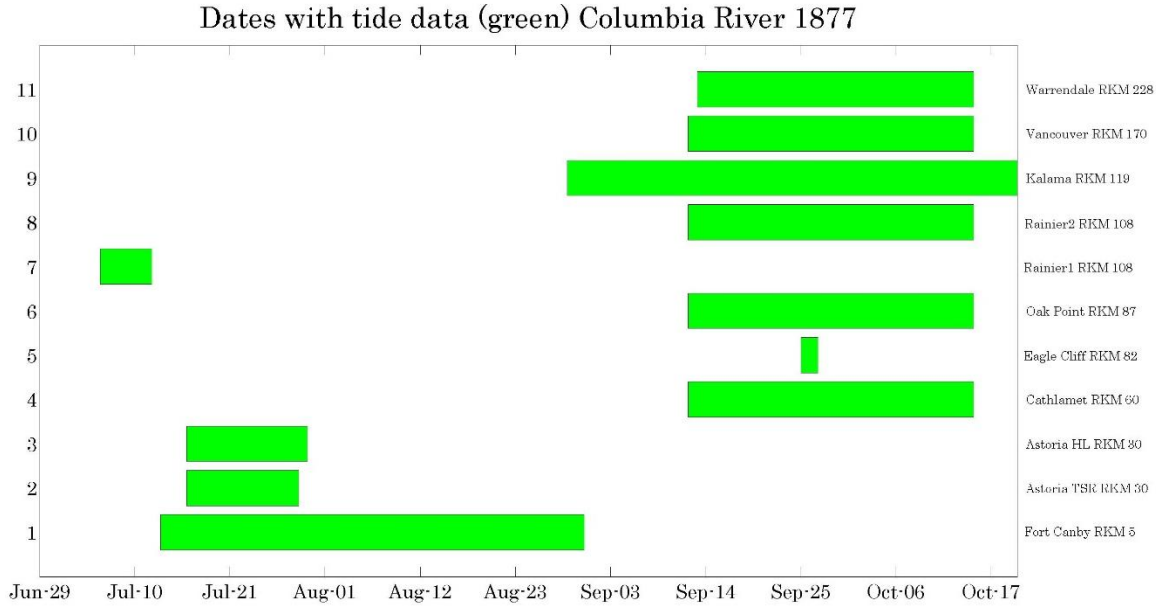
Figure 4-2: Locations and dates of 1870's LCR tide logs water surface elevation
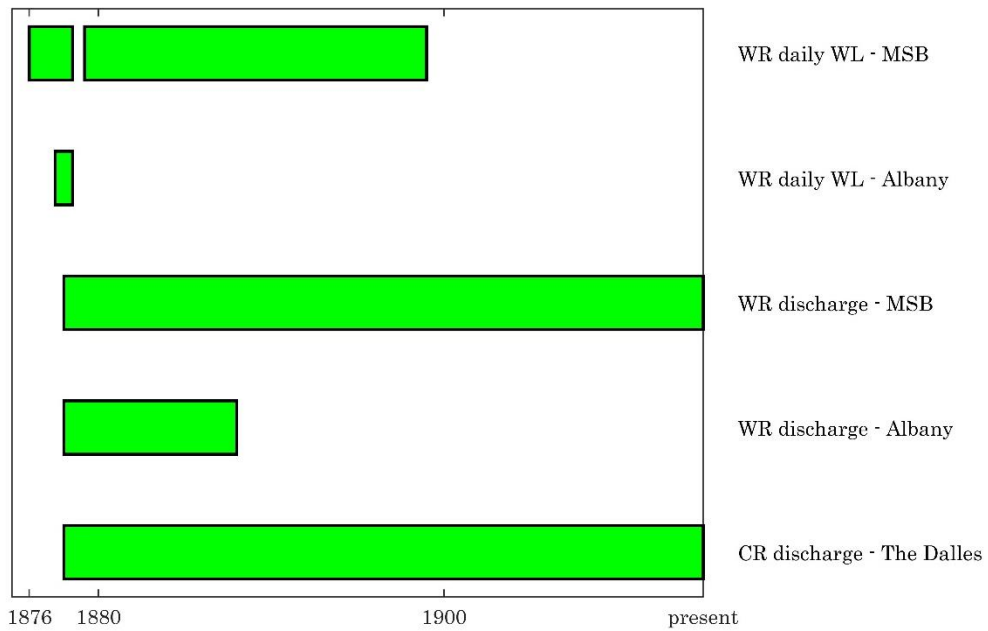
Figure 4-3: Location and dates of LCR hydrographic records used in the calibration of the Historic Model

At all locations except for Astoria and Warrendale, high/low tide data are used. Figure 4-4 is a photograph of a Columbia River tide log from the Vancouver, WA tide gauge for September 14, 1877. The tide log is the high/low format and the readings are 10 minutes apart and centered around the twice daily high and low tides. Water level is recorded for 90 minutes at low tide and 80 minutes at the subsequent high tide. In Warrendale, water level was measured every 30 or 60 minutes from 4:00 a.m. or 5:00 a.m. in the morning until 9:00 p.m. or 10 p.m. at night. Data shows that water level fluctuations due to the tidal signal are relatively small compared to discharge related fluctuations. The water level in Portland consists of once-a day water level measurements taken in the morning each day (Table 4-2), regardless of the tidal effects (the time of measurement changed over time).

Table 4-2: Amplitude of the five largest tidal constituents on the Columbia River in Astoria July 31 – August 31, 1874

Constituent	Period(hours)	Amplitude (m)
M2	12.4206	0.919±0.007
K1	23.9344	0.391±0.006
S2	12.000	0.266±0.006
O1	25.8193	0.251±0.006
N2	12.6583	0.163±0.007
Q1	26.8684	0.045±0.008

Figure 4-4: 19th century LCR tide log. [Talke, S.A., 1877 Vancouver, WA tide log. 2012. JPEG file].

Examples of the monthly tidal variations are plotted in Figures 4-5, 4-6 and 4-7 with additional examples located in the Appendix. Inspection of the records indicates slight variations in daily mean water level, possibly due to changing river discharge or the fluctuations due to the spring/neap cycle (Figure 4-5). Results show that, like today, 19th century LCR tidal range drops progressively from the mouth to upstream locations. The variability in the daily mean tide level (MTL) also increases going upstream. In Cathlamet in the estuary (Figure 4-5) the daily MTL is nearly unchanged over a month. In Vancouver at rkm 165, the daily MTL is influenced by river discharge (Figure 4-7).
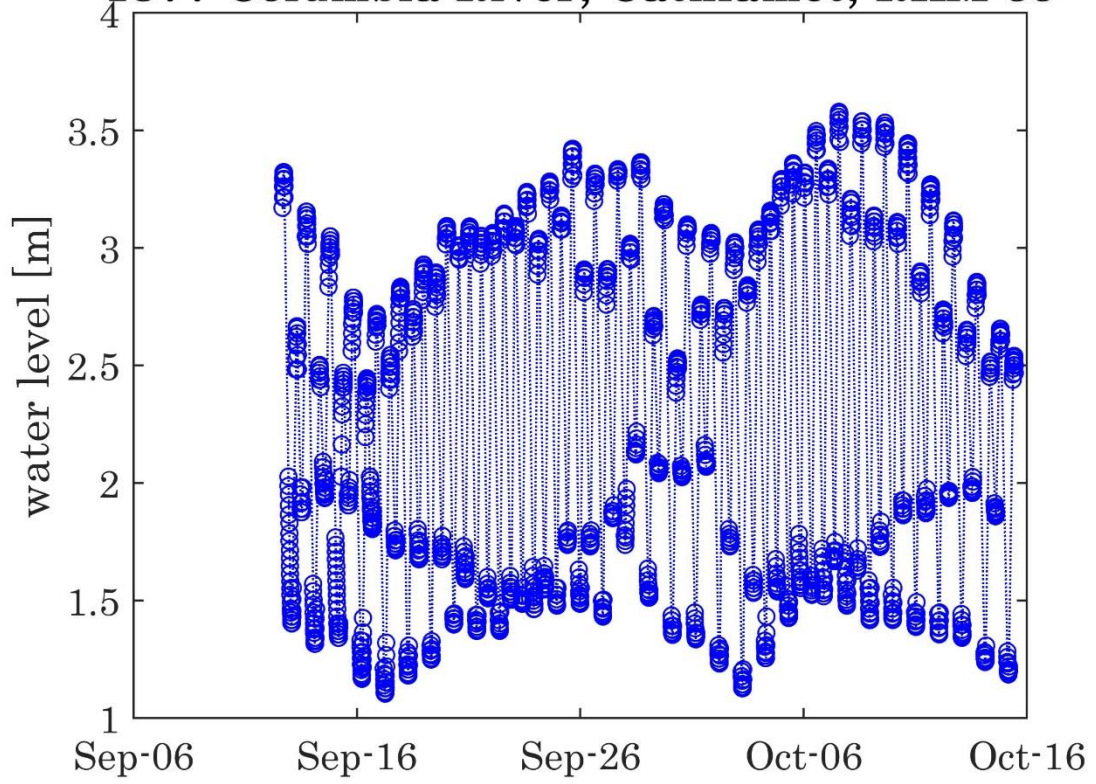
Figure 4-5: Columbia River water level, Cathlamet, WA, September12 – October 15, 1877.
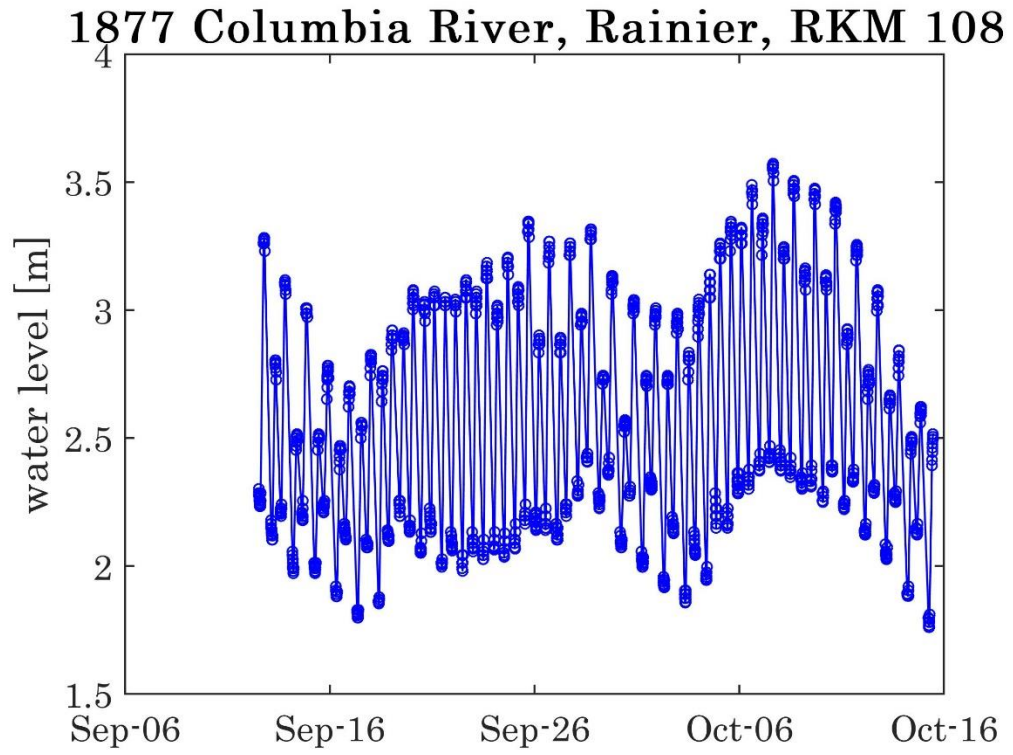
Figure 4-6: Columbia River water level, Rainier, OR, September 12 – October 15, 1877
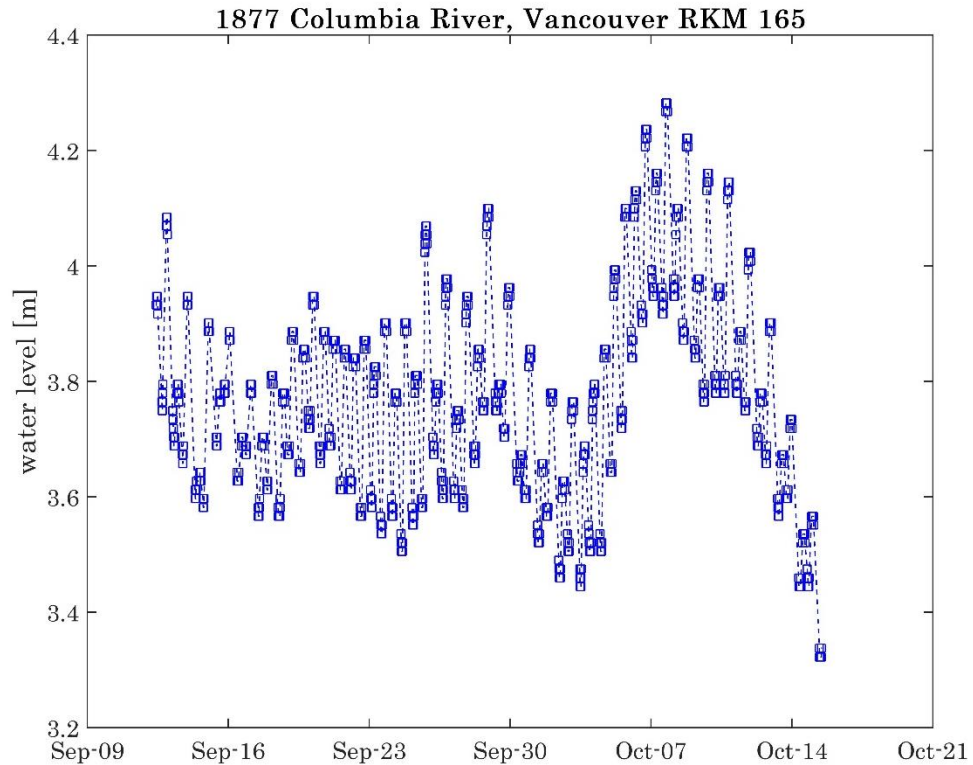
Figure 4-7: Columbia River water level, Vancouver, WA September 12 – October 15, 1877

Willamette River Water Level

Beginning in 1879 the U.S. Signal Corps began measuring and recording daily water level from the Willamette River in Portland. A time series of the water level is shown in Figure 4-8. The initial staff gage was located on a pile on the south side of Stark Street on the west bank of the Willamette River in downtown Portland, OR. In 1896 the staff gage was moved to the original Morrison Street Bridge and the United States Weather Bureau (USWB) (present-day National Weather Service) took over maintenance of the gauge. In 1922 the staff was relocated to the second Morrison Street Bridge. Finally, in 1958 the third present-day Morrison Street Bridge was completed and the gage was moved

to this location. The staff gage was replaced with a step stage recorder in the customs house beneath the bridge. The modern tide gage provides continuous water level readings and is still in operation [http://water.weather.gov]. U.S.G.S. also maintains a gage on the Morrison Street Bridge. At this location, water level records from 2007 to the present, and daily average discharge and High/Low records from 1974 to the present are available.

An additional source of water level information from the Willamette River are daily water level measurements from the 1876 to 1878 obtained from historic hydrographs plotted by the United States Army Corp of Engineers (USACE). Available readings were taken at the Stark Street gage in Portland from January 1876 to June 1878; however, Weather Bureau documents indicate that measurements began as early as 1872 by the city Engineer. A similar hydrograph from Albany, OR, is available from June 1877 to June 1878 [*USACE,* 1881-1915].
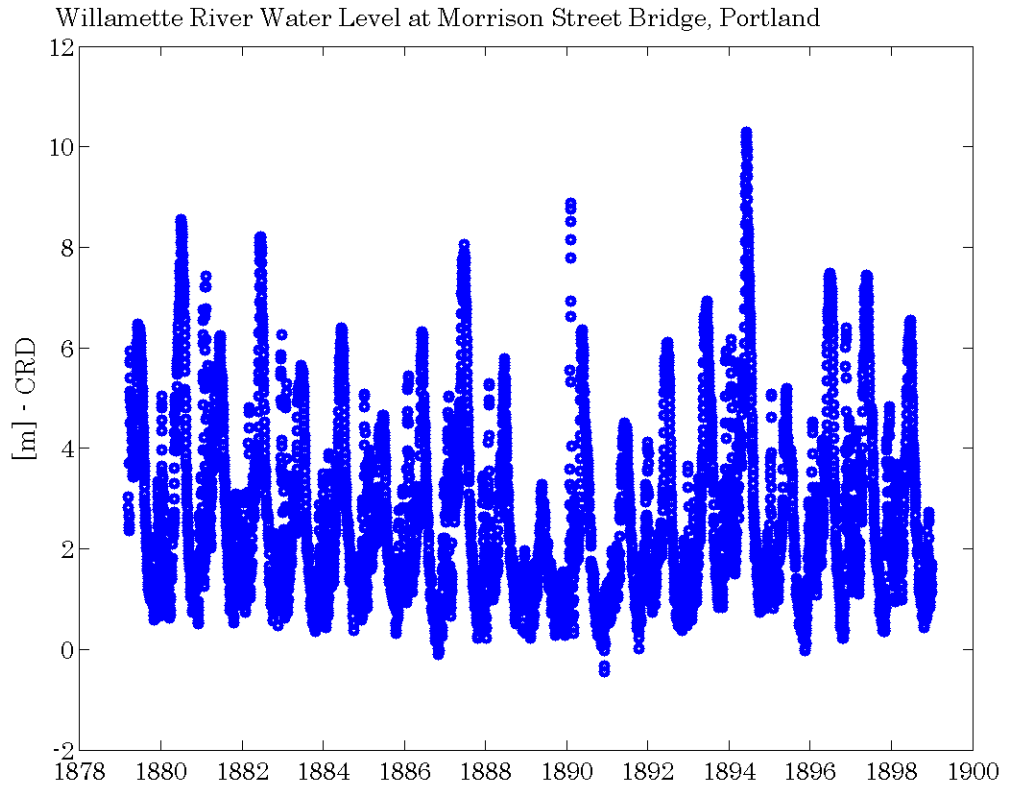
Figure 4-8: Willamette River water level at the Morrison Street Bridge in Portland, OR.

Surveying of Water Marks

While the datum of the National Weather Service gage is given relative to sea level, the definition of sea level changed multiple times in the early 20th century. Moreover, the level lines run from Portland to Astoria in 1898 are not considered accurate [*Burgette et al.*, 2009]. Thus, tying the zero of the historical water level measurements to the modern Columbia River Datum (CRD) is non-trivial. We approach the problem in two ways. First, we assess historical records and benchmarks available from the EV2 database [https://www.ncdc.noaa.gov]. Second, we resurveyed an extant floodmark in Portland from the 1894 Flood. The mark is within 0.5 km of the Morrison Street Bridge gage

A survey led by Tom Szymoniac of Portland State University measured the floodmark relative to a National Geodectic Survey (NGS) benchmark. The approximate location of the floodmark and the benchmark are shown in Figure 4-9, and a picture of the benchmark is shown in Figure 4-10. A forward and reverse loop indicated an agreement to within 0.023' with an NGS benchmark (Table 4-3), and is within the permissible limit of 0.055' for a first order, class II survey (see Appendix 7.3 for survey notes).

The survey placed the peak elevation of the 1894 Flood at 33.75' relative to CRD or 39.05' relative to NAVD88. This value is 0.75' higher than the elevation given by the water level records from the USWB at the Stark Street Gage. However, the result is consistent with corrected archival records of Morrison Street Bridge data from 1880-1914, which have had 0.7 feet added to them [http://www.portlandoregon.gov]. Based on this result the Willamette River water level from the late 19th century and early 20th century were adjusted by adding 0.75' to the reported value.

Table 4-3: Location of survey benchmark. Datasheet available at www.ngs.noaa.gov

PID	Location	NAVD Height [m]
RD 0457	45° 31' 03.72" N	34.26
	122° 40' 17.40" W	
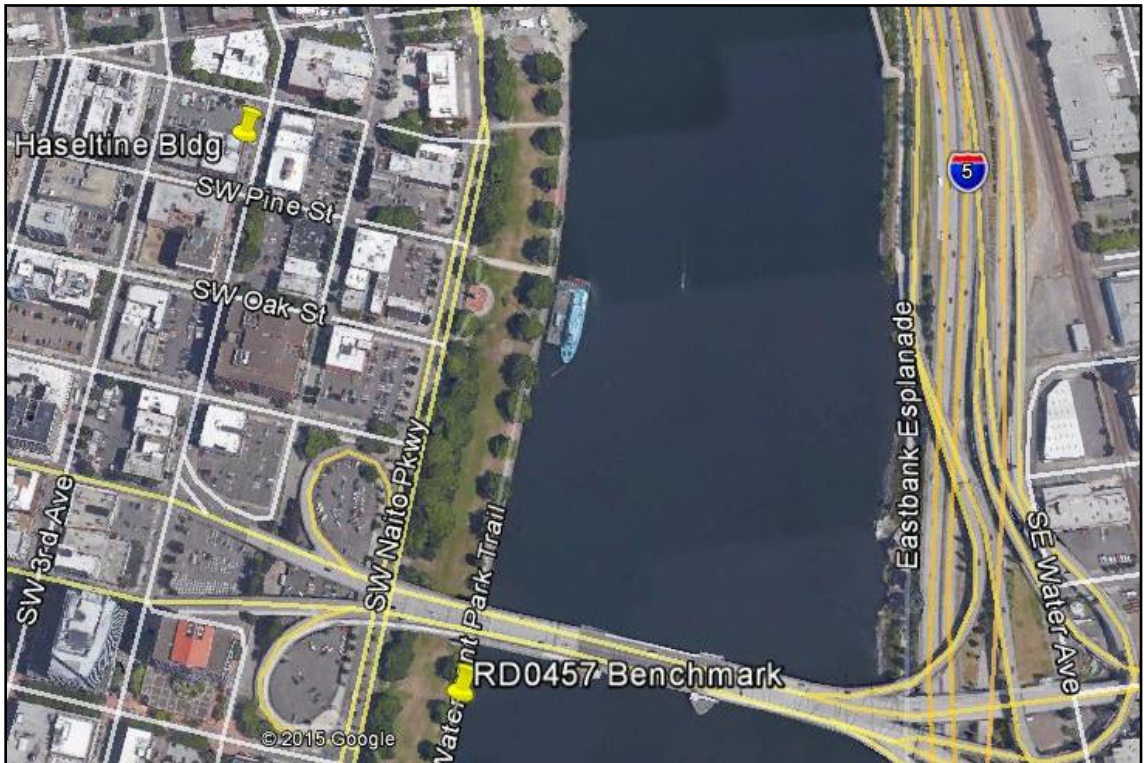
Figure 4-9: Location of the Haseltine Building (122 SW 2nd Ave, Portland) and NGS Benchmark RD0457. [Google Earth,2015].

Figure 4-10: Flood marks from the 1894 Spring Flood (top) and the 1948 Vanport Flood (bottom) on the Haseltine building. Photo available at www.waymarking.com

Columbia River Discharge

Starting in 1878 the USACE began measuring the daily average discharge from the Columbia River at The Dalles, OR. The daily statistics for site number 14105700 can be found online at http://waterdata.usgs.gov . The gage is located approximately 74 km upstream of Bonneville Dam (Figure 4.-11).

Figure 4-11: Satellite image of the Columbia River between Bonneville, OR and The Dalles, OR. [Google Earth, 2015].

Figure 4-12: Location and dates of Willamette and LCR hydrographic records of discharge
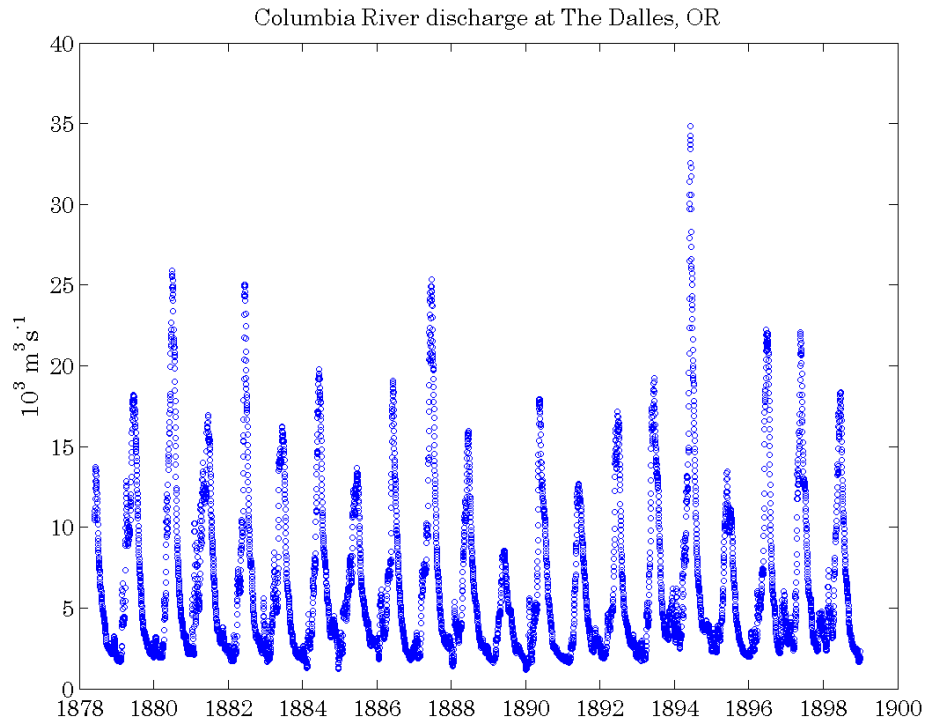
Figure 4-13: Daily average discharge from the Columbia River at The Dalles, OR 1878-98. Records retrieved from http://waterdata.usgs.gov

Willamette River Discharge

We include the Willamette River in our model since it is the largest tributary of the Columbia River and provides up to 25% of the streamflow of the Lower Columbia River [*Orem,* 1968]. Several other tributaries the Columbia River are being excluded from the model (Table 4-4). The three largest tributaries of the Columbia River downriver of the Willamette River are the Lewis River, the Cowlitz River and the Kalama River. The total average discharge from these tributaries are small compared to the Willamette River and Columbia River.

47

Table 4-4: Daily discharge from the three largest tributaries of the Columbia River downriver of the Willamette River. a – [Kimbrough et al., 2005], b – [Lower Columbia Fish Recovery Board, 2004], c –

	Ave Daily Discharge (CMS)
Cowlitz River (a)	258
Lewis River (b)	173
Kalama River (c)	35

The only observed stage and discharge data from Willamette River in the 19th century is from the Albany, OR gage (Figure 4-14), located about 190 km from the confluence with Columbia River and above the head-of-tides. The USGS has used water level records to estimate discharge at Albany since 1878. The discharge collected by the USGS for the Willamette River at Albany is mostly complete from 1878 to 1881, but there are many days missing between 1881 and 1892 (Figure 4-15). The discharge record from the Albany is used to hindcast the Willamette River discharge at Morrison Street Bridge. This section will detail the process used to develop flow estimates for the Willamette River in Portland, OR.
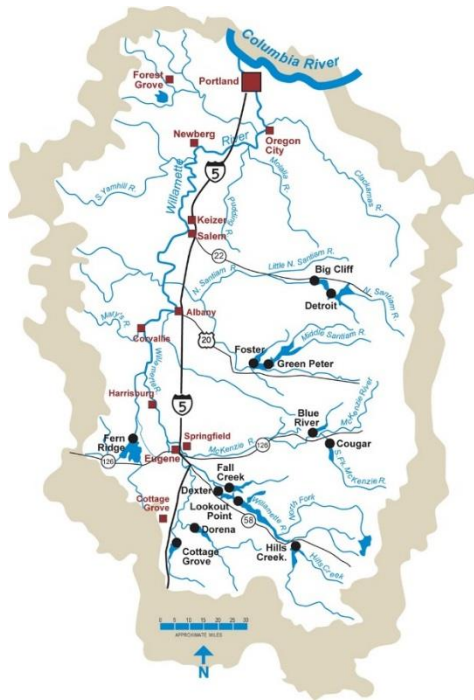
Figure 4-14: U.S. Army Corps of Engineers map of the Willamette River.
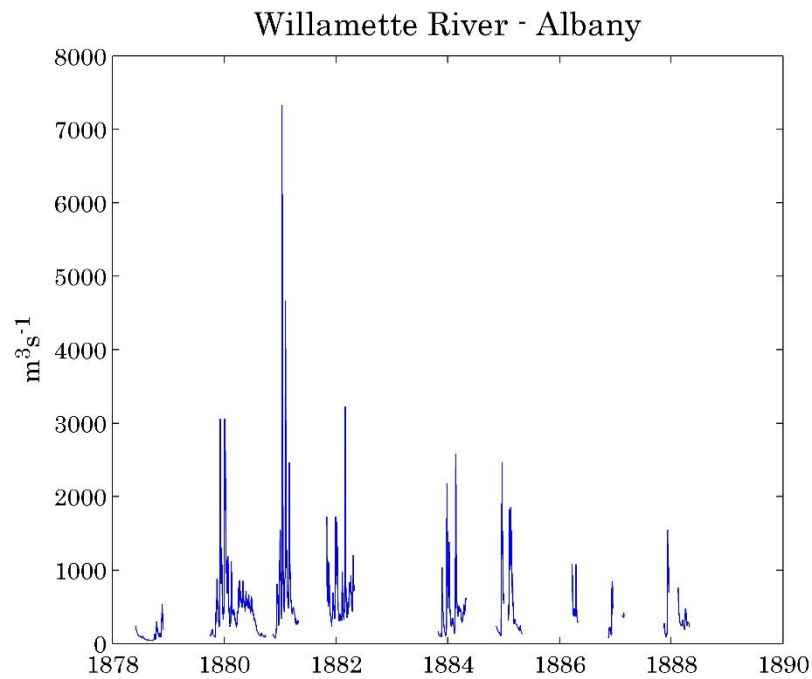
Figure 4-15: Daily average discharge from the Willamette River at Albany, OR Nov. 1878 to Apr. 1888. [USGS, 2012]

49

Water level at Morrison Street Bridge is dependent on Columbia and Willamette River discharge as well the tidal amplitude. An estimate of the Willamette River discharge in the 19th century is determined through an iterative model (D.Jay, unpublished data, 2011) using inputs of river discharge, water level and downstream tidal range. The process begins by using a forward model for the surface elevation at Morrison Street Bridge, where the elevation has six basis functions:

$$MSB = f(1, Q_{TD}^{m1}, Q_{TD}^{m2}, Q_{TD}^{m3}, Q_{WR}^{nn}, \frac{TPR^{ss}}{(1+Q_{TD}+Q_{WR})^{rr}}) \qquad (Equation\ 4.1.1)$$

MSB = Morrison Street Bridge surface elevation (CRD)
Q_{TD} = Columbia River discharge at the The Dalles lagged by one day in $10^3 m^3 s^3$
Q_{WR} = Willamette River discharge at Albany when available in $10^3 m^3 s^3$
TPR = Tidal range on the Columbia River at Tongue Point
[*m1*, *m2*, *m3*, *nn, ss, rr*] = [1, 2, 3, 0.63, 0.96, .0.51]

Tongue Point tidal range was determined from data after 1925, such that amplitudes may be altered from the historical condition; nevertheless, the neap-spring cycle is correctly timed. A regression analysis was then used to determine the coefficients for each of the basis function functions (Table 4-5).

Table 4-5: Coefficients for the six basis functions in equation 4.1.1

a0	a1	a2	a3	a4	a5
-1.32209	0.444791	-0.00260778	-0.0000756595	2.05729	0.582934

The coefficients and the exponents from the forward model (MSB elevation) are then used in an inverse model to determine discharge from the Willamette River at Morrison Street Bridge (equation 4.1.2).

$$Q_{Wst}(k+1) =$$

$$\left(Max \left[\left\{ .06^{nn}, \frac{1}{a_4(MBR_{(j)} - a_0 - a_1 Q_{TD(j)}^{m1} - a_2 Q_{TD(j)}^{m2} - a_3 Q_{TD(j)}^{m3} - \frac{a_5 TPR_j^{SS}}{\left(1 + Q_{WO} + Q_{TD(j)}\right)^{rr}}} \right\} \right] \right)^{1/nn}$$

(*Equation 4.1.2*)

The terms on the right side of the equation are the same as equation 4.1.1. The subscript j denotes the values for a given day. The Willamette River at Portland discharge is determine iteratively where Q_{WO} is the value for iteration k. The iteration is repeated six times or until the solution converges. The minimum discharge allowed is 60 CMS. A non-linear filter (1 day for high flows, up to 19 days for low flow) is applied to remove spurious neap-spring fluctuations. The resulting data set is provides an estimate of Willamette River discharge that is utilized in the historical water level analysis.
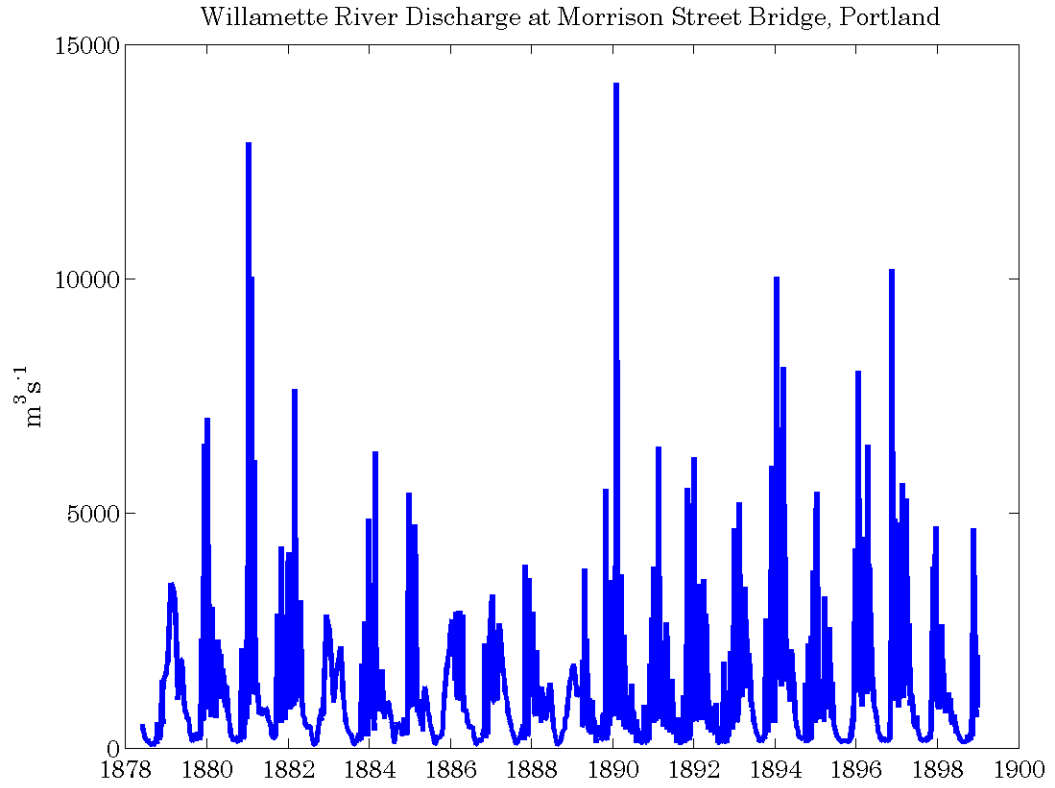
Figure 4-16: Willamette River discharge at Morrison Street Bridge in Portland, OR. Records provided by the Portland Water Bureau. [USWB, 2012].

CR discharge @ The

Tongue Pt TR via harmonic analysis

[*Pawlowicz et al.*, 2002; *Jay et al.*,

Morrison Street Bridge WL (Signal Service, USWB)

WR River discharge @ Albany (USWB)

Forward Model

$$MSB = f\left(1, Q_{TD}^{m1}, Q_{TD}^{m2}, Q_{TD}^{m3}, Q_{WR}^{nn}, \frac{TPR^{ss}}{(1 + Q_{TD} + Q_{WR})^{rr}}\right)$$

set k = 0

$|MSB\ WL_{OBS} - MSB\ WL_{MOD}| \leq \max error$

or $k < k_{max}$

increment k

n

yes

Coefficients

$a_0, a_1, a_2, a_3, a_4, a_5$

set k = 0

$|MSB\ WL_{OBS} - MSB\ WL_{MOD}| \leq \max error$

or $k < k_{max}$

increment k

n

yes

Exponents

$m_1, m_2, m_3, nn, rr, ss$

Figure 4-17: Flowchart of forward model of 19th century water level at Morrison Street Bridge, Portland, OR

53

Coefficients

a_0 , a_1 , a_2 , a_3 , a_4 , a_5

Exponents

m_1 , m_2 , m_3 , nn , rr , ss

CR discharge @ The Dalles (USGS)

Tongue Pt TR via harmonic analysis [*Pawlowicz et al.*, 2002; *Jay et al.*, 2011]

Morrison Street Bridge WL (Signal Service, USWB)

WR River discharge @ Albany (USWB)

set k = 0

Inverse Model

$$Q_{WR(k+1)} = Max\left[0.06^{nn}, f^{-1}\left(1, Q_{TD}^{m1}, Q_{TD}^{m2}, Q_{TD}^{m3}, Q_{WR}^{nn}, \frac{TPR^{ss}}{\left(1 + Q_{TD} + Q_{WR(K)}\right)^{rr}}\right)\right]$$

increment k

$|Q_{WR(k+1)} - Q_{WR(k)}| \leq max\ error$ or $k < k_{...}$

no

yes

Q_{WR} MSB
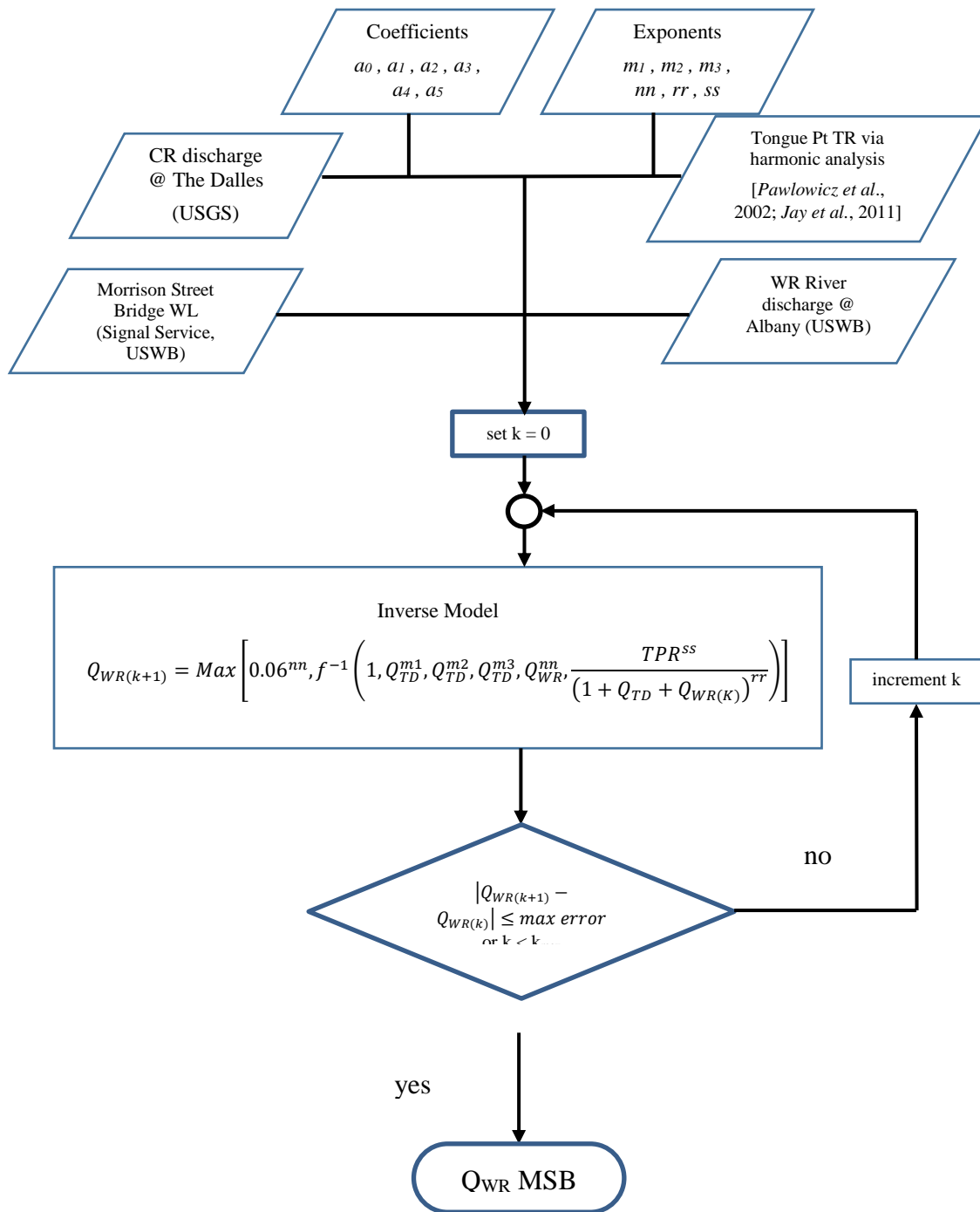
Figure 4-18: Flowchart of inverse model of 19th century Willamette River discharge at Morrison Street Bridge, Portland, OR

54

Morrison Street Bridge Rating Curve

The discharge records from the Columbia River and Willamette River along with the water level from the Morrison Street Bridge can be combined into a rating curve which relates water level to a given flow condition. A rating curve for the years 1879-98 is constructed for the Willamette River at Stark Street/Morrison Street Bridge Gage (Figure 4-19). In the rating curve, the Columbia River discharge from The Dalles is lagged by one day to account for travel time. The rating curve is representative of the time period of the Columbia River surveys conducted by the USC&CG in the late 19th century.

The Willamette River is subject to many short duration floods such as the 1890 event, which produced relatively high discharge for only a few days. To improve the rating curve estimate of Portland water level vs. Columbia River flow, the regression is limited to days with Willamette River discharge below 500 CMS. This reduces the non-Columbia induced variability in water level.
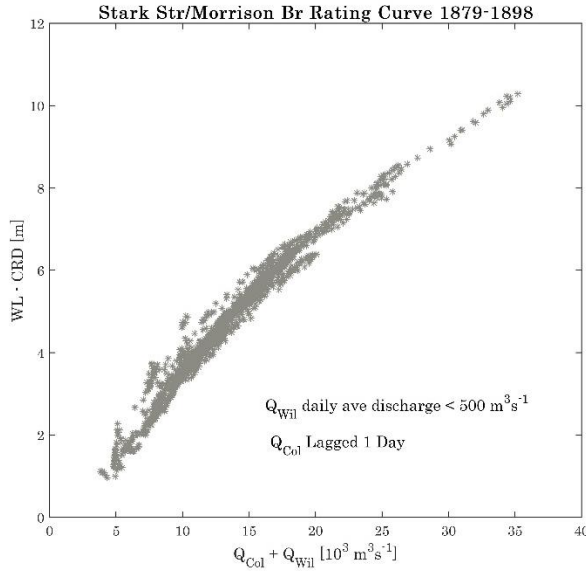
Figure 4-19: Rating Curve of Willamette River at Stark Street/Morrison Street Bridge from 1879-98.

USACE Flood Profile

The USACE Flood profile [*USACE*, 1963] provides several key pieces of information that are useful in the creation of the Historic DEM (Figures 4-23 & 4-24). The document provides the flood profile along the Lower Columbia River for the seven largest spring freshets between 1876 and 1963. The profile also provides the date and the peak surface elevation of the spring freshet at Vancouver, WA from 1876 to 1963. This information, combined with discharge data from the Willamette and Columbia River helps to verify the accuracy of historical flood simulations.

The flood profile also contains the approximate flood stage along the river. The approximate flood stage is used as a guide in estimating historical levee heights.
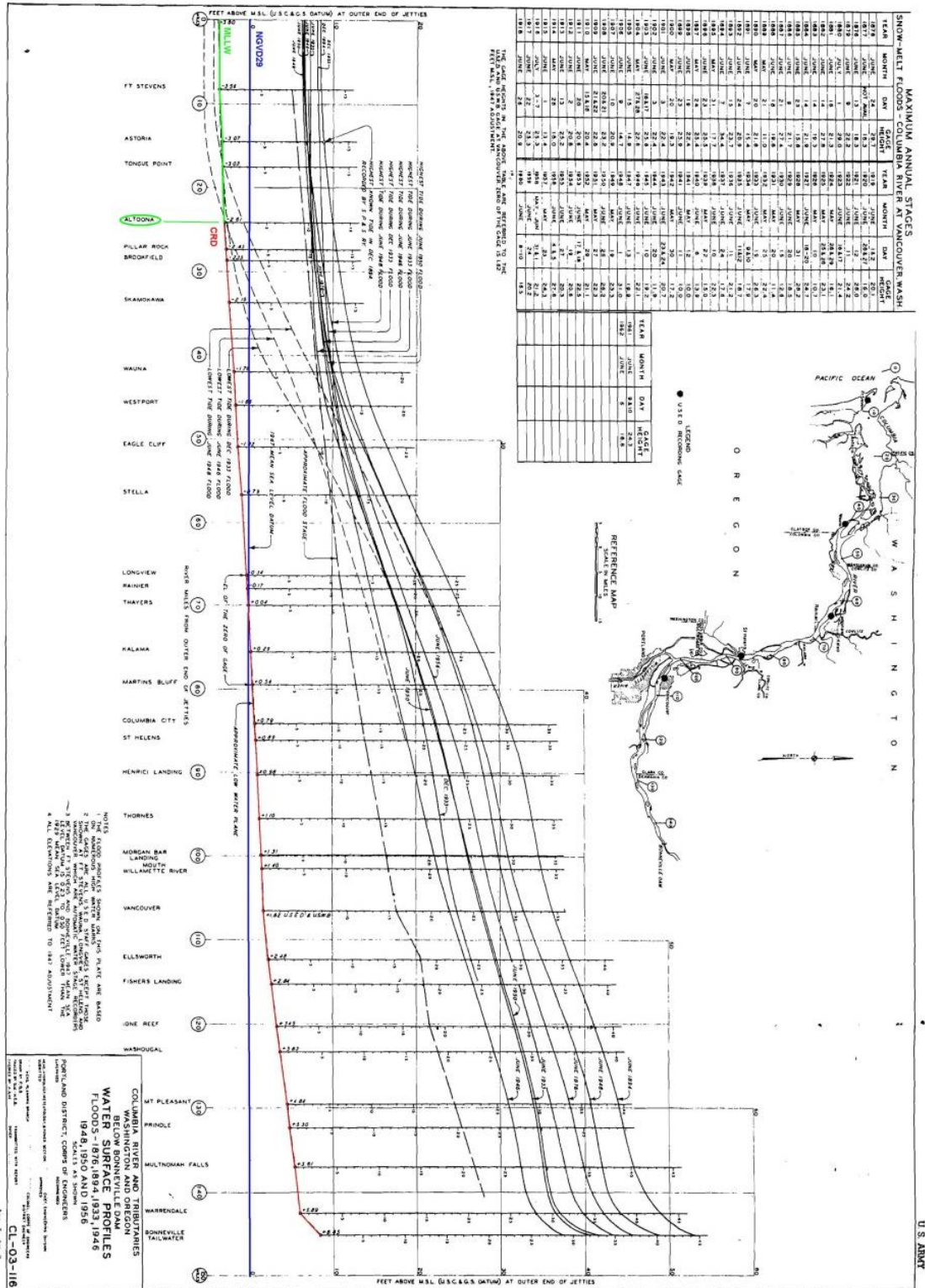
Figure 4-20: Columbia River water surface profiles for major floods in 1876, 1894, 1933, 1946, 1948, 1950 and 1956. [USACE, 1963]

MAXIMUM ANNUAL STAGES
SNOW-MELT FLOODS – COLUMBIA RIVER AT VANCOUVER, WASH.

YEAR	MONTH	DAY	GAGE HEIGHT	YEAR	MONTH	DAY	GAGE HEIGHT
1876	JUNE	24	29.7	1919	JUNE	1 & 2	20.1
1877	JUNE	NOT AVAIL.	18.3	1920	JUNE	26 & 27	16.0
1878	JUNE	13	18.3	1921	JUNE	12	26.0
1879	JUNE	9	22.2	1922	JUNE	11	24.2
1880	JULY	1	29.0	1923	JUNE	16 & 17	21.4
1881	JUNE	16	21.3	1924	MAY	28 & 29	16.1
1882	JUNE	14	27.8	1925	MAY	25 & 26	23.1
1683	JUNE	14	19.3	1926	MAY	10	10.7
1884	JUNE	14	21.9	1927	JUNE	16-20	24.7
1885	JUNE	23	15.8	1928	MAY	31	26.2
1886	JUNE	9	21.7	1929	JUNE	20	18.5
1887	JUNE	21	27.4	1930	JUNE	15	12.6
1888	JUNE	18	19.8	1931	MAY	20	11.4
1889	MAY	21	11.0	1932	MAY	25	22.4
1890	MAY	20	21.6	1933	JUNE	19	26.3
1891	JUNE	7	15.4	1934	MAY	9 & 10	17.9
1892	JUNE	24	20.9	1935	JUNE	11 & 12	16.7
1893	JUNE	15	23.7	1936	JUNE	11	21.2
1894	JUNE	7	34.4	1937	JUNE	24	17.6
1895	MAY	31	17.7	1938	JUNE	10	22.3
1896	JUNE	23	25.5	1939	MAY	22	15.0
1897	MAY	24	25.4	1940	JUNE	6	13.9
1898	JUNE	19	22.4	1941	MAY	12	10.0
1899	JUNE	23	25.9	1941	JUNE	11	10.0
1900	MAY	20	19.3	1942	MAY	30	17.2
1901	JUNE	3	22.4	1943	JUNE	23 & 24	20.7
1902	JUNE	3	22.4	1944	JUNE	20	11.9
1903	JUNE	16 & 17	25.8	1945	JUNE	10	19.2
1904	MAY	27 & 28	22.6	1946	JUNE	1	22.1
1905	JUNE	15	14.8	1947	JUNE	13	19.8
1906	JUNE	9	14.7	1948	JUNE	1	31.0
1907	JUNE	10	20.9	1949	MAY	19	23.3
1908	JUNE	20 & 21	23.2	1950	JUNE	26	26.2
1909	JUNE	21 & 22	22.6	1951	MAY	27	22.3
1910	MAY	15 & 16	20.4	1952	MAY	29	21.1
1911	JUNE	20	20.6	1953	JUNE	17 & 18	22.5
1912	JUNE	2	20.8	1954	JUNE	19	20.6
1913	JUNE	13	25.2	1955	JUNE	27	20.3
1914	MAY	28	18.0	1956	JUNE	4 & 5	27.6
1915	JUNE	1	13.4	1957	MAY	23	24.3
1916	JULY	3-7	25.3	1958	MAY - JUN	31 & 1	21.2
1917	JUNE	22	23.3	1959	JUNE	24	20.2
1918	JUNE	26	20.9	1960	JUNE	8-10	16.5

Figure 4-21: Maximum annual stages of snow-melt floods on the Columbia River Columbia River at Vancouver, WA. [USACE, 1963]

58

4.2   Bathymetry

To understand how anthropogenic changes affect tidal propagation it is necessary to have bathymetry information from past and the present. This project is made possible by the existence of 19th century maps, surveys and topography sheets (T-sheets). The maps contain information about river depths, floodplain vegetation, and infrastructure on the river and surrounding floodplain.

Historic DEM

The majority of the bathymetry and topography data used to produce a DEM consists of hydrographic surveys made by the US Coastal Survey and US Coast and Geodetic Survey between 1868 and 1901. A large fraction of the available historical bathymetry data set was digitized by the Wildlife Ecosystem Team at the University of Washington [*Burke*, 2010]. The resulting sample set covers the main stem of the Columbia River from the mouth to rkm 219 near Skamania Island. The sample set also covers the main stem of the Willamette River from the confluence with the Columbia River to a point approximately 11 kilometers upriver. Table 4-6 lists the LCR hydrographic surveys, location and year completed, and Figure 4-22 shows the physical location of each of the surveys. USC&GS documents from that period typically included elevation to about MLLW, such that additional information is needed for the floodplains (see below).

The digitized data points were compiled into a digital elevation model with NAVD88 as a vertical datum. The data were originally in latitude and longitude based on the NAD83 system for spatial coordinate but were changed to Washington North coordinates for convenience in determining linear distances between points. The spatial

59

coordinates were then converted to Washington South coordinate system for use in the Delft3D model. Figure 4-23 shows the original area covered by the digitized data points from the Wildlife Ecosystems Team (WET). Because the samples from the WET Team were coarser than desired, samples were interpolated in ArcGIS to a spatial density of 30m. Figure 4-24 shows the outline of the Historic DEM from WET and the outline of the final Historic DEM. The following sections will the compilation of the final digital elevation model.

Table 4-6: Digitized hydrographic surveys from the WET Team [Burke, 2005]

H-sheet #	Year	Title	Scale
H1015	1867	No.1 From Three Tree Pt to Gray's Bay	1:10,000
H1016	1868	No. 2 Inside Passage from Tongue Pt to Welch's Is	1:10,000
H1017	1868	Sheet No. 3	1:10,000
H1018	1868	From Cape Disappointment to Tongue Pt	1:20,000
H1019	1868	Entrance of the Columbia River	1:20,000
H1335	1875	Cathlamet Point to Head of Puget Is	1:10,000
H1336	1876	Head of Puget Is to Head of Grim's Is	1:10,000
H1368	1877	Head of Grim's Is to Mt Coffin	1:10,000
H1369a	1877	Mt Coffin to Coffin Rock	1:10,000
H1369b	1877	Coffin Rock to Foot of Deer Is	1:10,000
H1524	1884	North End of Deer Is to Columbia City, OR	1:10,000
H1671	1885	Columbia River (Willow Bar)	1:10,000
H1673	1885	Willamette and Columbia Rivers	1:10,000
H1711	1886	From Columbia City to Head of Bachelor Is	1:10,000
H2506	1900	Ryan's Pt to Hood's Bar	1:10,000
H2529	1900	Hood's Bar to Head of Lady's Is	1:10,000
H2550	1901	Lady's Is to Rooster Rock	1:10,000
H2574	1901	Rooster Rock to Multnomah Falls	1:10,000
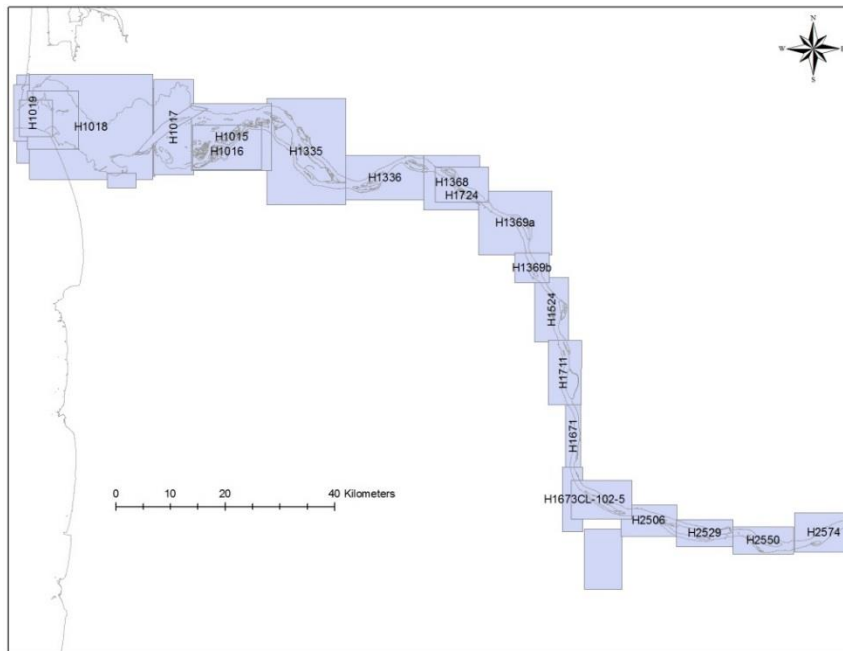
Figure 4-22: Extent of the each hydrographic survey provided by the WET Team.

61
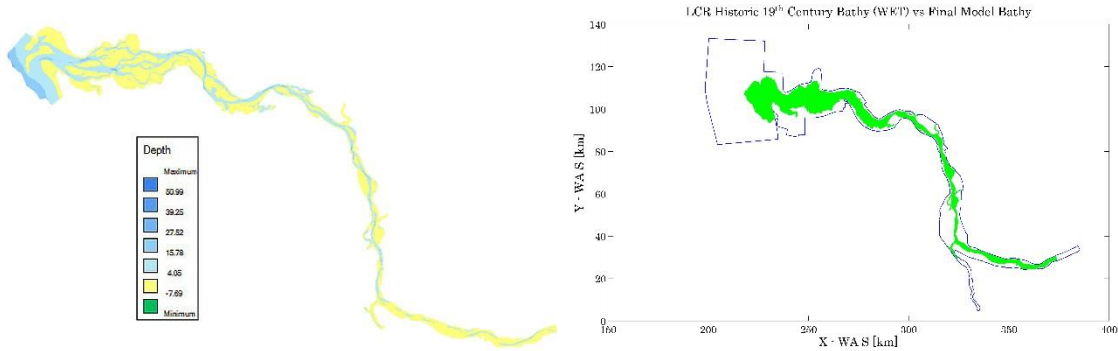
Figure 4-23: left) Historic DEM from WET in Delft3D format. Depth in meters relative to NAVD88, and positive downwards. [Burke, 2005]

Figure 4-24: (right) Extent of final Historic DEM (blue line) and WET DEM (green).

Figure 4-24 shows that the final model grid contains samples that extends out into the Pacific Ocean and along the Oregon and Washington coast. This is necessary because the Columbia River plume exerts an influence on the water levels at least 40km from the mouth of the Columbia River [*Horner-Devine et al*, 2009]. The model grid is set extended approximately 40 km from the mouth of Columbia River to a point where vertical water level fluctuations due to the plume are minimized. The water depths in the coastal domain were interpolated from a National Geophysical Data Center, Pacific Ocean digital elevation model [*NGDC,* 2003].

Topographic Survey Sheets

Historical topography sheets (T-sheets) produced by the USC&GS were used as a supplemental tool in the creation of the Historic DEM [*Burke,* 2005]. These digitized maps do not contain any depth information but are on the same coordinates system as the Historic DEM. They are useful because they contain information about surfaces features such as

intertidal mudflats, marshes, swamps, channels and forests, locations which were not surveyed by the H-Sheets (which measured bathymetry below MLLW). The T-sheets are therefore valuable for approximating the historical floodplain and were used to infer historical differences (or lack thereof) between the modern and historical periods. An example is Minaker Island and Karlson Island just north of Knappa, OR. Comparisons of historical T-sheets (Figure 4-25) to the modern topography (Figure 4-26) obtained from satellite imagery shows that, in this case, many of large scale features of the wetland have not significantly changed. Hence, to first order, the modern floodplain topography above MLLW can be used in the historical DEM (see the description of Lidar bathymetry below). However, close inspection often shows features in the modern topography that are not present in the historical DEM or T-sheets. These features, which include roads, levees, pile-dikes, and other constructed features, were manually removed from the modern flood-plain, to the extent possible. By this manual method, the modern bathymetry was used to fill in the floodplain of the Historic DEM.

Figure 4-25: (left) Topographic survey t1234 (1870) So. Side of the Columbia River from John Day's Rvr to Warren's Ldg [Burke, 2010]

Figure 4-26: (right) Image of Minaker Island and Karlson Island [Google Earth, 2014]

63

Table 4-7: digitized 19th century U.S.C. & G.S. topographic sheets of the Lower Columbia River [Burke, 2005]

Name	Year	Description	Scale
t1112lam83	1868	So. Side of the Columbia Rvr from Pt Adams to Young's Bay	1:10,000
t1138lam83	1869	Columbia Rvr from Cape Disappointment to Chinook Pt	1:10,000
t1123lam83	1868	Columbia Rvr from Young's Bay to John Day's Rvr	1:10,000
t1139lam83	1869	Colmbia Rvr from Chinook Pt to Gray's Pt	1:10,000
t1234lam83	1870	So. Side of the Columbia Rvr from John Day's Rvr to Warren's Ldg	1:10,000
t1235lam83	1870	Columbia Rvr Warren's Ldg to Three Tree Pt	1:10,000
t1249lam83	1870	Columbia Rvr from Gray's Bay to Snag Is	1:10,000
t1250lam83	1871	Columbia Rvr from Three Tree Pt to Puget Is	1:10,000
t1250lam83b	1871	Columbia Rvr from Three Tree Pt to Puget Is	1:10,000
t1331lam83	1872	Columbia Rvr in the vicinity of Cathlamet and Westport	1:10,000
t1401alam83	1874	Columbia Rvr Cape Horn and vicinity	1:10,000
t1401blam83	1874	Columbia Rvr from Wallace's Is to Oak Pt	1:10,000
t1431alam83	1876	Columbia Rvr between Long. 123°02' and Long. 123°09'	1:10,000
t1431blam83	1874	Columbia Rvr vicinity of Wallace's Is	1:10,000
t1454lam83	1877	Columbia Rvr vicinity of Mt Coffin	1:10,000
t1455alam83	1877	Columbia Rvr including the mouth of the Cowlitz Rvr	1:10,000
t1455blam83	1877	Columbia Rvr from Cottonwood to Deer Is	1:10,000
t1495lam83	1879	Columbia Rvr from near Kalama to Columbia City	1:10,000
t1542lam83	1882	Columbia Rvr vicinity of Bachelor's Is	1:10,000
t1562lam83	1884	Columbia Rvr from Willow Bar to Foot of Hayden's Is	1:10,000
t1563lam83	1880	Columbia Rvr Columbia City to Bachelor's Is	1:10,000
t2007lam83	1890	Columbia Rvr from Lower End of Hayden's Is to Sta. Wintlet	1:10,000
t2085lam83	1891	Columbia Rvr from Sta. Wintlet to Head of Government Is	1:10,000
t2522lam83	1900	Columbia Rvr vicinityof Lady's Is Hood's Bar to Head of Government Is	1:10,000
t2577lam83	1901	Columbia Rvr Lady's Is to Rooster Rock	1:10,000

Navigation Maps

Historical navigation maps were also used as a source of information from the late
19th century LCR. A search at the Oregon Historical Society in Portland yielded several
useful navigation maps from the late 19th century and early 20th century (Table 4-8). These
maps provide channel depth and show natural features such as sand bars and shoals and

man-made features such as pile dikes. Although the maps do not provide elevations outside

of the river channel, they do show lakes, marshes and streams. The historic elevation of

these features can be estimated from nearby modern analogs.

Table 4-8: Supplementary map sources a. [Pengra, 1862], b. [Cutts et al., 1870], c. [Rockwell, 1876], d. [Rockwell et al., 1888], e. [McIndoe and Thomson, 1911]

Year	Location	Reach	Sources
1862	Columbia River	Sauvie Island	Oregon Survey (a)
1870	Columbia River	Mouth to Astoria	U.S.C. & G.S. (b)
1876	Young's River	Near Astoria	U.S.C. & G.S. (c)
1888	Columbia River	Fales Landing to Portland	U.S.C. & G.S. (d)
1911	Willamette River	Portland to Oregon City (3 sheets)	U.S.C. & G.S. (e)

Figure 4-27: Photograph of 1888 map of the Willamette River in Portland. Depth measured in feet. [Rockwell et al., 1888]

LiDAR Bathymetry

The bathymetry provided by the WET is not sufficient to model a large flood on the Lower Columbia River. It must be supplemented with modern bathymetry, by multibeam surveys of the waterways in the LCR and LiDAR derived elevations above the water/land interface [*USACE*, 2010]. The dataset is gridded and has a resolution of 0.5m. The extent of the dataset is shown in Figure 4-28.
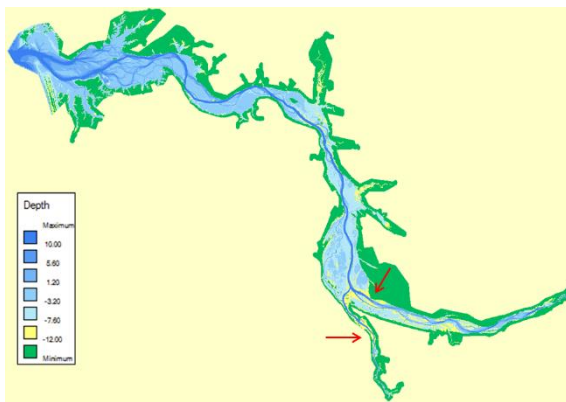
Figure 4-28: LiDAR bathymetry of the Lower Columbia River from Bonneville to the mouth. Data includes the Willamette River from Oregon City, OR to the confluence with the Columbia River. Depth is in meters positive upwards referenced to NAVD88

4.3   Delft3D Grid

In constructing the Delft3D hydrodynamic grid for the model, several factors need to be taken in consideration. The grid should be aligned with the velocity vectors of the river flow, and the cells should be as close to rectangular as possible. The grid for the LCR should have enough resolution to capture the flow of the water in a channel, but having too fine a resolution will slow computational time and utilize a large amount of computer storage space [*Deltares,* 2010a, 2010b]. The grid is divided into six domains (figure 4-29). Breaking the grid into domains makes it easier to modify the grid, run simulations and

define the bed roughness. Domain decomposition also allows each sub-domain to run in parallel.
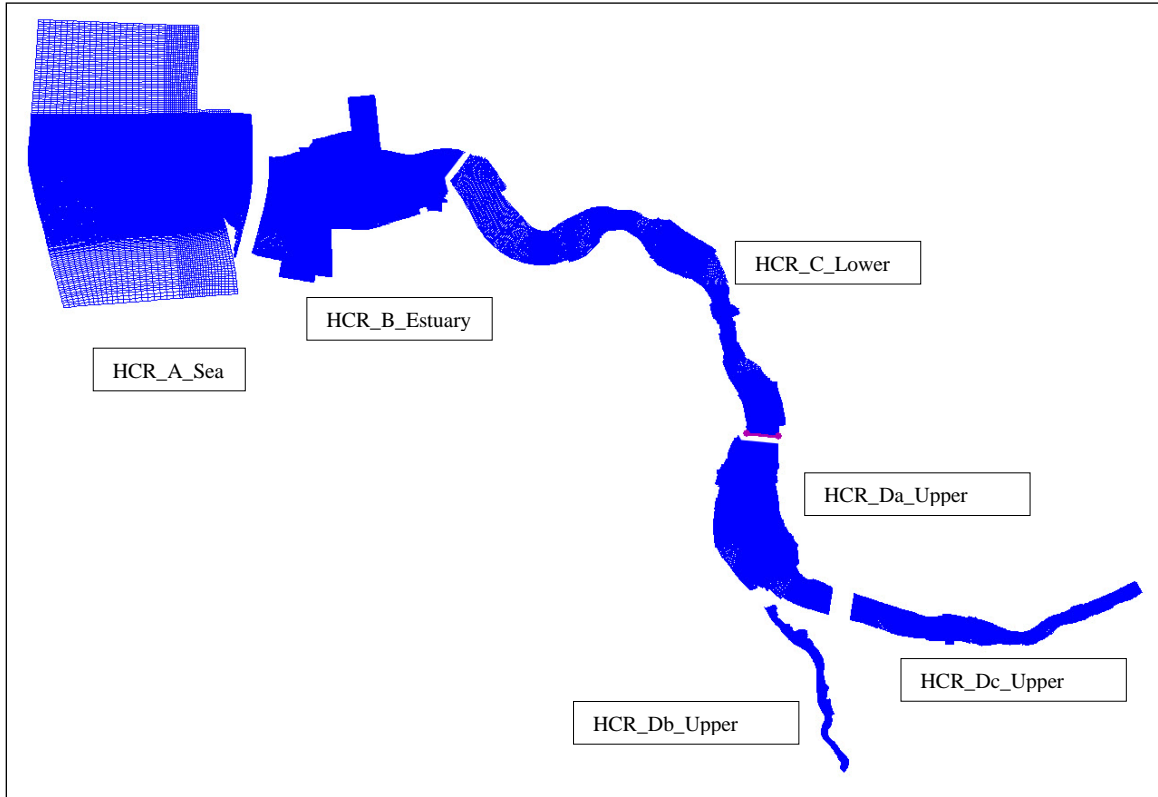
Figure 4-29: Domains within the Delft3D Historic Columbia River Model.

For data analysis purposes, observation point are located every 5km along the Columbia River shipping channel (Figure 4-30). The water level and water velocity at each observation point are extracted from the model every 10 minutes (Modern Model) or 15 minutes (Historic Model).
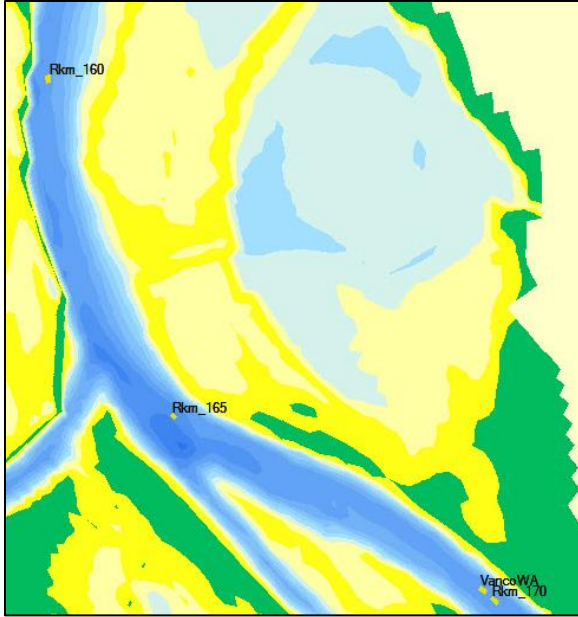
Figure 4-30: Observation points in the Modern Model located every 5km in the river channel

Boundary Conditions

Four different types of boundary conditions are applied to the model. Two of the boundary conditions are related to the Pacific Ocean tides. The other two boundary conditions are the Willamette River discharge at Oregon City, OR, and the Columbia River discharge at Bonneville, OR. In applying the boundary conditions several assumptions are made.

1. The ocean boundary is not influenced by the river

2. Tides at the ocean boundary have not changed significantly since the late 19th century

68

3. The discharge of the Columbia River at Bonneville and the Willamette River at Oregon City accounts for the majority of discharge of the Lower Columbia River. Other discharge inputs are minor and can be neglected.

4. A barotropic model is sufficient to model a flood in the tidal-river portion of the estuary.

5. Water at the ocean boundary has a salinity of 31.5 ‰, density of 1022 kg m^{-3} and temperature of 20°C.

6. Water discharged from the Willamette River and Columbia River has no salinity, a density of 1000 kg m^{-3} and temperature of 20°C.

4.3.1.1 Pacific Ocean Water Level Boundary

The Delft3D model is forced from the ocean by the incoming tides. The ocean tides travel parallel to the coast in the form of a Kelvin wave. The amplitude and phase of the oceanic tides are defined at the extreme southwest and northwest points on ocean boundary (Figures 4-31 & 4-32). Tidal phase and amplitude of the nine largest constituents at these points are obtained from the Oregon State University Tidal Prediction Software (OTPS) tide model (using the Pacific Northwest regional sub-model) [*Egbert and Erofeeva*, 2002]. The tidal phase and amplitude are defined at the red dots (Figures 4-31 & 4-32) and interpolated along the dotted line at the western edge of the ocean boundary.
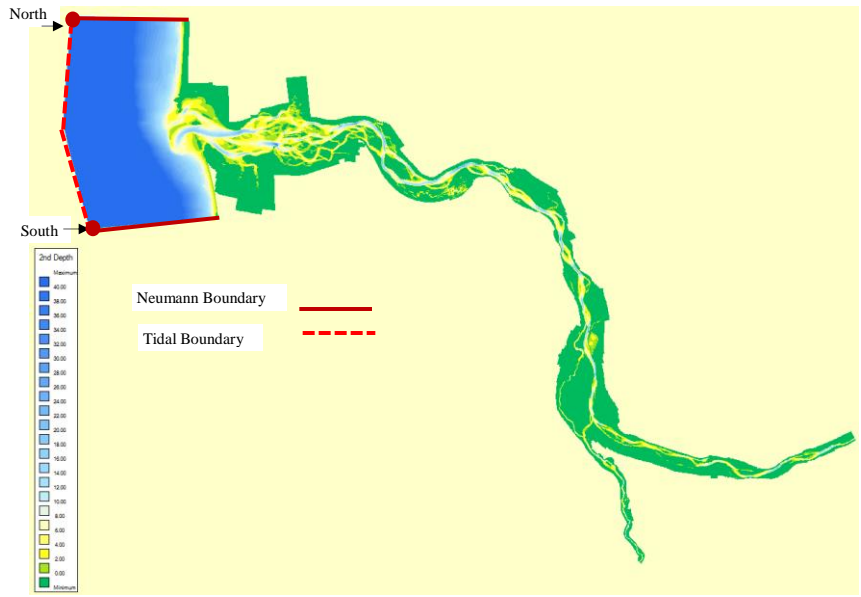
Figure 4-31: Historic Columbia River Model with open sea boundaries
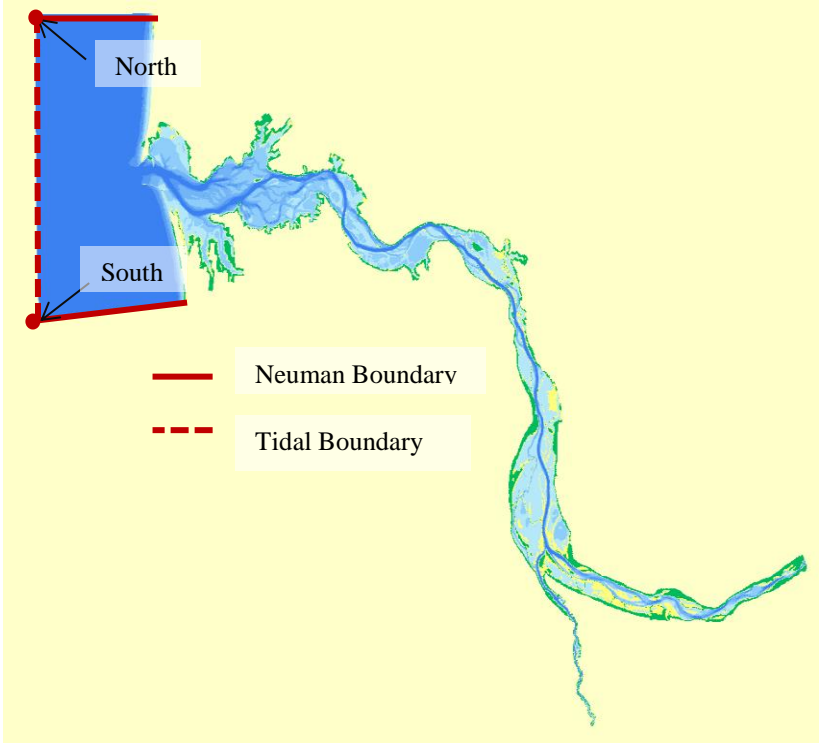
Figure 4-32: Modern Columbia River model with open sea boundaries

Table 4-9 below shows the amplitude and phases of the eight largest astronomically forced constituents at the North and South boundary of the Historic Model, and Table 4-10 shows the same information for the Modern Model. The Pacific Ocean is deep in the vicinity of the tidal boundaries; therefore overtides can be neglected.

Table 4-9: Amplitude and phase of tidal constituents at the open sea boundary – Historic Columbia River Model. Phases referenced to G.M.T.

Constituents	Period (hrs)	North Boundary		South Boundary	
		Amp (m)	Phase (°)	Amp (m)	Phase (°)
M2	12.4206	0.890	232.6	0.912	232.9
S2	12.0000	0.248	259.6	0.252	260.5
N2	12.6584	0.187	206.5	0.190	207.4
K2	11.9673	0.066	249.9	0.067	251.3
K1	23.9344	0.426	240.2	0.426	239.7
O1	25.8194	0.265	224.6	0.263	224.6
P1	24.0659	0.131	235.4	0.131	236.1
Q1	26.8684	0.047	213.6	0.047	214.4

Table 4-10: Amplitude and phase of tidal constituents at the open sea boundary – Modern Columbia River model. Phases are referenced to G.M.T.

Constituents	Period (hrs)	North Boundary		South Boundary	
		Amp (m)	Phase (°)	Amp (m)	Phase (°)
M2	12.4206	0.883	231.4	0.913	232.2
S2	12.0000	0.247	258.8	0.253	260.2
N2	12.6584	0.187	206.0	0.190	207.3
K2	11.9673	0.066	249.6	0.067	251.3
K1	23.9344	0.424	239.6	0.428	239.5
O1	25.8194	0.264	224.2	0.264	224.3
P1	24.0659	0.131	235.4	0.131	236.0
Q1	26.8684	0.047	213.6	0.047	214.4

4.3.1 Water Level Cross Boundary (Neumann)

A conceptual image of the grid for a coastal boundary is shown in Figure 4-33. The grid is similar to our model because it has two tidal boundaries describing the tidal amplitude and tidal phases at a point, and two Neumann boundaries for the slope of the

water level along a line [*http://en.wikipedia.org/wiki/Neumann_boundary_condition*]. An analogy

can be made to describe how tidal boundaries are applied on the LCR grid. The tidal

amplitude is defined at points A and B, or the North and South tidal boundaries. The

Neumann boundaries are along lines A-A' and B-B'. The slope of the water level along

the line A-A' is adjusted to match the slope the water level at point A, likewise the slope

of the water level along line B-B' is adjusted to match the slope of the water level at point

B.
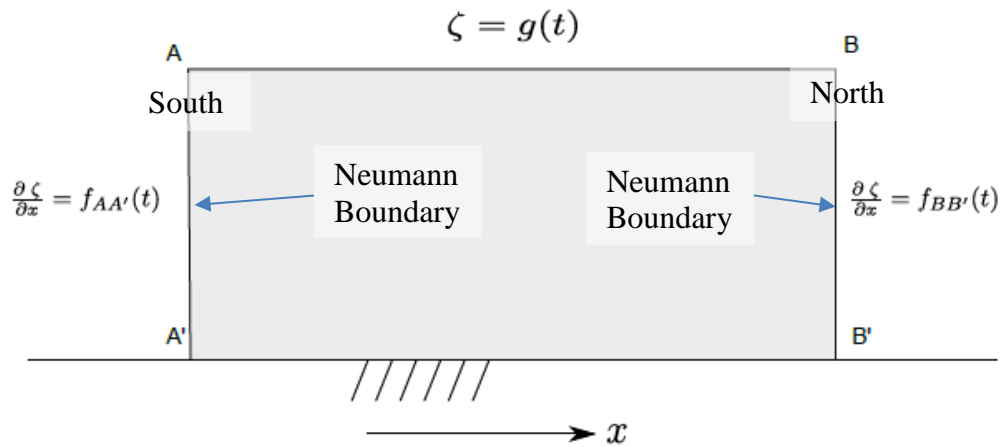
Figure 4-33: Hydrodynamic model of coastal area with three open boundaries with offshore boundary (A-B at deep water) and two cross shore boundaries (A-A' and B-B'). Taken from Deltares [2010].

Discharge Boundaries

The model contains discharges boundaries for the Willamette River at Oregon City

and for the Columbia River at Bonneville (Figures 4-34 & 4-35). The boundaries are

defined at roughly the same locations for the Historic and the Modern Model. In a Delft3D

flow simulation, water is discharged evenly across the cell faces covered by the discharge boundary. The instantaneous discharge rate in CMS $[L^3T^{-1}]$ is specified at the beginning of the simulation and at specified times during the simulation. The Delft3D program interpolates the discharge rate between these time points.
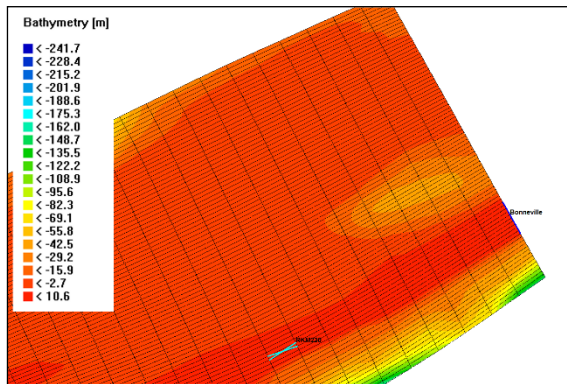
Figure 4-34: Discharge boundary for the Columbia River at Bonneville in the Historic Columbia River model
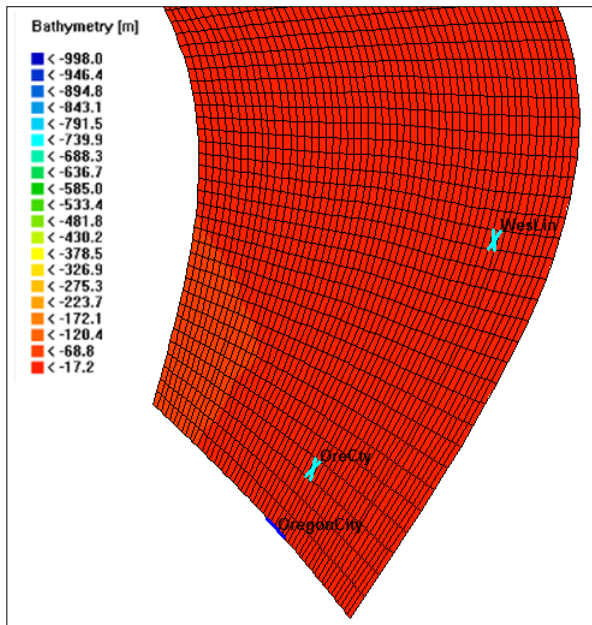
Figure 4-35: Discharge boundary for the Willamette River at Oregon City in the Historic Columbia River model

Historic Columbia River Model Roughness

A depth variable roughness is used in this model to help simulate variations in roughness caused by wetlands and the floodplain. To define a depth variable roughness, each domain is divided into regimes which are defined relative to channel depth. The channel is defined as the part of the river that is always inundated. Because MHHW and MLLW change from the mouth going upriver, the depth of the channel friction regime relative to NAVD-88 is adjusted accordingly. The floodplain is then defined as all elevations above the channel (above MLLW). The channel is given a higher Chézy coefficient – i.e. less roughness – than the floodplain. Both the Historic and Modern Model were calibrated with the assistance of another graduate student at Portland State University [*Mahedy*, 2016].

The Chézy coefficients (C) of the areas that are periodically inundated are maintained at C = 50 throughout 3 of the 6 domains in the Historic Model. The floodplain roughness is set higher than the channel roughness due to vegetation. Figure 4-36 shows the Chézy coefficients in the six domains in the Historic Model. The roughness parameterization for the modern model is given in Appendix 7-5. These roughness coefficients were chosen to produce an optimal agreement with tides measured during low flow conditions (the 1877 data set) and with the rating curve of water level in Portland (high flow conditions), as discussed below.
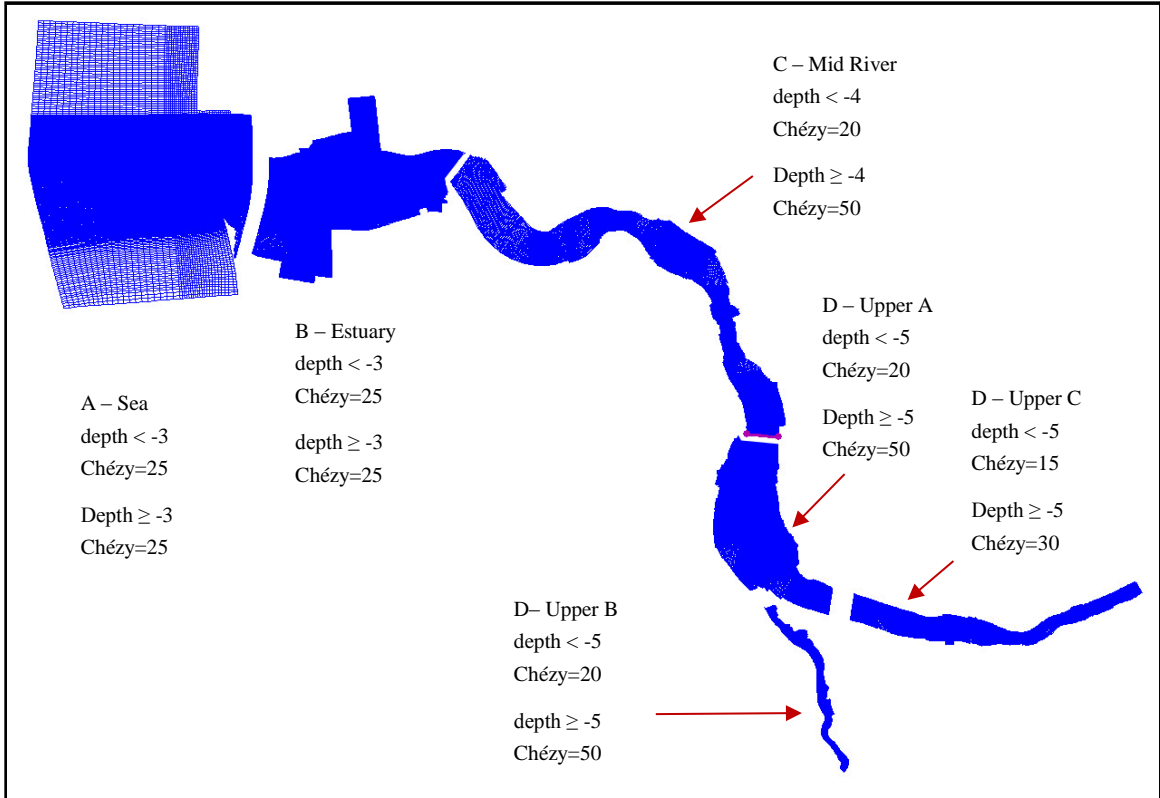
Figure 4-36: Roughness values used in the Historic Columbia River Model. All depths are referenced to NAVD88.

4.4   Numerical Simulations

Numerous numerical simulations were performed on the Historic and Modern Model in order to calibrate for the progression of the tide, upstream water level and the interaction between tides and river discharge. Simulation of model floods were also run to evaluate the response of the LCR to flood waves. This section provides a brief description of the simulations run on the models.

The first simulations are calibration runs to model the decay of the tide throughout the LCR as it progresses upriver. The Historic Model is calibrated to the tidal decay

throughout the LCR from a low discharge period in 1877 (Table 4-11). The calibration period corresponds to the 19th century tide logs from 1877 (section 4.1). The modern model is calibrated to the tidal decay throughout the LCR from a low discharge period in 2005 (Table 4-12).

The second calibration runs are used to calibrate upstream water level in the Portland/Vancouver area as function of discharge (Table 4-11). The upriver calibration is used to adjust the model so that the modeled water level matches the rating curve of the Morrison Street Bridge gauge (section 4.1). The Historic Model is calibrated to match a rating curve of daily water level and river and river discharge at Morrison Street Bridge in Portland. The modern model is calibrated to match the discharge dependent tidal elevation and tidal range at Portland and Vancouver.

The final set of runs are flood simulations on both the Historic and Modern Model. The flood simulations are used to evaluate the response of the LCR to flood waves from the Columbia River. The discharge boundaries are modeled as a Gaussian distribution imposed on a baseline flow (Tables 4-11 & 4-12).

Table 4-11: Simulations run on the Historic Model

Run Type	Columbia Rvr discharge	Willamette Rvr discharge	Duration
tidal decay	Sep-Oct, 1877 meas	Sep-Oct 1877 meas	30 days
water level	5,000 CMS constant	250 CMS constant	6 months
water level	10,000 CMS constant	250 CMS constant	6 months
water level	15,000 CMS constant	250 CMS constant	6 months
water level	20,000 CMS constant	250 CMS constant	6 months
water level	25,000 CMS constant	250 CMS constant	6 months
water level	30,000 CMS constant	250 CMS constant	6 months
flood pulse	normal distr 25 kCMS	250 CMS constant	6 months

Table 4-12: Simulations run to calibrate the Modern Model

Run Type	Columbia Rvr discharge	Willamette Rvr discharge	Duration
tidal decay	Aug-Oct, 2005 meas	Sep-Oct 2005 meas	30 days
water level	2,500 CMS constant	250 CMS constant	6 months
water level	5,000 CMS constant	250 CMS constant	6 months
water level	7,500 CMS constant	250 CMS constant	6 months
water level	10,000 CMS constant	250 CMS constant	6 months
water level	12,500 CMS constant	250 CMS constant	6 months
water level	15,000 CMS constant	250 CMS constant	6 months
water level	25,000 CMS constant	250 CMS constant	6 months
flood pulse	normal distr 20 kCMS max	250 CMS constant	6 months

5 Results

The following section discusses (a) the analysis of in-situ water levels from 1876 to the present; (b) the calibration of the Historic and Modern Model and (c) the results of a 6-month flood simulation in both Historic and Modern Model.

5.1 Water Level Analysis

Mean water levels in the Portland/Vancouver area have substantially changed over the last 150 years, particularly between April and September (Fig. 5-1). During the month of June, historical water levels between 1879 and 1898 were more than 3m higher than between 1989 and 2009, on average. A large part of the change can be attributed to the changing hydrograph at The Dalles (figure 5-1), which produces a reduced backwater effect in Portland during the seasonal spring freshet. Conversely, increased Columbia River Flow during the winter months slightly increases water levels. Nonetheless, a portion of the reduced spring levels - as we show below - is likely attributable to a reduced river slope, such that the same river discharge results in a lower mean water level today than in the past (see also Jay et al., 2011). The Willamette River hydrograph has also changed over time, and may influence the seasonality of water levels as well (figure 5-2).
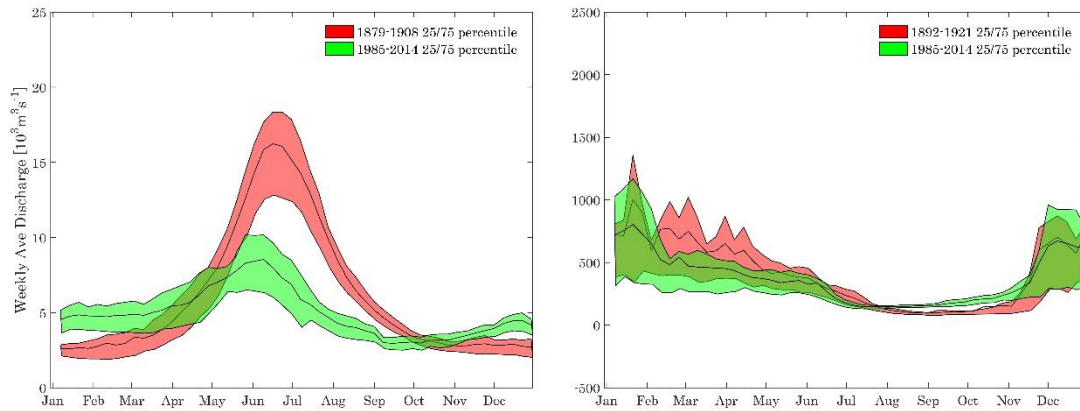
Figure 5-1: (left) 25/75 percentile of Columbia River discharge at The Dalles in the historical and modern periods.

Figure 5-2: (right) 25/75 percentile of Willamette River discharge at Salem in the historical and modern periods.

The effect of Columbia River discharge on historical and modern water levels in Portland is graphically shown in Figure 5-4 and 5-5. The effect of the Willamette River is minimized by requiring that $Q_{Willamette} < 500$ CMS. Historically, every additional 2700 CMS in discharge at The Dalles resulted in a ~1m rise in Portland, up to about 15,000 to 20,000 CMS. For higher flows, the slope reduced to approximately 1m in increased water level for every 4300 CMS. The reduction in slope around 15,000 CMS occurs at a water level of ~6m above CRD. This appears to be the approximate level of the historical river bank in the Portland/Vancouver area estimated from the USACE Flood Profile (Figure 4-20) and the Historic rating curve for Morrison Street Bridge (Figure 5-4). Thus, the reduced slope is caused by overbank flow, which tends to spread additional discharge over a larger area and reduce the rate of water level increase.

79

For modern water levels in Portland, an approximately 1m rise occurs for every 3000 CMS, up to~15000 CMS (Fig. 5-6); hence, compared to the historical conditions, more discharge is required today to produce the same rise in water levels. The reasons for this altered rating curve are investigated later using our numerical model; nonetheless, the data show that even without an altered hydrograph, water levels would be lower in Portland today than historically. Since Columbia River flows larger than 15,000 CMS are now uncommon, we also use our numerical models to investigate how the modern system would react to the larger discharge magnitudes which were common in the 19th century.
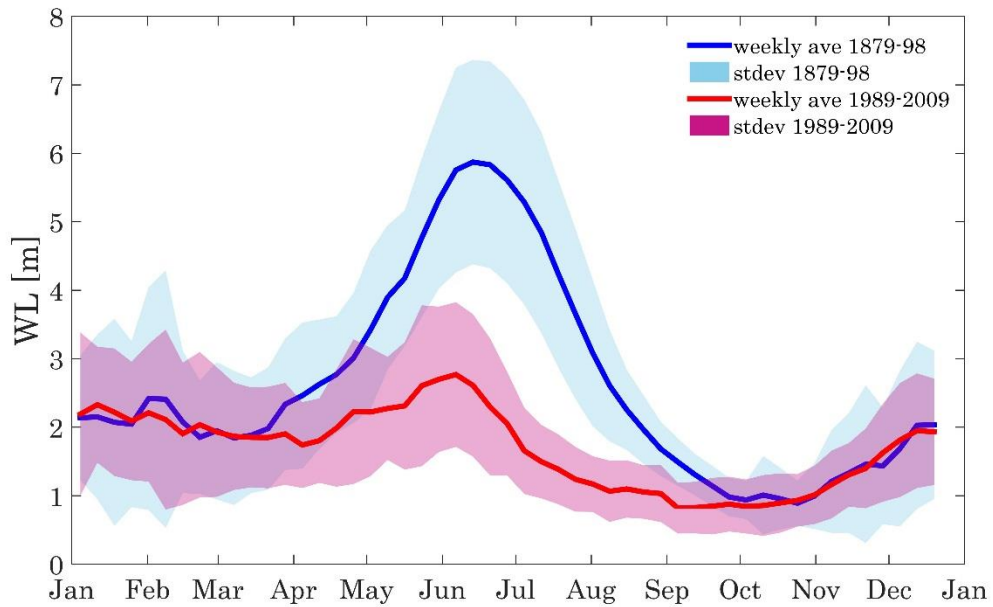
Figure 5-3: Comparison of mean monthly water level +/- 1 standard deviation of the Willamette River at Morrison Street Bridge from the late 19th century (1879-98) and the modern period (1989-2009). Measurements referenced to CRD.
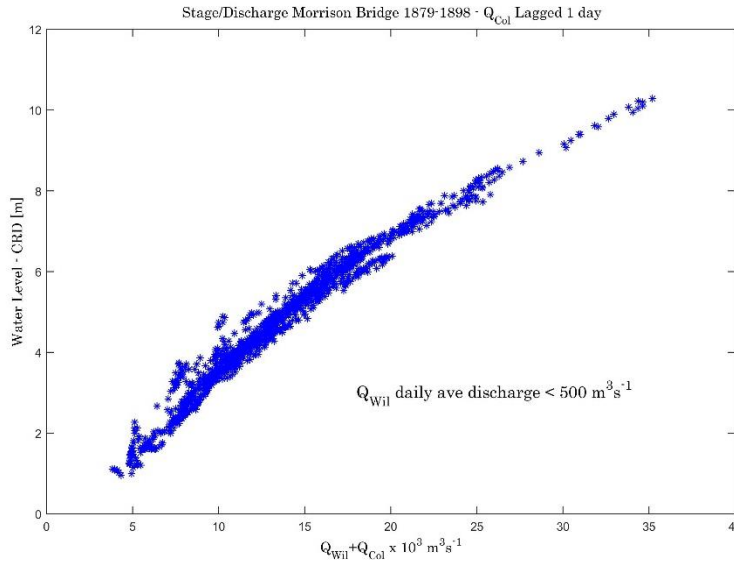
Figure 5-4: Rating curve for the water level at the Stark Street/Morrison Street Bridge gauge. Days with Willamette River discharge higher than 500 CMS are removed.

Water Level Statistics

The water-level data shown in Figure 5-5 is converted to a rating curve using a nonlinear regression approach (see *Jay et al.*, [2011]). Mean water level (MWL) statistics obtained from the regression are then used to calibrate and validate the historical and modern models. Since hourly data is available from 1986-pressent, additional statistics such as MLLW and MHHW are calculated and used to calibrate the modern model.

The flow regression model relates tidal range at Vancouver and Portland to coastal tidal range (here, Astoria) and the total discharge [*Jay et al.,* 2011], based on theoretical considerations of how rivers and tides interact nonlinearly [*Kulkuka & Jay*, 2003]:

$$LLW = a_0 + a_1 Q^{m_1}{}_{TD} + a_2 Q^{m_2}{}_{WR} + a_3 \left(\frac{TR^2}{(Q_{TD}+Q_{WR})^{n_1}} \right), \qquad (5.1.1)$$

$$MWL = b_0 + b_1 Q^{m_1}{}_{TD} + b_2 Q^{m_2}{}_{WR} + b_3 \left(\frac{TR^2}{(Q_{TD}+Q_{WR})^{n_1}} \right), \qquad (5.1.2)$$

$$HHW = c_0 + c_1 Q^{m_3}{}_{TD} + c_2 Q^{m_4}{}_{WR} + c_3 \left(\frac{TR^2}{(Q_{TD}+Q_{WR})^{n_1}} \right), \qquad (5.1.3)$$

where a_i, b_i, c_i and m_i, are regression coefficients ($i = 1$ to 4), n_1 is an additional flow coefficient, Q_{TD} is the daily averaged Columbia River discharge at The Dalles, Q_{WR} is the daily averaged Willamette River discharge at Portland, and TR is the greater diurnal tidal range at Astoria. Flow is input in units of kCMS, and discharge from the Columbia River at The Dalles is lagged one day to account for travel time. The results of the regression for modern data are given in Table 5-1.

Q_{TD} daily ave. Col Rvr discharge at The Dalles in 1000 CMSlagged 1day

Q_{WR} daily ave. Wil Rvr discharge at Portland in 1000 m^3s^{-1}

$m_{i = 1,2}$ flow exponents for the Wil Rvr and Col Rvr

TR Columbia River tidal range at Tongue Point in Astoria

Table 5-1: Flow coefficients for the Columbia River and Willamette River water level regression Portland and Vancouver. [*Jay et al.,* 2011]

CR LLW - Vancouver, 1999-2008				WR LLW, Morrison Str Br, 1999-2008			
	Estimate	Confidence Interval			Estimate	Confidence Interval	
a0	-1.210	-1.229	-1.192	a0	-1.063	-1.079	-1.047
a1	0.294	0.292	0.296	a1	0.218	0.216	0.218
a2	0.656	0.652	0.664	a2	0.656	0.651	0.660
a3	0.111	0.107	0.115	a3	0.096	0.092	0.100
TD flow exponent (m1)			1.1	TD flow exponent (m1)			1.2
WR flow exponent (m2)			0.9	WR flow exponent (m2)			0.95
n1			0.75	n1			0.7
CR MWL - Vancouver, 1999-2008				WR MWL, Morrison Str Br, 1999-2008			
	Estimate	CI			Estimate	CI	
a0	-0.824	-0.840	-0.807	b0	-0.652	-0.667	-637
a1	0.273	0.272	0.275	b1	0.198	0.197	0.199
a2	0.600	0.595	0.605	b2	0.598	0.593	0.602
a3	0.151	0.147	0.154	b3	0.138	0.135	0.142
TD flow exponent (m1)			1.1	TD Flow			1.2
WR flow exponent (m2)			0.9	WR Flow			0.95
n1			0.75	n1			0.7
CR HHW - Vancouver, 1999-2008				WR HHW, Morrison Str Br, 1999-2008			
	Estimate	CI			Estimate	CI	
a0	-0.332	-0.351	-0.313	b0	-0.132	-0150	-0.114
a1	0.242	0.241	0.244	b1	0.175	0.173	0.176
a2	0.517	0.512	0.523	b2	0.493	0.488	0.498
a3	0.211	0.207	0.215	b3	0.202	0.197	0.206
TD flow exponent (m1)			1.1	TD flow exponent (m1)			1.2
WR flow exponent (m2)			0.9	WR flow exponent (m2)			0.95
n1			0.75	n1			0.7

Table 5-2: Discharge used in 1999-2008 water level analysis at Morrison Street Bridge in Portland

Willamette River (kCMS)	Columbia River (kCMS)
0.5	2.5
0.5	5.0
0.5	7.5
0.5	10.0
0.5	12.5
0.5	15.0

A similar methodology was used for developing the rating curve for historical water levels. A bin averaging approach is used to analyze the Morrison Street Bridge data. The discharge is divided into 500 CMS bins from the minimum to the maximum discharge.

The measured water level within each discharge bin are then averaged and a nonlinear regression (Equation 5.1.4) is applied to the resulting data,

$$WL = \beta_0 + \beta_1 Q_{Wil}^{\beta_2} + \beta_3 Q_{Col}^{\beta_4}$$ *(Equation 5.1.4)*

This analysis indicates that a difference in the rating curve slope occurs when the discharge reaches approximately 18 kCMS, though the change in slope occurs gradually over a range of discharge between 15-20 kCMS (see discussion in Chapter 4). Above this threshold, overbank flow occurs and water would begin flowing over levees, reducing the slope of the rating curve. Hence, the inflection point is also helpful in determining levee heights, which traditionally are considered to occur at about the level of the 2 year flood. Here, the inflection is essentially the same as the two-year return flood, estimated by *Naik & Jay*, [2011] to be 20 kCMS based on Columbia River flows at Beaver, OR.
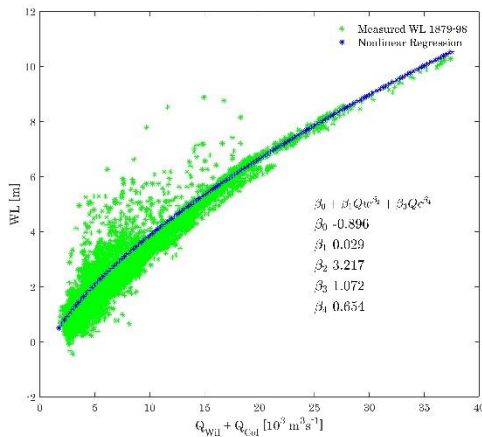
Figure 5-5: (left) Nonlinear regression of the Stark Str/Morrison Street Bridge rating curve from 1879-98.
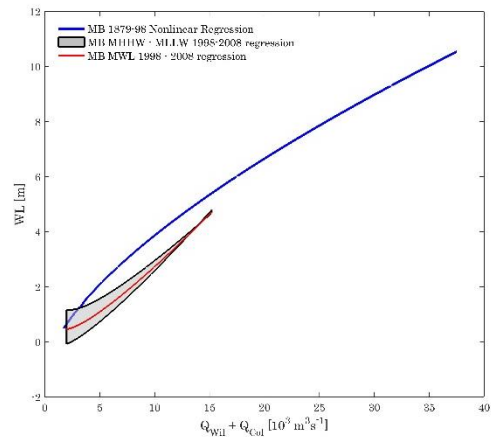
Figure 5-6: (right) Nonlinear regression of Stark Str/Morrison Street Bridge daily water level (1879-98) with nonlinear regression of MHHW, MWL and MLLW from 1999-2008.

A comparison of the modern and historical rating curves (Figure 5-2) demonstrates the magnitude of historical change over the past century. Most obviously, modern peak flows are much lower, and the modern curve lies below the historic curve for every flow rate between 2.5 kCMS and 15 kCMS; therefore, the same river flow produces a *lower* river stage today (0.5 to 1m lower) than historically (see also [*Jay et al.*, 2011]). Also, the modern curve is slightly concave up. Extrapolated beyond 15 kCMS, the modern curve would intersect and exceed the historical rating curve around 20 kCMS. Since not enough data are available to statistically evaluate the modern system response above 15 kCMS, it is unclear whether extrapolation to larger flows is valid. Hence, we use our model results to evaluate whether a 'cross-over' will occur or whether the modern system water levels are always below historical norms.

5.2   Model Calibration

An iterative approach to calibrate the roughness was used for both the Historic and Modern Model. First, roughness values in the channel were adjusted until low-flow model simulations were able to reproduce the spatial variation in tidal constituents, specifically M_2, S_2, K_1 and O_1. Next, model roughness in the flood plain was adjusted until the model simulations reproduced the WL rating curve in Portland and Vancouver (see Table 5-1 and Figures 5-5 and 5-6). Channel roughness in the Historic Model ranged from Chézy coefficient values in the range of 5 to 55, compared to 59 to 96 (estuary) in the modern model. The historical floodplain was best modeled with a Chézy coefficient of 5 to 25.

Spatial Calibration of a Low Flow Event

Historic Model

The Historic Columbia River Model is calibrated so that model output matches tide data collected in September-October 1877 at the end of the summertime dry period (see section 4-1 and Appendix 7-1). Though no discharge measurements on the Columbia River are available for this period, Portland water levels varied between 2-4 feet over this period (Figure 5-7 below), corresponding to a nearly constant flow between 2 to 4 kCMS according to the rating curve developed in section 5.1 (see Fig. 5-5). This is similar to the 1878 Columbia River discharge from September 1878 to Jan 1879 (Fig. 5-10). We cannot easily separate Willamette River and Columbia River flow based on the graph in Fig. 5-5, but we do have some information about the Willamette River in 1877 and 1878. Willamette River water level measurements in Albany in 1877 (Fig. 5-8), along with 1878 Albany discharge measurements (Fig 5-9), suggest that the Willamette River discharge from August to September was small in both years. Since water level in the 1877 low discharge period is similar to the 1878 low discharge period, we run the 1877 calibration using river boundary conditions obtained from Willamette and Columbia River discharge measurements from the same period in 1878. The slight differences in flow between 1877 and 1878 will have a negligible effect on tidal constituents. Much larger flow variation than the 1-2 kCMS measured in 1877 and 1878 is required to substantially affect tidal characteristics. This is suggested by the envelope of tide range in Figure 5-6 (modern rating curve), and is discussed later.
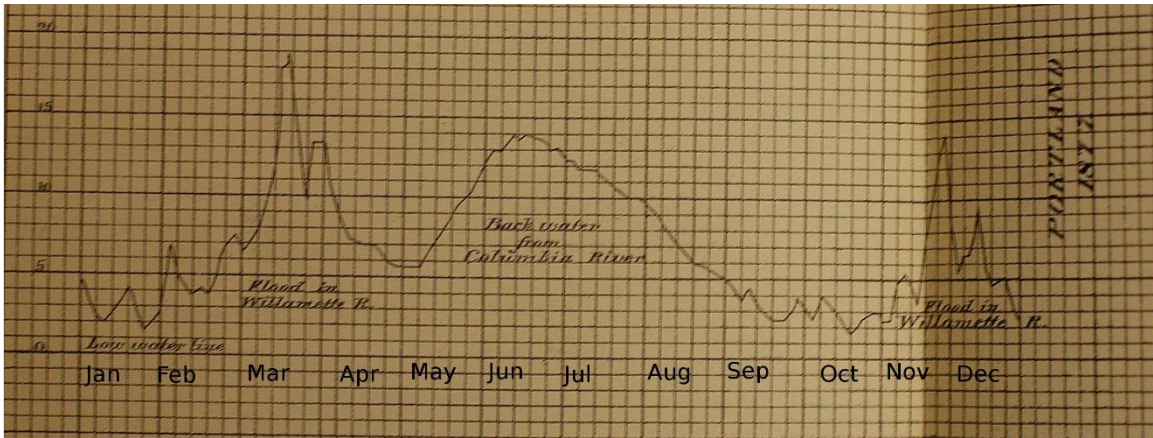
Figure 5-7: Water level measured in Portland, 1877, extracted from a larger graph including Portland and Albany data from 1876-1888 (US Army Corps Annual Report, 1878, Appendix JJ).
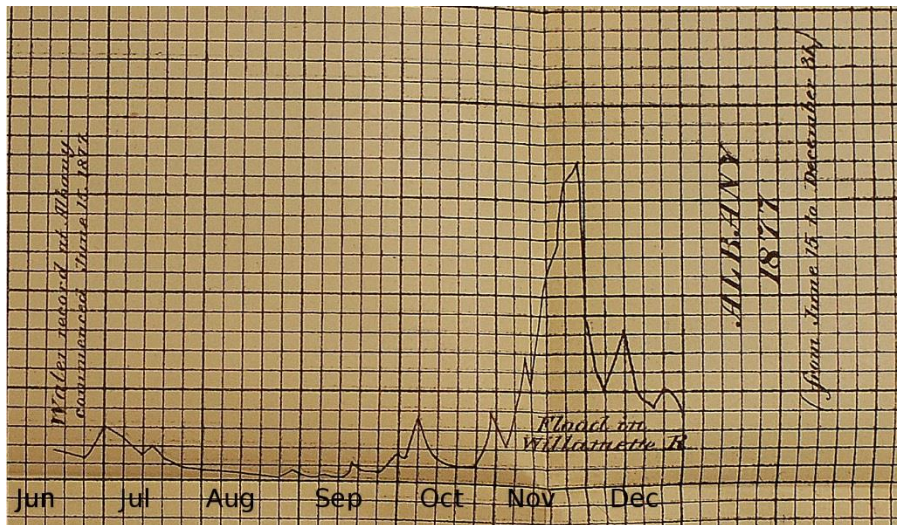
Figure 5-8: Water level measured in Albany, 1877, extracted from a larger graph including Portland and Albany data from 1876-1888 (US Army Corps Annual Report, 1878, Appendix JJ).
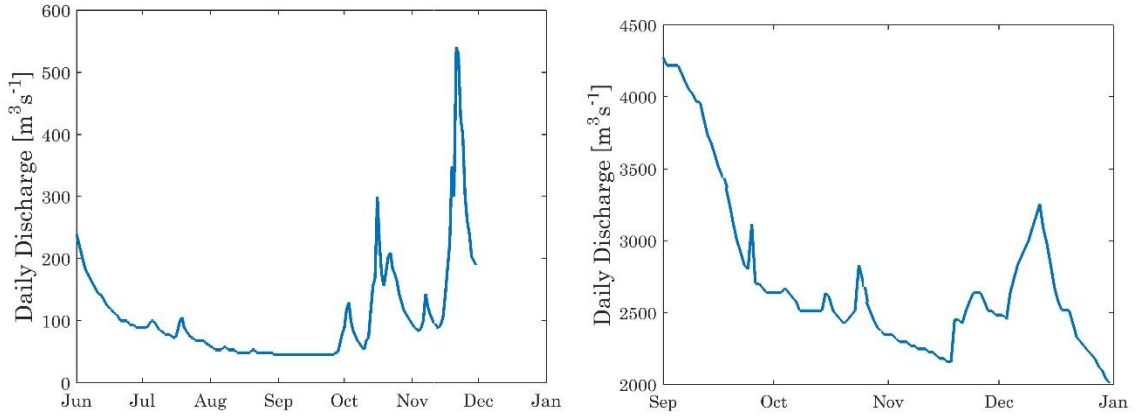
Figure 5-9: (left) Estimated Willamette River discharge in Albany, OR from Jun 1878

Figure 5-10: (right) Columbia River discharge from The Dalles from 1878 – Jan 1879.

Table 5-3: Stations used in the calibration of the Historic Model

Station	RKM
Fort Stevens, WA	3
Astoria, OR	20.3
Cathlamet, WA	59.2
Oak Point, WA	85.2
Rainier, WA	106
Vancouver, WA	169.1

Figure 5-11 shows the shows the spatial calibration of tidal amplitude of the semidiurnal (twice-daily) constituents M_2, and S_2 against the 1877 measurements. The solid lines denote model results. The statistics described below are based on the difference between the measured tidal amplitude [●] (Appendix 7-2) and the model output [■] at observation points located as close to the coordinates of the in-situ tide gage. The results indicate an overall good fit between model results and data.

In figure 5-11 the M_2 constituent peaks in amplitude near rkm 25, then decreases in amplitude as it moves upriver. There is a noticeable drop in amplitude at rkm 160,

coincident with the confluence of the Willamette River. The decrease in amplitude is likely due to the topographic divergence related to the tide propagating into the Willamette River, and/or the shallow bathymetry at the confluence of the Willamette River and Columbia River. The root mean square error(RMSE) for the M_2 constituent is 0.055m, which is approximately 5% of the total M2 amplitude at the entrance, but closer to 50% of the M_2 amplitude near Vancouver (rkm 170). Overall, the calibration is an accurate representation of the tidal behavior in this period, and is of a similar order of magnitude as modern model results. However, the precision of the model results (and/or undiagnosed problems with the in-situ measurements) means that some uncertainty is connected with upstream tidal processes at low flow. The second diurnal constituent, S_2, is much smaller in amplitude and does not show the pronounced peak of the M_2 tide. The S_2 tide has a peak amplitude of approximately 0.25m at the mouth and the amplitude decreases steadily beyond river kilometer 25. The RMSE for the S_2 tide is 0.033m or approximately 12% of the amplitude at the mouth.

The two diurnal constituents K_1 and O_1 do not show the pronounced peak of the M_2 tide (Figures 5-11 & 5-12) and behave similarly to the S_2 tide. Both constituents begin to decrease in amplitude beyond river kilometer 25, and also exhibit a sharp drop in amplitude near the confluence of the Willamette River. The RMSE for the K_1 constituent is 0.041m, or approximately 8% of the amplitude at the river mouth and 12% of the amplitude at Vancouver. The RMSE for the O_1 constituent is 0.016m, or approximately 7% of the amplitude at the river mouth and 16% of the amplitude Vancouver. The calibration of the K_1 and O_1 constituents replicates the spatial trends seen in the observed data but is slightly

less accurate in predicting the amplitude than the M_2 calibration. One reason for the lack of accuracy of the K_1 and O_1 tides is that their amplitudes are substantially smaller than the M_2 tide (Figures 5-11 & 5-12), and the harmonic analysis estimates are less certain. The M_2 calibration is most accurate in terms of the ratio of the RMSE to the amplitude. Considering the measuring equipment of late 19th century, and the potential errors in flow measurement, along with the fact that other smaller streams have been excluded from the discharge model input, this can be considered to be a good calibration.

Figure 5-11: Spatial evolution of M2 and S2 tidal amplitude for Historic Model during low flow event in 1877.
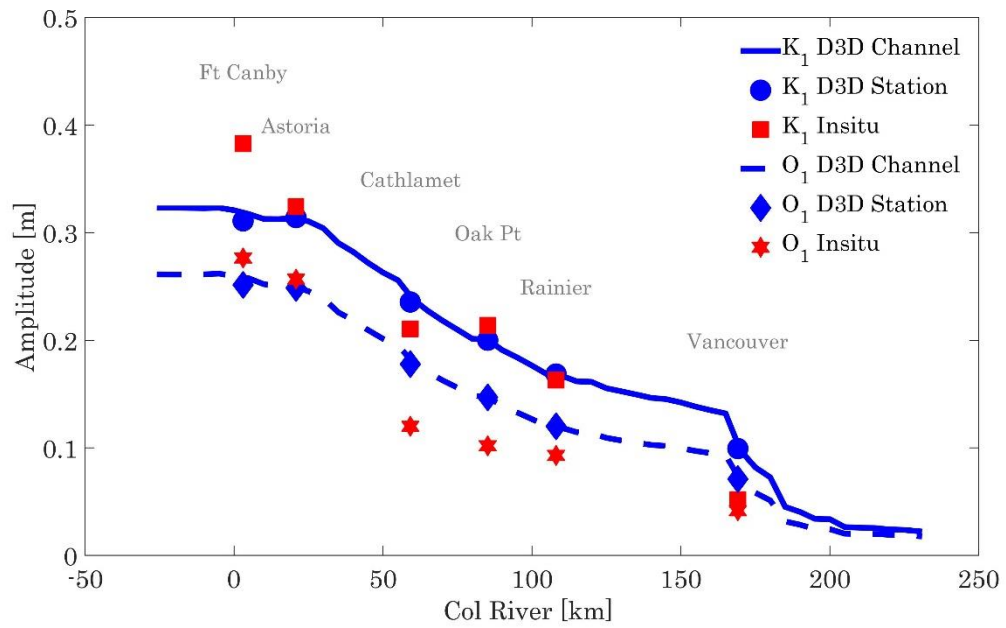
Figure 5-12: Spatial evolution of the K1 and O1 tidal amplitude for Historic Model during low flow event in 1877.

Modern Model

The low discharge period from September 1-30, 2005 is used for calibration of the modern model, with the exception of Hammond, which was calibrated using August 1-30, 1988 data. The model skill is determined by comparing the harmonic constituents from the tide stations during the analysis period to harmonic constituents from model locations representative of the tide gauges. Overall, the RMSE for the modern model is better than the Historic Model, likely reflecting more reliable water level, flow and bathymetry data.

In Figure 5-13 the M_2 tide peaks near river kilometer 50. This location is 25 km upriver of downtown Astoria (rkm 24 in the modern river channel), or approximately 20km further upstream than the M_2 peak in the Historic Model. The peak amplitude of the M_2 tide is 1m in the modern river. As with the Historic Model, the M_2 tide has a pronounced drop in amplitude at river kilometer 170, near the confluence of the Willamette and Columbia Rivers. The RMSE of the M_2 calibration at the reference stations is 0.057m, which is nearly identical to the historical model. This represents approximately 5% of the peak M_2 amplitude and 17% of the amplitude at Vancouver (rkm 171). The second diurnal constituent, S_2, shows a similar, though less pronounced amplitude peak near river kilometer 50. The peak amplitude of the S_2 tide was 0.34 m. Similar to the M_2 tide, the S_2 tide also has a pronounced drop in amplitude near river kilometer 170. The S_2 tide has a RMSE of 0.024m or approximately 5% of the peak amplitude and 18% of the amplitude at Vancouver.

The K_1 and O_1 calibration are shown in figure 5-14. Both constituents show a prolonged amplitude peak up to river kilometer 35 and then a steady drop in amplitude up

92

to river kilometer 170. The K_1 tide has a peak amplitude of 0.4m and a RMSE of 0.02m. The O_1 tide has a peak amplitude of 0.27m and a RMSE of 0.007m. All constituents but M_2 exhibit a smaller RMSE in the modern model, likely because of improved temporal coverage in the data (which are hourly) and improved time-keeping.

A second measure of the accuracy of a model is the phase offset or the progression of the phase as it propagates upriver. The phase offset is the change in phase measured from a reference location. As the tide enters the river it progresses upstream and its phase speed reduces because the river is shallower than the deep ocean. Here, the phase offset is measured from the gauge station closest to the mouth of river, Tongue Point, at river kilometer 28 (Hammond is excluded because data is from 1988). Figure 5-15 shows the phase offset of the M_2, S_2, K_1 and O_1 tides. In all cases the modeled phase offset from Tongue Point to Vancouver is slightly lower than the measured phase offset. The K_1 tide has the highest deviation between measured and modeled phase offset.

Overall the modern model has lower RMSE for the four largest constituents. The modeled amplitudes are also closer to the measured amplitudes at Vancouver. This indicates that the Modern Model likely does a better job than the Historic Model of representing the spatial evolution of the tidal constituents.

Table 5-4: Stations used in the calibration of the Modern Model

Station	RKM
Hammond	14.5
Astoria	28
Skamokawa	54.2
Wauna	66.9
Longview	106.7
Saint Helens	138.6
Vancouver	171.1

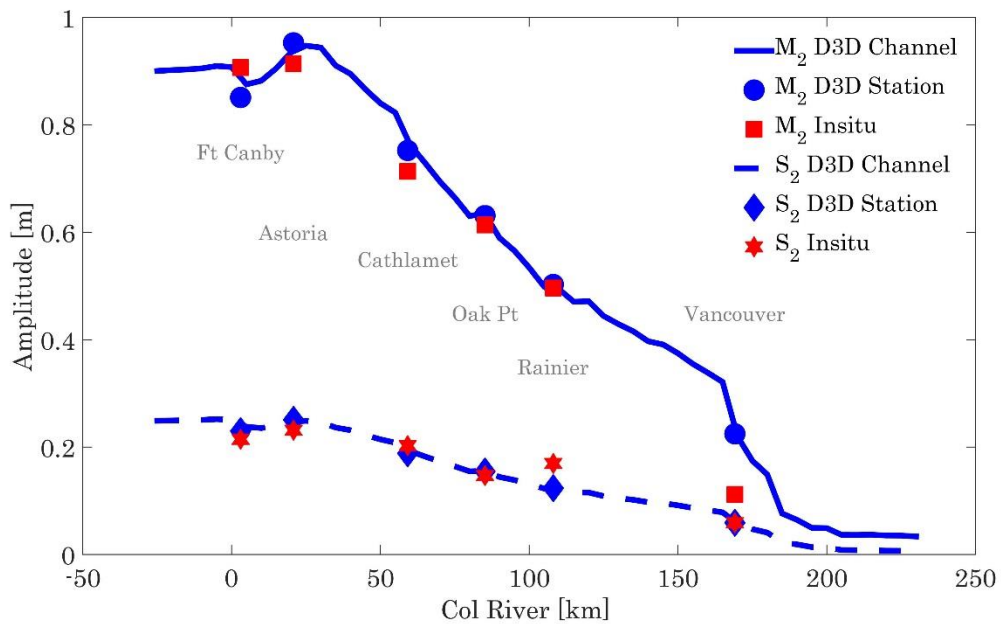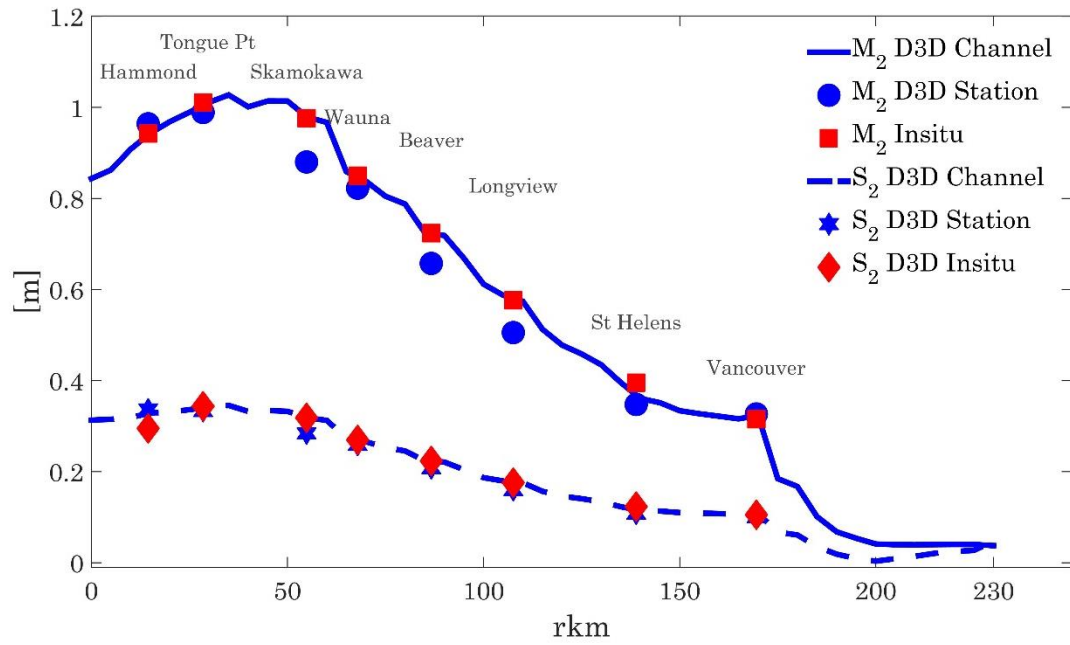*Figure 5-13: Spatial evolution of M2 and S2 tidal amplitude during low flow event in 2005.*
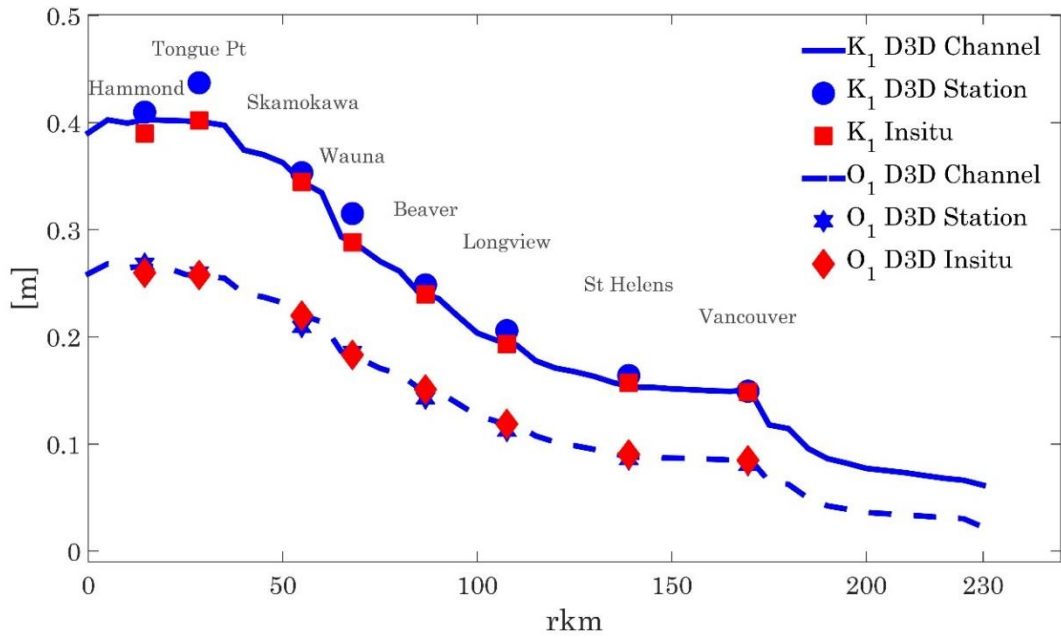
Figure 5-14: Spatial evolution of K1 and O1 tidal amplitude during low flow event in 2005.
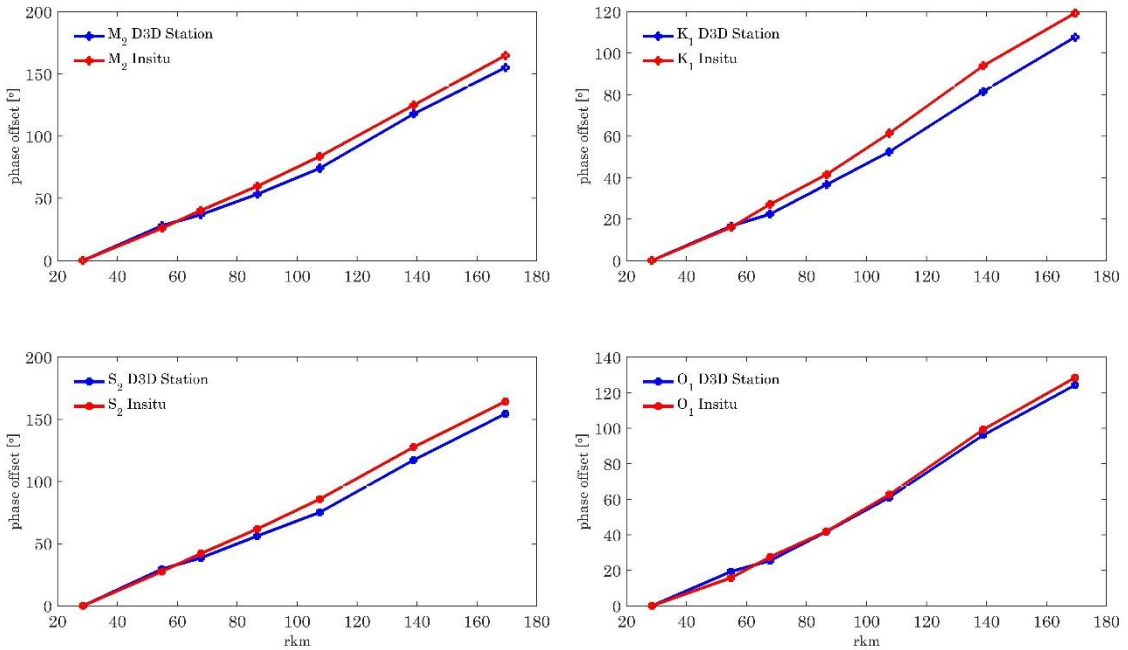
Figure 5-15: Phase offset of the M2 , S2 , K1 and O1 tide in the modern model. Phases are relative to local time.

95

Upriver Water Level Calibration

To calibrate and validate the depth variable friction coefficients, a number of different constant flow scenarios were tested and compared against observed data (Tables 4-11 and 4-12). The flow regression discussed previously in section 5.1 are used to validate both the Historic and Modern Model for high flow events.

Historic Model

The Delft3D model is calibrated to match the variability in the mean water level due the river discharge. The water level calibration are plotted against the rating curve at Morrison Street Bridge (Figure 5-16). The Historic Model slightly overestimates the measured daily water level at discharge up to 15 kCMS. Tidal forcing at Portland is almost absent in the modern river above 15 kCMS, and is negligible in the historic model results. As a consequence, at higher discharge the modeled mean water level can be compared directly to measured gauge data. Above 15 kCMS the modeled water level nearly matches the rating curve.
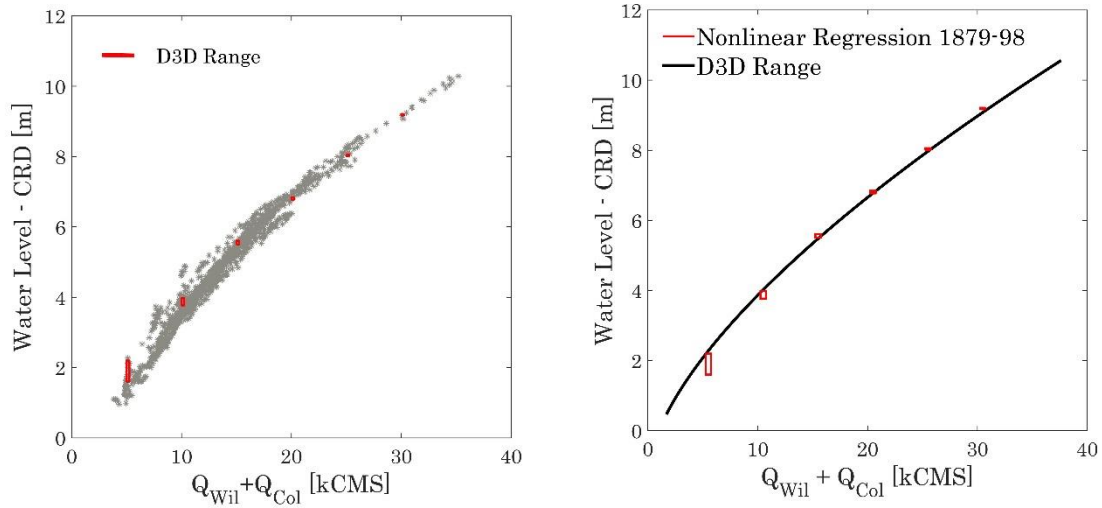
Figure 5-16: (left) Delft3D model output overlaid on rating curve for Stark Str/Morrison Street Bridge. Red rectangle are maximum – minimum water levels for each discharge condition.

Figure 5-17: (right) Delft3D output overlaid with regression of the Stark Str/Morrison Street Bridge rating curve from 1879-98.

Modern Model

Unlike coastal or estuary stations like Astoria, the water level in the Portland area is highly dependent on river discharge. The MLLW and MHHW changes by 5m between 2.5 kCMS and 15 kCMS total discharge. The tidal range is also dependent on river discharge, going from over 1m at the lowest discharge of 2.5 kCMS to nearly zero at 15 kCMS discharge (see Figures 5-18 & 5-19).

The D3D model reasonably reproduces both the rating curve and the tidal variability (MHHW and MLLW) as a function of river flow and coastal tidal range (Figures 5-18 & 5-19). As river flow increases for a constant coastal tide range, modeled mean water levels in Portland increase, but tidal range - represented by gray fill - decreases. . Modeled mean water levels are biased slightly higher than measurements (0.1-0.15m) for all river flows. Similarly, the RMSE for MLLW is 0.06m and the RMSE for MHHW is

0.18m, indicating that the modeled tidal range is slightly larger than that predicted by the regression model fit to in-situ data. The modeled friction used in the calibration is therefore a compromise between two competing goals; while decreasing friction might help reduce mean water levels to match the regression model (desired), it would also lead to slightly increased tidal range (undesired). The $O(0.1m)$ errors indicates that the D3D model is not perfectly simulating the estuary and tidal river. Including baroclinic effects within the estuary and higher grid resolution might eventually help further improve the model; however, we note that the model error is small relative to the annual variation in water level and that results are well within the 95% confidence interval of the regression. Further, we note that the regression model is based on in-situ data that are inherently non-stationary, and hence includes the net effects of processes not included in our calibration and model, including small tributaries, minor tidal constituents, wind effects, and pseudo-tides produced by daily discharge variations ("power peaking"). Considering the simplified tidal forcing and the steady-flow boundary conditions, we consider the calibration more than adequate. Since most models do not calibrate both water level slope and tides (e.g., Elias et al., 2012), this calibration represents a more stringent test of model skill than is usually performed.

Comparison of model and regression results shows that water levels at Vancouver are not as well modeled as water levels at Portland, and exhibit larger RMSE values (Figure 5-19). Part of the difference lies in the shape of the rating curve; while the regression (grey fill) is concave up and nonlinear, the D3D model WL curve (red dots) is almost linear vs. flow. A linear curve suggests that velocity and width are approximately constant, such that

an incremental increase in discharge Q results in a proportional increase in water level h; in other words, dh/dQ is constant. The concave upward curve (an increasing rate of dh/dQ as Q increases) is only possible if river velocity becomes smaller (a decrease in width with increasing water level would achieve the same effect, but is physically implausible). Since frictional effects become less prominent as depth increases, the most likely river behavior is the exact opposite, i.e., river velocity should increase and dh/dQ should decrease. In the modern situation, bedform amplitudes increase at high flows. It is therefore suggested that the non-linearity in the regression curve (Figure 5-18) is likely related to the changing hydrograph, specifically the lack of high flow events with levee overtopping. More data at high discharge would constrain the curve to bend concave downward, as in the historical case. While this observation helps explain the difference between model and results, we note also that Vancouver lies in an area in which the river slope and the gradient in tidal constituents is large (see Figure 5-19). Hence, slight errors in the modeled spatial variation of tides and river slope will have a disproportionately large effect. Both of these factors likely contribute to the larger RMSE at Vancouver.
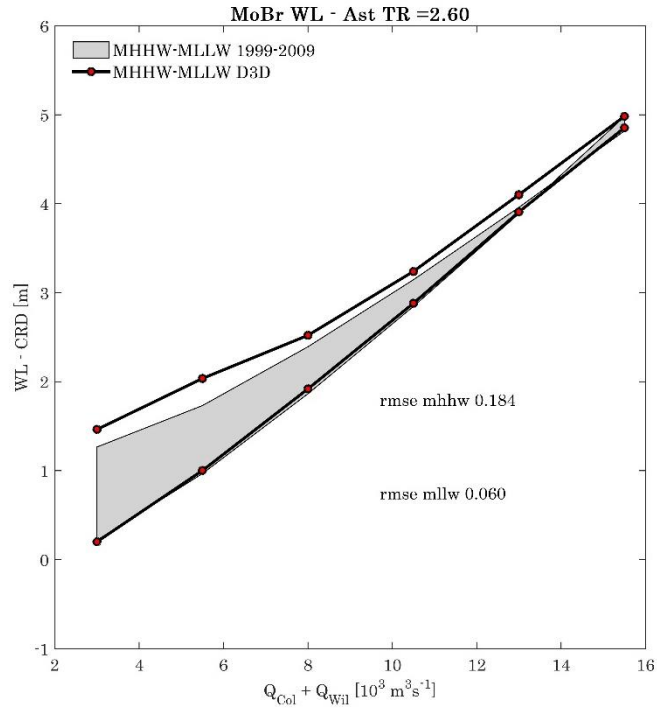
Figure 5-18: Comparison of Delft3D (Modern Model) constant flow simulations of MHHW & MLLW (red dots) versus regression of MHHW+10% CI, MLLW-10% CI at Morrison Street Bridge (grey fill) [Jay et al., 2011]
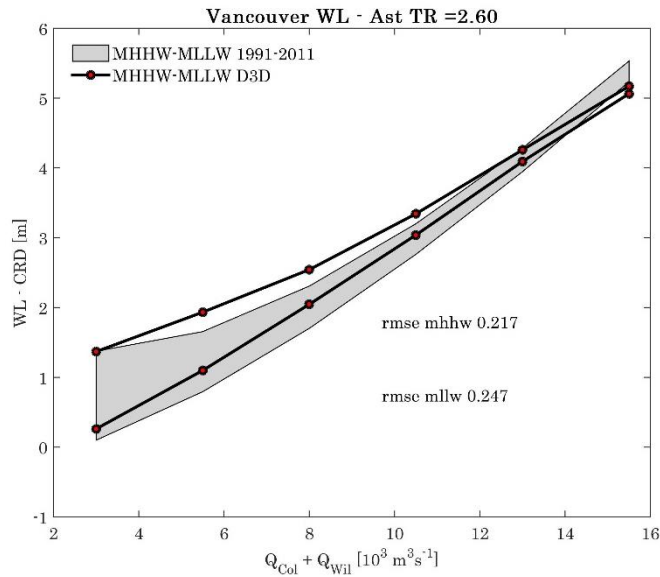
Figure 5-19: Comparison of Delft3D constant flow simulations (Modern Model) of MHHW & MLLW (red dots) versus regression of MHHW+10% CI, MLLW-10% CI at Vancouver, WA (grey fill) [Jay et al., 2011]

100

Comparison of historical and modern tides and water levels

The historical and modern model largely replicate the spatial variability in river slope and the tidal constituents observed in data. As observed in Figure 5-11, the historical M_2 peaks near rkm 25, then decreases as it moves upriver. A noticeable drop in amplitude occurs at rkm 160, at the confluence of the Willamette River. By comparison, the Modern M_2 tidal constituent follows a similar pattern but is larger than the historical M_2 at all locations (Figure 5-13). In the Modern Model there is an extended region of high peak M_2 amplitude from rkm 25-60. The changes in tidal amplitude and spatial structure suggest that the propagation of long-waves in the estuary and tidal river has fundamentally changed (see section 5.3 below for further discussion).

In both the Historic and Modern Model, the K_1 and S_2 constituents do not show the pronounced estuarine peak as the M_2 tide. Both constituents begin to decrease in amplitude beyond rkm 25 in the Historic Model, with a sharp drop in amplitude occurring near the confluence of the Willamette River at rkm 160. The pronounced drop in amplitude is likely influenced by the bifurcation of tidal flow between the Willamette and the Columbia River, but may also have a frictional component. Old USACE documents form the 19th century often discuss the necessity of dredging point bars and shallows around the confluence of the Willamette and Columbia, indicating a frictional environment.

The tidal calibrations are run under low flow conditions, which maximize the tidal intrusion. To estimate how the water surface slope has changed, a constant flow simulation using a Columbia River discharge of up to 15 kCMS and Willamette River discharge of 250 CMS is analyzed (Tables 4-11 and 4-12). At the larger discharge the tidal intrusion is

minimized, and particularly in the upstream portion of the river, changes in water level are due primarily to river discharge. Although the Vancouver and Portland are considered to be in the fluvial section of the LCR, tidal fluctuations are significant during a large portion of water year under both historical and modern conditions.
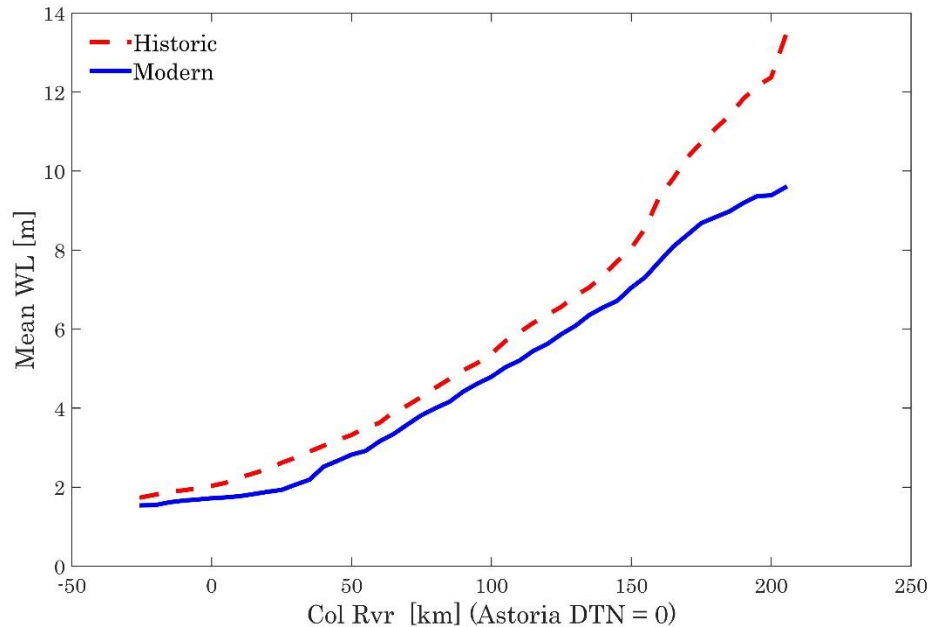
Figure 5-20: Comparison of mean water level for Historic and Modern Model at 15 kCMS constant flow in the Columbia River.

5.3 Analysis of a Large Flood Event

To investigate how changes to bathymetry and roughness have altered flood propagation, we simulate a large (19th century) spring freshet in both the Historic and Modern Model. These quasi-steady floods occurred over a 4-6 month time scale and were historically the primary mechanism of flooding in the Portland/Vancouver area (for example, in 1862, 1876, 1880, 1894, and 1948) (see Figure 4-20). Modeling a spring

freshet forms the basis for understanding how the hydrodynamics of floods (and flood risk) have changed. However, when choosing an historic event to model and compare to measurements, we are limited on the one hand by the availability of tide data in Astoria (1853-1876) and on the other hand by the availability of discharge measurements (1879-present). A compromise solution is to model the 1880 flood event, which exhibited a hydrograph in Portland that is very similar to the 1876 event (Figure 5-21).
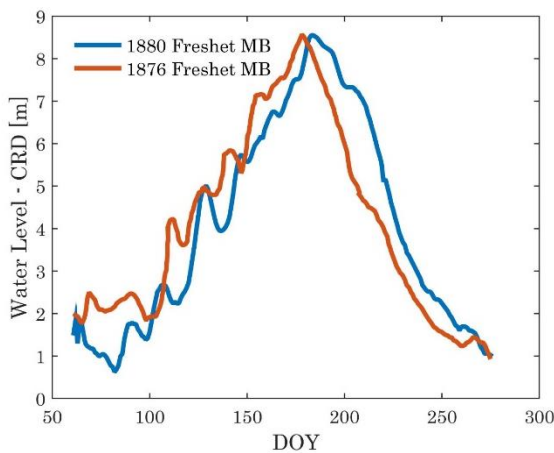
Figure 5-21: Surface elevation of the 1876 and 1880 Columbia River freshet at Morrison Street Bridge in Portland

The 1880 freshet is one of the 3 largest recorded freshets since 1878, and measured 25.9 kCMS discharge at The Dalles [*Henshaw & Dean*, 1915]. Several smaller peaks are superimposed on the larger 6 month event, possibly due to rain events, warmer weather, or inflow from upstream tributaries such as the Snake River. The discharge time series (Figure 5-22) roughly approximates a Gaussian distribution with a baseline flow of approximately 2.5 kCMS, though the curve is slightly asymmetric and exhibits a shorter, steeper rise and a longer, gentler tail. Based on this observation, we approximate the

freshet to first order with a Gaussian curve as follows, using the parameters given in Table 5-5.
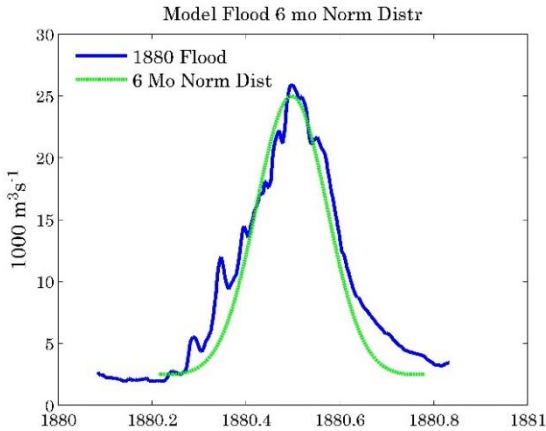
Figure 5-22: Columbia River discharge at The Dalles from 6 mo model flood and 1880 Columbia River freshet

Table 5-5: Gaussian distribution parameters for fitting 1880 freshet

Start Date	March 4, 2005
Peak Date	June 1, 2005
End Date	August 30, 2005
Duration	179 days
Baseline Discharge	2.5 kCMS
Peak Discharge	25 kCMS
σ	8 kCMS
μ	0

The smoothed Gaussian curve approximates the primary features of a natural Columbia River freshet, without including the shorter time period fluctuations that might introduce non-stationary effects and make interpretation more difficult. This Gaussian discharge, along with tidal boundary conditions from March 3rd to Aug. 30, 2005, are applied to both the Historic and Modern Model and results are compared. Willamette River flow is assumed to be a constant 250 CMS.

104

The results for the flood simulations are next analyzed for spatial patterns of inundation, river slope and velocity. Simulation results confirm the qualitative expectation that inundation patterns due to floods have changed over time (Figure 5-23). The figures are plotted using the same color scale so that a comparison of the inundation can be made. In the Historic Model, much of North Portland and Sauvie Island are inundated by the flood. By contrast, modern levees prevent inundation of these areas in the Modern Model. We note that the extent of flooding might be larger if the effects of other coastal tributaries are included.
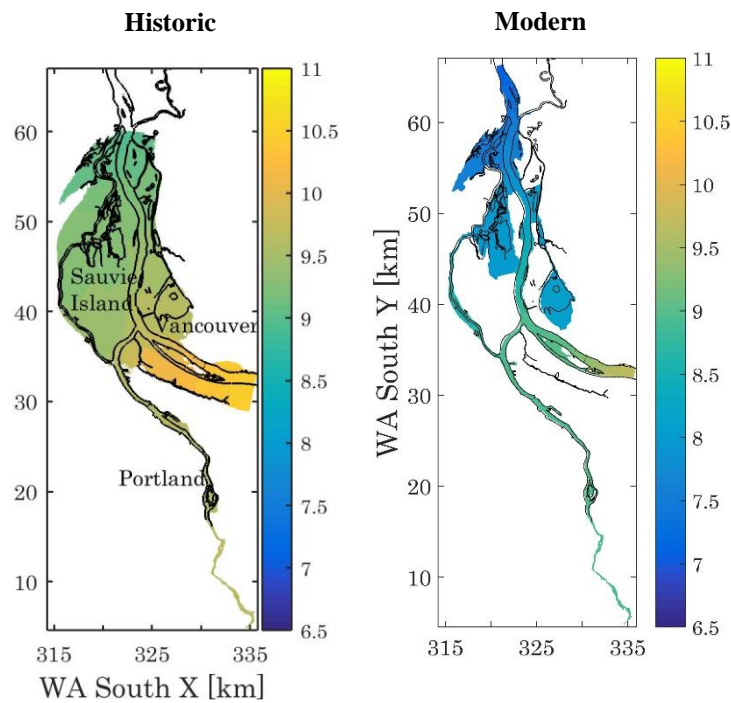
Figure 5-23: Inundation from 25 kCMS flood in the (left) Historic Model and (right) Modern Model. The figures are plotted on the same scale.

On a large spatial scale, mean water levels decrease monotonically in the downstream direction in both Historic and Modern Model (Figure 5-24). Nonetheless,

peak water levels are noticeably higher in the Historic Model than the Modern Model at all observation points between Vancouver (rkm 165) and Bonneville Dam (rkm 230). Historical MWL also exceeds modern MWL at Longview (rkm 105), Wauna (rkm 65), and Astoria (not shown), but the difference becomes much less noticeable downstream. Instead, changes in tidal fluctuation become much more obvious, with tides much larger in the Modern Model (Figure 5-24). As discussed earlier, this reduction in tidal damping is likely related to a decrease in frictional effects (see analysis below). A consequence is that during peak discharge the tidal intrusion is 130 km in the modern case, but just 80 km in the historical case. Tidal intrusion defined here as tidal range < 1% of tidal range at the mouth of the river. Spring and neap tidal ranges and water levels are compared as a function of river km in Fig. 5-25. As can be seen, the simulated tidal range has more than doubled at Wauna, Longview, and St Helens in the modern condition.
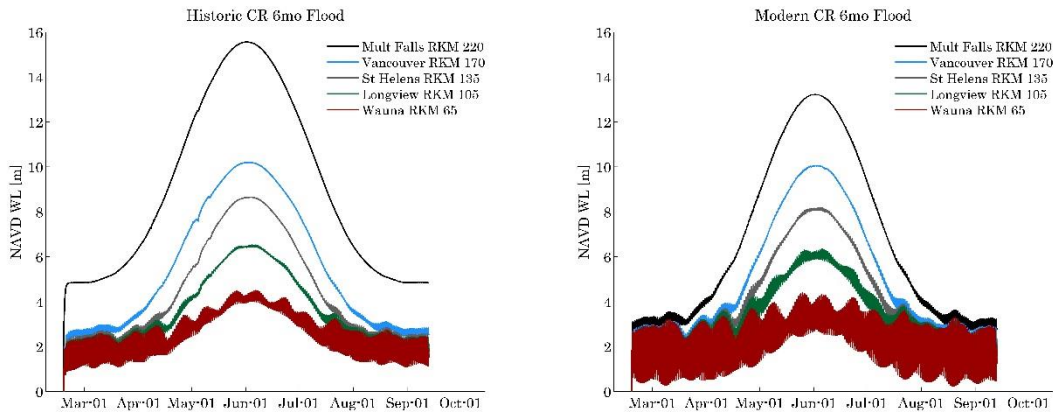
Figure 5-24: 6 Peak water levels from the 6 month Normal Distribution Flood on the (left) Historic Model (right) Modern Models
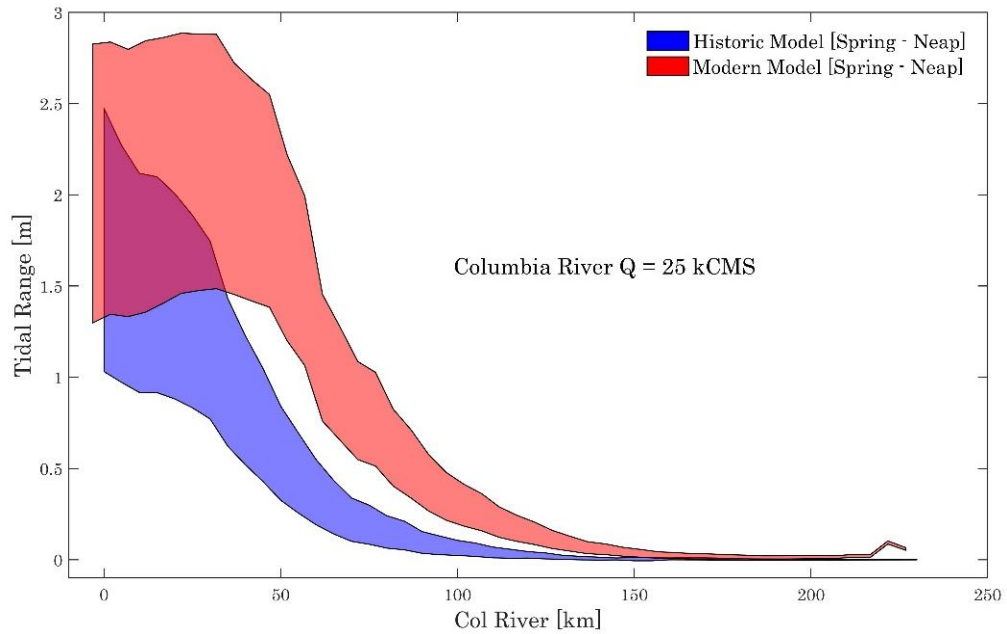
Figure 5-25: Spring and neap tidal range as a function of river kilometer in the Historic and Modern Model.

As a result of tidal influence, flood risk downstream of Longview is now highly dependent on tidal phase during the simulated spring freshet. This is evident in Figure 5-26, which shows the difference in simulated peak water levels between the Historic and Modern Model as a function of river kilometer. Downstream of Longview in the model, the peak water level is dependent on the timing of the flood and whether spring tides and flood peaks coincide.
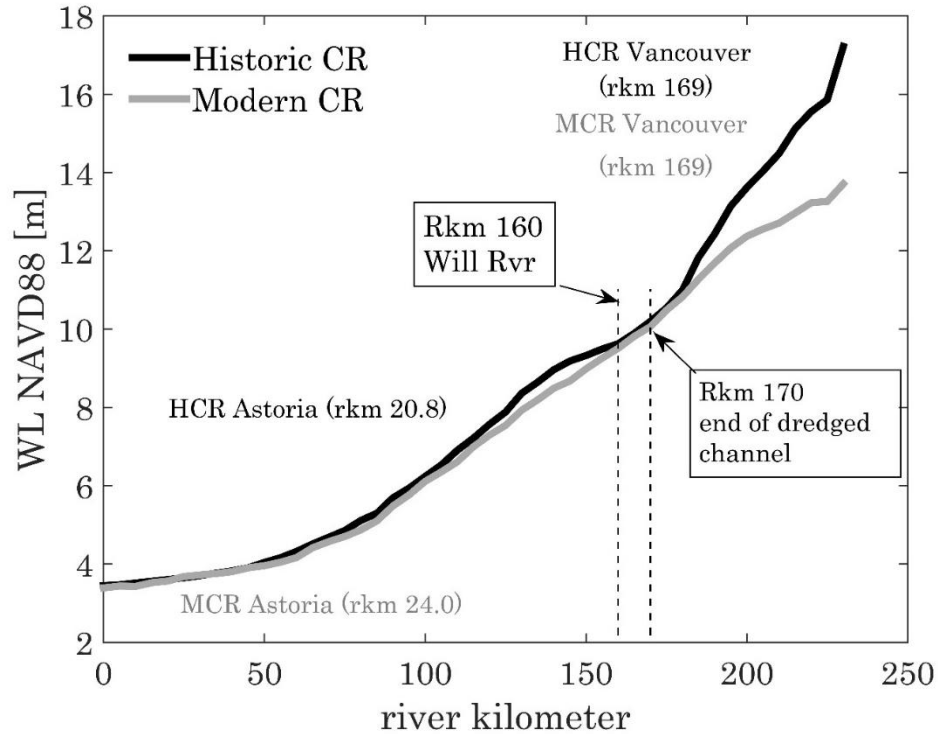
Figure 5-26: Peak water levels for 6mo simulated freshet in the Historic and Modern model.

To help interpret the water level trends, we note that two conflicting changes have occurred over time. First, the channel and floodplain in the Historic Model (sec. 4.3) is rougher than the Modern Model (appendix 7.5). The larger bed roughness creates a steeper surface slope (sec. 3.4) and higher water levels at each point, because a larger pressure gradient is required to drive the same flow. Conversely, in the modern model, the floodplain is constrained by levees, which limit inundation area. Therefore, an increase in river flow should (in theory) lead to a larger increase in height in the modern model than the historic model, all other variables being equal. This observation is encapsulated by considering flow through a cross-section, $h = Q/(ub)$, where h is the water surface elevation relative to the bed, Q is river discharge, b is width, and u is mean channel velocity. Taking

the derivative with respect to flow, we find that the rate of change in water level with an

incremental change of flow ($\frac{dh}{dQ}$) is :

$$\frac{dh}{dQ} = \frac{1}{ub} - \frac{Q}{u^2 b}\left(\frac{du}{dQ}\right) - \frac{Q}{ub^2}\left(\frac{db}{dQ}\right), \qquad \text{(Equation 5.3.1)}$$

where the first term on the right hand side is a constant for a given flow rate (u), and $\frac{du}{dQ}$

and $\frac{db}{dQ}$ are the rates of change of velocity and width, respectively, with an incremental

change in flow. Since $\frac{db}{dQ}$ has decreased in the modern model due to channelization and

levee construction, the lhs term $\frac{dh}{dQ}$ must necessarily increase, unless changes in sectionally

averaged velocity (second term on rhs) outweigh changes in width (third term on rhs).

Because flow velocity is governed by the momentum equation, a physical approach is

required to assess which terms dominate.
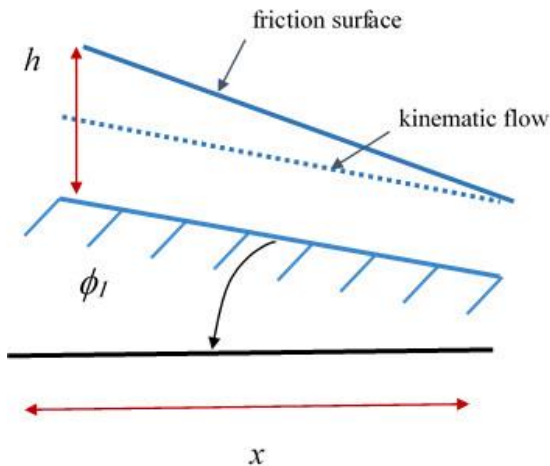
Figure 5-27: Schematic of friction surface with flow moving to the right. In kinematic flow Sf = S0
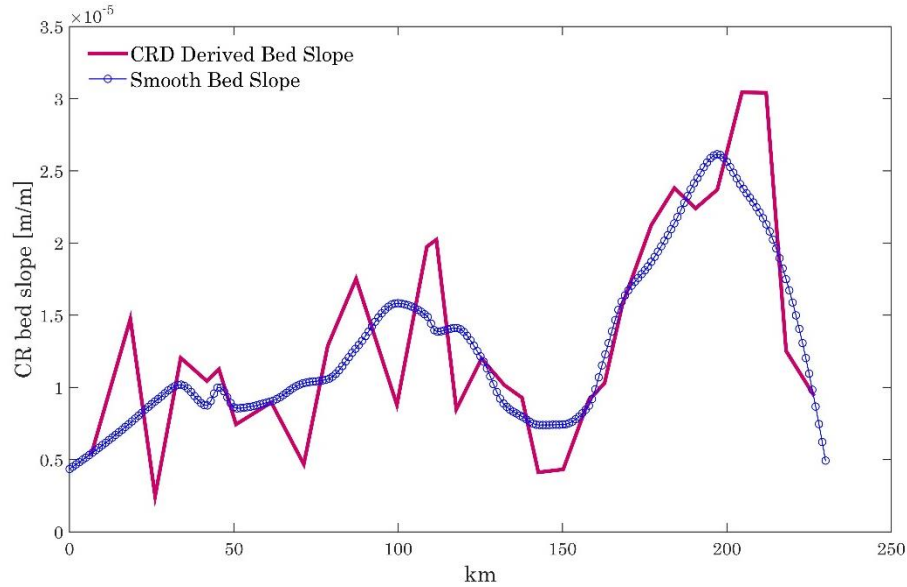
Figure 5-28: Columbia River bed slope derived from USACE estimates plot of CRD [USACE; 1963]

To better understand the secular change in water levels, we scale the terms in the 1-D St. Venant equation using results from both the Historic and Modern Model. Scaling terms of the 1-D St. Venant equation helps elucidate what factors control the momentum balance and can illustrate changes in the nature of the flood progression over time. This equation, which assumes a constant bed slope and a straight channel, is a useful simplification that allows us to investigate the fundamental physics, but is probably most valid over relatively straight sections of channel with constant width and depth (relative to CRD). The St. Venant equation is described below:

$$\frac{1}{g}\frac{\partial u}{\partial t} \; + \; \frac{u}{g}\frac{\partial u}{\partial x} \; + \; \frac{\partial h}{\partial x} \; = \; S_O \; - \; S_f, \qquad \text{(Equation 3.4.1)}$$

| *dynamic wave* | *dynamic quasi-steady wave* | *diffusive wave* | *kinematic wave* |

110
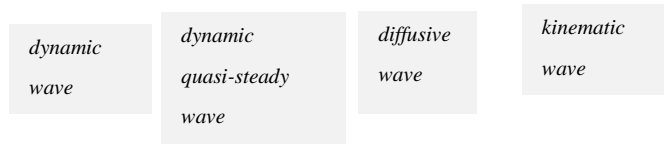
Where:

g acceleration due to gravity $[L^2T^{-2}]$

h water surface elevation relative to CRD $[L]$

u mean flow velocity $[LT^{-1}]$

t time $[T]$

x along stream direction $[L]$

S_O Bed slope (gravitational forcing) - $[LL^{-1}]$

S_f friction slope $[LL^{-1}]$

In equation 3.4.1 above the first two terms on the left hand side are the local acceleration ($\left[\frac{1}{g}\frac{du}{dt}\right]$), and convective acceleration term ($\left[\frac{u}{g}\frac{du}{dx}\right]$). The final term on the left hand side is the pressure gradient measured with respect to the Columbia River Datum (CRD). The CRD, an extreme low water datum, was established in 1911 [*Hickson,* 1912] and it still being used today. Therefore, the CRD should be an acceptable datum for measuring pressure gradients for both the Historic and Modern Model. The bed slope on the right hand side of equation 3.4.1, S_0, was estimated by taking the derivative of CRD.

In order to understand how the flood progresses in the modern and historical system, it can be examined with respect to three phases of the flood at Vancouver on the Columbia River (Figure 5.29). The numbers indicate rising water (1), peak water level (2) and falling water level (3). In the figures below, the water level (relative to CRD), velocity and acceleration are tidally averaged (~24.84 hours) at each observation point. A comparison of historical and modern models show that there has been an increase in depth averaged channel velocity in the Modern model (Figured 5-30 & 5-31) downriver of rkm 150 during the peak of the flood (2).
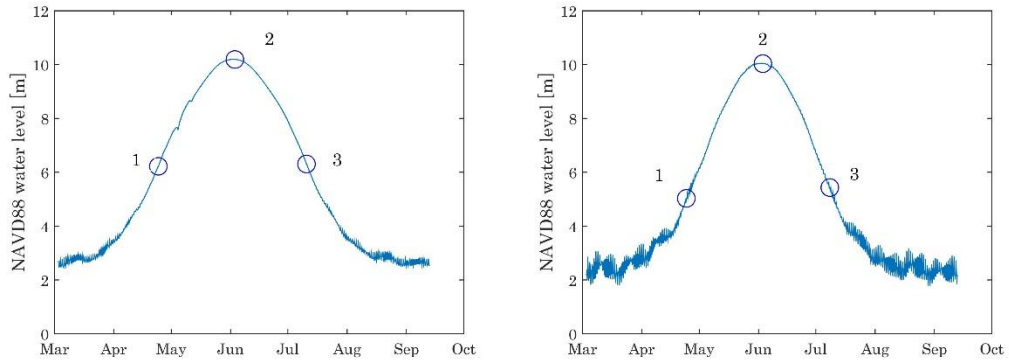
Figure 5-29: Water level near Vancouver during the 6 mo simulated freshet. (left) Historic Model (right) Modern Model
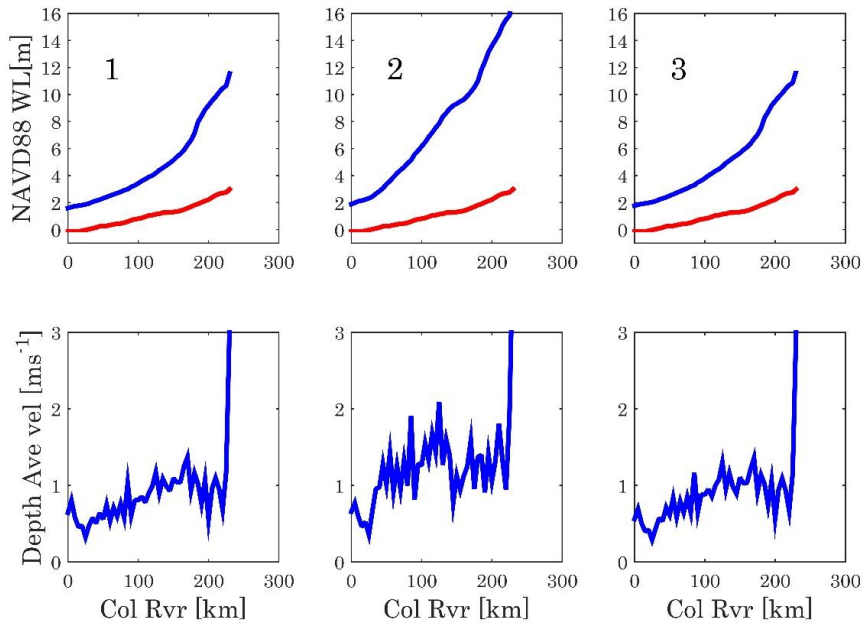
Figure 5-30: Historic Model (top) Water level along channel at three different phases of the flood. Red line is CRD (bottom) Depth average channel velocity at three different phases of the flood
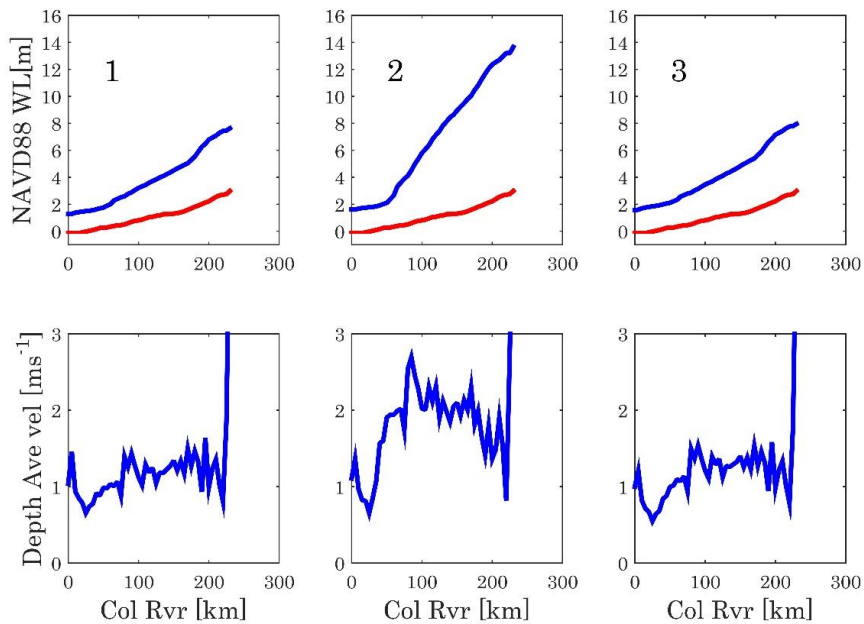
Figure 5-31: Modern Model (top) Water level along channel at three different phases of the flood. Red line is CRD (bottom) Depth average channel velocity at three different phases of the flood

An examination of the acceleration terms in the St. Venant Equation can elucidate the type of flood wave and whether there have been changes in the nature of the flood waves. The along channel magnitude of tidally averaged (~24.84 hr) magnitude of the two acceleration terms in the Historic Model is shown in Figure 5-32 and the Modern Model in Figure 5-33. Results indicate that during the three phases of the flood the acceleration is much smaller than other terms and can be neglected in both Historic and Modern model.

113
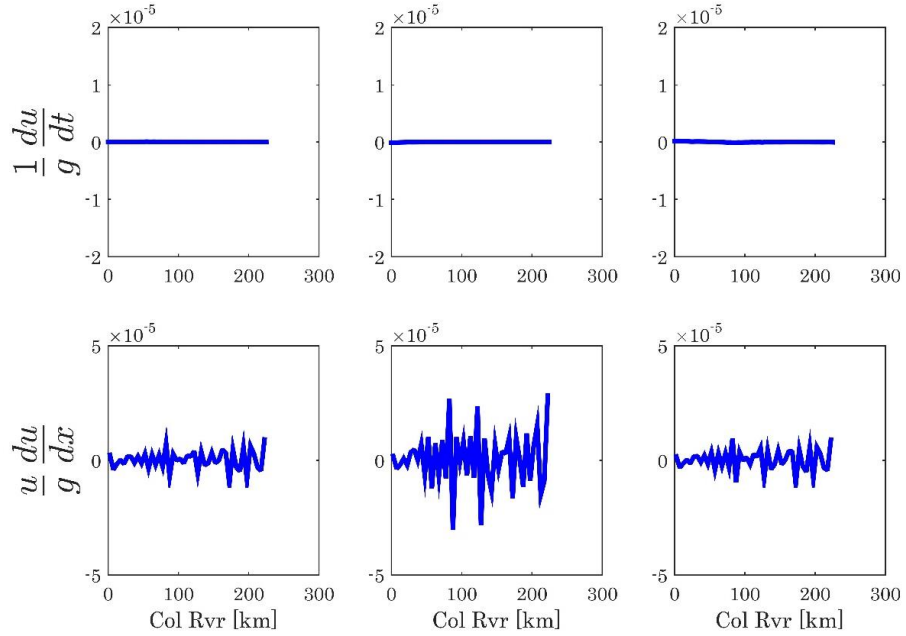
Figure 5-32: Historic Model (top) [(1/g)(du/dt)] as a function of the river for the 6mo simulated freshet (bottom) [(u/g)*(du/dx)] as a function of the river for the 6mo simulated freshet*
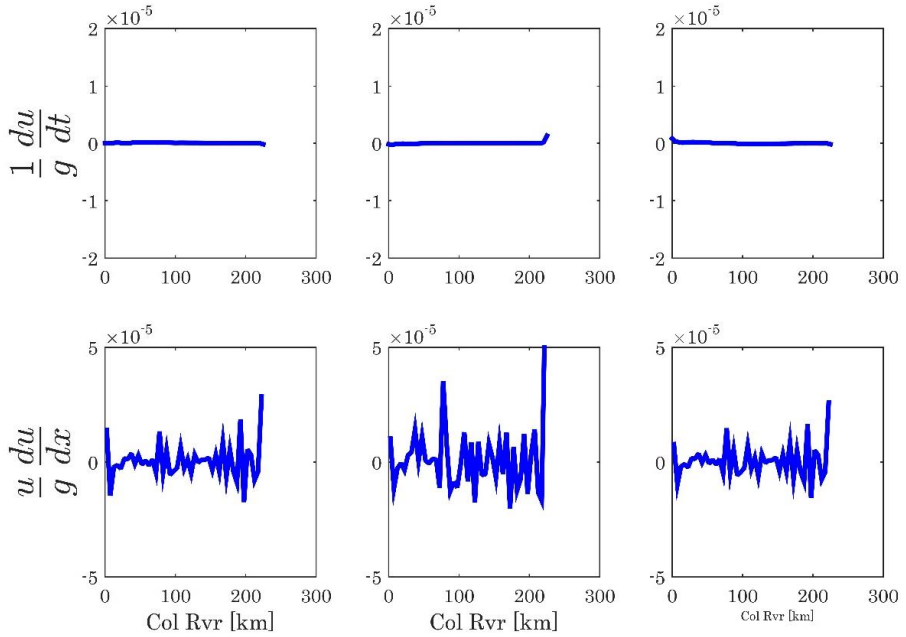
Figure 5-33: Modern Model (top) [(1/g)(du/dt)] as a function of the river for the 6mo simulated freshet (bottom) [(u/g)*(du/dx)] as a function of the river for the 6mo simulated freshet*

114

The final term on the left hand side of the St Venant Equation is the water level gradient, *dh/dx*. A comparison of the magnitude of *dh/dx* in the Historic and Modern Model shows that at all three phases of the flood the water level gradients are roughly the same order of magnitude as the calculated bed slope, S_0 (Figure 5-28). During the three phases of the flood, and at most locations, the water level gradients in the Historic Model are larger than the Modern model. It is probable that the larger bed roughness in the Historical Model (greater friction and likely larger S_f) leads to this increased pressure gradient (larger $\frac{dh}{dx}$), assuming that bed slope is similar. There are two notable exceptions. First, during the peak of the flood the water level gradients in the vicinity of Portland and Vancouver (rkm 170), are much smaller than compared to the peak of the Modern Flood (Figures 5-34 and 5-35). A likely scenario is that during the peak of the flood, the natural levees in the Historic Model were overtopped and the flood was spread over a large area (Figure 5-23). In the Modern model, higher level levees prevented overtopping and create larger water level gradients. Second, in the Modern model, water level gradients during the peak of the flood are higher than the Historic Model near Wauna (rkm 65, Figures 5-34 &5-35). It is possible that in this section of the river, the levees in the Modern model constrain floodplain inundation and create higher water level gradients. This would seem to suggest that at most locations, the rougher channel bed in the Historic Model created higher water level gradients, but that the effect of higher levees limiting floodplain inundation can also create higher water level gradients in the Modern Model.
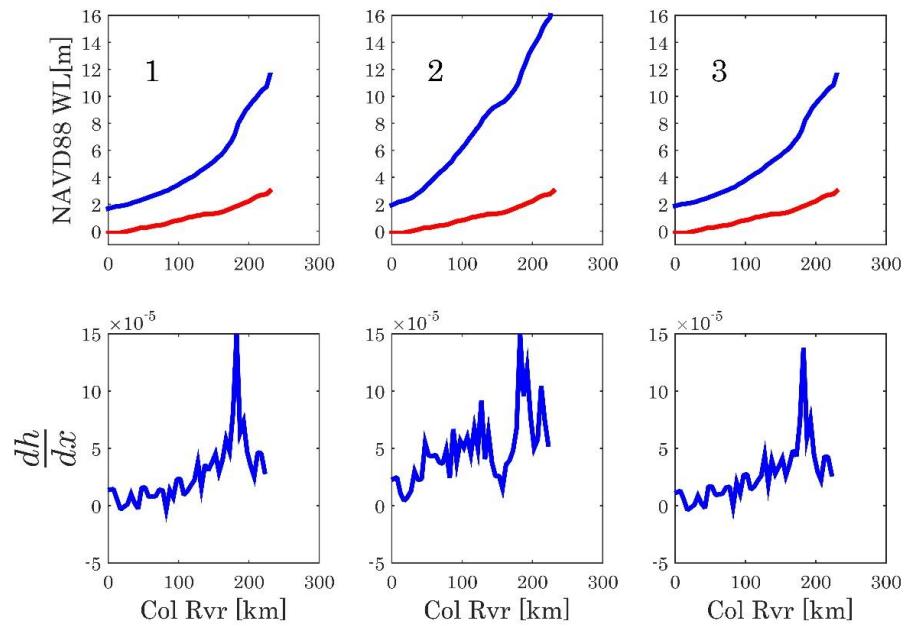
Figure 5-34: Historic Model (top) Water level along channel at three different phases of the flood. Red line is CRD (bottom) water level gradients during three phases of the flood.
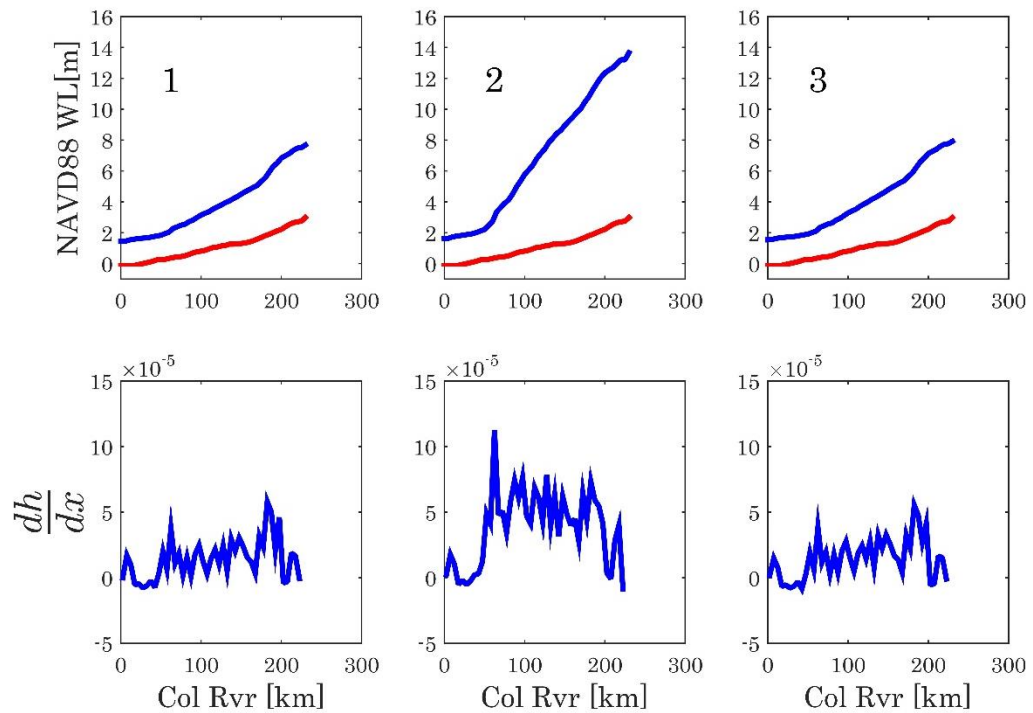
Figure 5-35: Modern Model (top) Water level along channel at three different phases of the flood. Red line is CRD (bottom) water level gradients during three phases of the flood.

116

To summarize, results during the peak flood suggest that the Historic and Modern *dh/dx* terms are of similar magnitude in the Columbia River, particularly downstream of the confluence with the Willamette River (rkm 160). Upstream of this location the Historic *dh/dx* is much larger than the Modern model. In both historic and modern models, acceleration terms are found to be negligible. Hence, the full St. Venant equation (Equation 3.4.1) reduces to an equation for a diffusive wave (Equation 3.4.3),

$$\frac{dh}{dx} = S_0 - S_f$$ (*Equation* 3.4.3).

Since we assume that S_0 (CRD) has not changed significantly over time, any variations in *dh/dx* over time must be balanced by changes to the friction slope, S_f. The friction slope can depend on many factors, but in the simplest case the friction is related directly to the Chézy roughness, such that a decrease in roughness (lower Chézy) causes an increase in surface slope (Equation 5.3.2). In Equation 5.3.2 C is the Chézy roughness, *v* is the mean channel velocity and *m* is the hydraulic radius:

$$S_f = \frac{v^2}{C^2 m}$$ (*Equation* 5.3.2)

During a large flow event such as the 1880 spring freshet, the average slope *dh/dx* between Portland and the ocean is modeled to be approximately the same in both the historic and modern situation. Since modeled roughness is larger historically (smaller Chezy), this implies that the historical velocity must also have been smaller, on average, to retain the same S_f. This is consistent with model results; note that the hydraulic radius was different somewhat as well, but is in each case approximately equal to the depth. Because the modern flow velocity is larger and confined within levees, the rate of change of height

117

with an incremental increase in flow (dh/dQ) is larger now than historical in the peak flood condition in Figure 5.29. Hence, if extrapolated beyond the 1880 peak flood condition, river water levels in the modern condition would likely begin to exceed historical water levels in the Portland-Metro area. More simulations are necessary to confirm this inference.

6   Discussion & Conclusions

The most prominent changes in the LCR since the late 19th century are the increase in channel depth and loss of tidally inundated wetlands [*Jay et al.*, 2014, 2016]. In this study, model simulations tidal analysis, and water level analysis are used to gain insight into the evolution of tidal processes in the LCR and investigate the role that changing bathymetry has had on those changes. Water level and discharge records from the LCR and Columbia basin from the late 19th century are instrumental in understanding tidal propagation and how the LCR responds to large flood events. From a physical perspective, changing water levels suggest that long-term changes in tidal propagation are a response to bathymetry changes such as dredging, dikes and filling of wetlands. To help understand how these bathymetry changes have affected water levels and tidal propagation, a Historic Model of the LCR has been developed. The model is developed from digitized, georeferenced surveys, georeferenced topography sheets and historical navigation maps. The development of this Historic Model along with the existence of a Modern Model allows for simultaneous simulations. The model outputs of water level and velocity are then analyzed with respect to 1-D St. Venant equations.

Water level analysis shows that given the same flow, mean water level were higher and the tidal range was smaller during the late 19th century (Figure 5-3) over the measured range of modern variability. The water level comparison is limited to Columbia River discharge of less than 15 kCMS because management of modern flows has eliminated large floods. These results confirm the analysis of mean water levels at Vancouver from 1904 to 2010 [*Jay et al.*, 2011]. Using the assumption that the oceanic tides have not

substantially changed, the model also shows that tidal propagation and tidal amplitudes within the LCR have been altered.

The Historic Model (Figure 4-29) requires a much lower Chézy coefficient, to reproduce observed tides than the Modern model (7.5). The changed friction is in part due to the effect of vegetation in increasing effective bed roughness [*Arcement & Schneider*, 1989]. It is likely that the heavily vegetated floodplain in the historical Columbia River was more frictional, which caused large floods to be slower and have a steeper water level vs. flow relationship for elevated flood flows. A consequence of the altered physical characteristics is that the characteristics of wetland flooding have changed over time, in part due to the altered physics with the LCR [*Kukulka & Jay*, 2003b].

Within the channel, the larger historical roughness may be caused by larger historical bedforms, sand bars, and obstructions such as snags. It is possible, however, that the increased roughness is also necessary to compensate, in part, for unrecognized errors in the historical bathymetry and datum. In terms of bathymetry, tidal theory indicates that a deeper and smoother channel will have a higher wave celerity. *Friedrichs & Aubrey,* [1990] showed that in convergent channels, the friction term in the momentum equation is inversely related to the channel depth. The implication is that given the same bedforms, waves in a deeper channel are less damped than in a shallow channel. It is also probable that the historical bathymetry was rougher due to a less regular channel alignment and a larger volume of sediment and larger sediment being directed downstream from unregulated flow [*Templeton & Jay*, 2012]. Reduced friction has led to two distinct changes in wave propagation. There has been an increase in tidal amplitude in the Modern

model, which is shown by the increase in M_2 amplitude in the spatial calibration of the Historic and Modern Model (Sec. 5.2). There has also been a decrease in water level gradients in the Modern model for the typically observed modern flow range (Sec. 5.2).

Jay et al., [2011] concluded that human modification of the river system (alteration of system topography, sand removal, flow regulation and diversion) along with changing oceanic tides have given rise to increases in tidal amplitude at Vancouver in the Columbia River. The changes in tidal amplitude between the Historic and Modern Model can be seen in both the spatial calibrations (Sec. 5.2) and the simulation of the freshet (Sec 5.3). These changes in tidal amplitude are likely due to the increase in the mean channel depth and the lower bed roughness as seen in the higher Chézy channel roughness (less friction) in the Modern Model.

Comparison of a rating curve at the Morrison Street Bridge in Portland from the late 19th century (1878-98) to the early 21st century (1999-2008) show that for most modern discharge conditions there has been a drop in water level. This would suggest that there has been a reduction in bed friction caused by the increased channel depth in the Willamette River and reduction in the large bedforms. The simulation of the freshet showed a similar result, i.e., generally higher water level gradients in the Historic Model.

The scaling of the simulated freshet (6 month duration, 25 kCMS peak discharge) indicate that in both the Historic and Modern Model, flood waves scale as diffusive waves. With the assumption of similar bed slopes in the Historic and Modern Model, the balance is now between water level gradients and a friction slope. In the Historic Model, higher bed friction and a shallower channel produced higher water level gradients than the Modern

Model except when levee overtopping cause the flood to spread over an extremely large area. In the Modern Model, lower bed friction and a deeper channel produce lower water level gradients than the Historic Model except in the cases where higher levees constrain the flow and prevent floodplain inundation. The scaling of the simulated freshet show that alterations to the river system have caused a change in the propagation of flood waves.

In this study we showed a direct link between wave propagation (tidal and flood) and bathymetry in the LCR. While the modern LCR has been extensively modeled [*Elias et al.*, 2012] no such hydrodynamic models exist for the historical LCR. The utility of the Historic Model is that now we have the ability to reach beyond conceptual descriptions of historical tidal processes and can start to quantitatively understand the processes that dominated the historical LCR.

The implementation of the Delft3D Historic Model accurately models a large flood event and is useful in understanding the nature of interactions between flood waves, but there is still considerable room for improvement. Much of the bathymetry outside of the river channel was taken from modern sources. Further analysis of historical maps would help to more accurately define the bathmetry. Current work on the both the Historic and Modern Model involves developing methods to determine land features to improve the definition of the bed roughness. Currently the only freshwater inputs are from the Willamette River and the Columbia River. In terms total discharge these two rivers account for 95% of the total discharge of the Columbia River at Beaver, but during winter floods (particularly rain-on-snow events), Western Sub-Basin rivers can account for more than

half the discharge. Additionally smaller rivers are also important to hydrodynamic processes such turbidity and play a role the salinity structure in the estuary.

In this study the models are calibrated with 2D (depth averaged) simulations. This is a safe assumption beyond the limit of salinity intrusion and in a large flood. In reality the estuary is strongly baroclinic (with depth variable density); the Columbia River varies between a moderately stratified estuary to a highly stratified salt wedge estuary depending on the tidal conditions [*Jay & Smith*, 1990; *Valle-Levinson*, 2010; *Kärna & Baptista*, 2015].

Despite these shortcomings, utilization of hydrodynamic models to understand historical processes and contrast them to modern conditions shows strong promise. This study has touched mostly on extreme events such as flood waves. This is an obvious topic to study in that most of the largest known freshets occurred in the 19th century. A keen understanding of past processes can help to understand how processes evolved over time. Two key factors that affect biology throughout the LCR are water temperature and salinity. We know from historical records that the water temperatures in the LCR were several °C colder than today (unpublished data, S., Talke). While there are no measurements of salinity in the historical LCR we know from model results that the extent of salinity intrusion in the LCR has increased. A future project could be to model the temperature/salinity along channel in the historical LCR. A study of this nature would go a long way towards understanding the connection between river conditions and river biota during the late 19th century.

There are numerous questions that could be posed about the processes in the LCR that have evolved over the past 150 years. With the completion of a hydrodynamic model we now have a valuable tool to help us gain a clearer understanding.

7 References

Arcement Jr, G.J., V.R. Schneider (1989) Guide for Selecting Manning's Roughness Coefficients for Natural Channel and Floodplains United States Geological Survey Water-supply Paper 2339, *pubs.usgs.gov/wsp/2339/report.pdf*

Aubrey, D.G., P.E. Speer (1985), A study of nonlinear propagation in shallow inlet/estuarine systems, Part 1: Observations, *Estuarine Coastal Shelf Science 21*, 185-205

Bottom, D.L., C.A. Simenstad, J. Burke, A.M. Baptista, D.A. Jay (2005) Salmon at River's End: The Role of the Estuary in the Decline and Recovery of the Columbia River salmon, Technical Memorandum NMDS-NWFSC-68, NOAA, Seattle, WA

Burke, J.L. (2010), Georeferenced historical topographic survey maps of the Columbia River Estuary, School of Aquatic and Fishery Sciences, University of Washington, Seattle, WA

Chernetsky, A.S., H.M. Schuttelaars, S.A. Talke (2010), The effect of tidal asymmetry and temporal settling lag on sediment trapping in tidal estuaries, *Ocean Dynamics 60*(5), 1219-1241

Cunge, J.A., F.M. Holly, A. Verwey (1980) Practical aspects of computational river hydraulics, Pittman Publishing Ltd., London, UK

Cutts, R.D., C. Rockwell, E. Cordell, G. Davidson, C.P. Patterson (1870), Columbia River: sheet no. 1: The Survey, 1870, map, United States Coast & Geodectic Survey

De Jonge, V.N., H.M. Schuttelaars, J.E. van Beusekom, S.A. Talke, H.E. Swart (2014), The influence of channel deepening on estuarine turbidity levels and dynamics, as exemplified by the EMS estuary, *Estuarine, Coastal and Shelf Science 139*, 46-59

Deltares (2010), Delft3D-FLOW, Simulation of multi-dimensional hydrodynamic flow and transport phenomena, including sediments, User Manual, Rotterdamseweg, The Netherlands

Deltares (2010), Delft3D –RGFGRID, Generation and manipulation of curviliniear grids for Delft3D-FLOW and Delft3D-WAVE, User Manual, Rotterdamseweg, The Netherlands

Egbert, G.B., S.Y. Erofeeva (2002), Efficient Inverse Modeling of Barotropic Ocean Tides, *Journal of Atmospheric and Ocean Technology 19*(2), 183-204

Elias, E., G. Gelfenbaum, A.J. Van der Westhuyen (2012), Validation of a coupled wave-flow model in a high energy setting: The mouth of the Columbia River, *Journal of Geophysical Research: Oceans 117*(C9)

Foreman, M. (1977), revised 1996, Manual for tidal heights and analysis prediction. *Technical Report Pacific Marine Report 77-10*, Institute of Ocean Services, Patricia Bay Victoria, BC, Canada

Friedrichs, C.T., D.G. Aubrey (1994), Tidal propagation in strongly convergent channels, *Journal of Geophysical Research: Oceans (1978-2012) 99*(c@), 3321-3336

Giese, B.S., D.A. Jay (1989) Modelling Tidal Energetics of the Columbia River Estuary, *Estuarine, Coastal and Shelf Science 29*(6), 549-571

Godin, G. (1985), Modification of river tides by the discharge, *Journal of waterway, port, coastal and ocean engineering 111*(2), 257-274

Green, G. (1837), On the motion of waves in a variable canal of small depth and width, *Transaction of the Cambridge Philosophical Society 6*, 457-462

Henshaw, F.F., H.J. Dean (1915), Surface water supply of Oregon (1878-1910), *US Geological Survey Supply Paper 370*, Government Printing Press, Washington, DC

Hickson, R.E. (1912), A Report on the Establishment of River Gauges on the Lower Columbia River & Willamette Rivers, *U.S. Army Corps of Engineers,* As submitted to Major J.F. Indoc

Holland, P.W., R.E. Welsch (1977), Robust regression using iteratively reweighted least-squares, *Communications in Statistics-theory and Methods 6*(9), 813-827

Ianniello, J.P. (1979), Tidally induced currents in estuaries of variable breadth and depth, *Journal of Physical Oceanography 9*(5), 962-974

Ippen, A. T. (1966) Tidal dynamics in estuaries, I: Estuaries of rectangular section, in *Estuaries and Coastline Hydrodynamics*, edited by A.T. Ippen, pp. 492-522, McGraw-Hill, New York

Jay, D.A. (2009) Evolution of tidal amplitudes in the eastern Pacific Ocean, *Geophysical Research Letters 36*(4), L04063

Jay, D.A, A.B. Borde, H.L Diefenderfer (2016) Tidal-Fluvial and Estuarine Processes in the Lower Columbia River: II. Water Level Models, Floodplain Wetland Inundation, and System Zones, *Estuaries and Coasts*, 1-26

Jay, D.A., K. Leffler, S. Degens (2011) Long-term evolution of Columbia River tides, *Journal of Waterway, Port, Coastal and Ocean Engineering 137*(4), 182-191

Jay, D.A, K. Leffler, H.L Diefenderfer, A.B. Borde (2014) Tidal-Fluvial and Estuarine Processes in the Lower Columbia River: I. Along-Channel Water Level Variations, Pacific Ocean to Bonneville Dam, *Estuaries and Coasts 38*, 415-433

Jay, D.A., T. Kukulka (2003), Revising the paradigm of tidal analysis – the uses of non-stationary data, *Ocean Dynamics 53*(3), 110-125

Jay, D.A., P. Naik (2011) Distinguishing human and climate influences on the hydrological disturbance processes in the Columbia River, USA, *Hydrological Services Journal 56*(7), 1886-1209

Kammerer, J.C. (1990) Largest Rivers in the United States, Open-File Report 87-242, US Geological Survey, Water Resources Division, Reston, VA, 2 pp.

Kärnä, T., A.M. Baptista, J.E. Lopez, P.J. Turner, C. McNeil, T.B. Stanford (2015), Numerical modeling of circulation in high-energy estuaries: A Columbia River estuary benchmark, *Ocean Model 88*, 54-71

Kärnä, T., A.M. Baptista (2016), Evaluation of a long-term hindcast for the Columbia River estuary, *Ocean Model 99*, 1-14

Kimbrough, R.A., G.P. Ruppert, W.D. Wiggins, RR. Smith, D.L. Kresch (2005), Water Resources Data-Washington Water Year 2005, *WA-050-1*, U.S. Geological Survey

Kukulka, T.A., D.A. Jay (2003), Impacts of Columbia River discharge on salmonid habitat: 2. Changes in shallow-water habitat, *Journal of Geophysical Research: Oceans (1978-2012) 108*(C9), 17 pp

Lanzoni, S., G. Seminara (1998), On tide propagation in convergent estuaries, *Journal of Geophysical Research: Oceans (1978-2012) 103*(C13), 30793-30812

Leffler, K.E., D.A. Jay (2009), Enhancing tidal harmonic analysis: Robust (hybrid L1/L2) solution, *Continental Shelf Research 29*(1), 78-88

Lower Columbia Fish Recovery Board (2004), Lower Columbia Salmon Recovery and Fish & Wildlife Subbasin Plan Volume II – Subbasin Plan Chapter G – NF and EF Lewis, Northwest Power and Conservation Council

Mahedy, A. (2016) Comparative numerical modeling of floodplain inundation frequency and extent in the historic and modern Lower Columbia River estuaries, thesis (unpublished), Portland State University, Portland, OR, 2015

McIndoe, J.F., E.B. Thomson (1911), Willamette River, Oregon, from Portland to Oregon City (in three sheets), map, U.S. Army Corp of Engineers, Washington DC

Mofthakhari, H.R., D.A. Jay, S.A. Talke, T. Kukulka, P.D. Bromirski (2013), A novel approach to flow estimation in tidal rivers, *Water Resources Research 49*(8), 4817-4832

Mofthakhari, H.R., D.A. Jay, S.A. Talke (2016), Estimating River Discharge Using Multiple-Tide Gauges Distributed Along a Channel, *Journal of Geophysical Research: Oceans 121*(4) 2078-2097, doi: 10.1002/2015JC010983

Moussa, R., C. Bocquillon (1996), Criteria for choice of flood-routing method in nature channels, *Journal of Hydrology 186*(1), 1-30

Naik, P., D.A. Jay (2011), Distinguishing human and climate influences on the Columbia River: changes in mean flow and sediment transport, *J. Hydrology 404*(3), 259-277

National Geophysical Data Center (NGDC) (2003), U.S. Coastal Relief Model – Northwest Pacific, National Geophysical Data Center, NOAA, Boulder, CO

Orem, H.M. (1968), Discharge in the Lower Columbia River Basin, 1928-1965, US geological Survey Circular 550, p. 24.

Parker, B.P.(2007) Tide analysis and prediction, US Department of Commerce, National Oceanic and Atmospheric Administration, National Ocean Service, Center for Operational Oceanographic Products and Services, 378 pp.

Pawlowicz, R., B. Beardsley, S. Lentz (2002), Classical tidal harmonic analysis including error estimates in MATLAB using T_TIDE, *Computers and Geosciences 29*(8), 929-937

Pengra, B. F., (1862), Township no. 2 North Range no. 1 West Willamette Meridian, map, Oregon Surveyors General Office, Eugene, OR

Rockwell, C. (1876) Columbia River at Youngs River and Lewis And Clark River, map, United States Coast & Geodectic Survey, Washington, DC

Rockwell, C., H. Lindenkohl, A. Lindenkohl, H.C. Evans, A. Peterson, F. Courtenay, H.M. Knight (1888), Columbia River: Fales Landing to Portland: sheet no. 6: The Survey, 1888, map, United States Coast & Geodectic Survey, Washington, DC

Talke, S.A., D.A. Jay (2013), Nineteenth Century North American and Pacific Tidal Data: Lost or Just Forgotten?, *Journal of Coastal Research 29*(6a), 118-127

Thomas, D.W. (1983), Changes in the Columbia River Estuary Habitat Types over the Past Century, Columbia River Estuary Data Development, Astoria, OR, 51 pp and appendices

Thorn, F.M. (1888), Columbia River Sheet No. 6 Fales Landing to Portland, United States Coast & Geodetic Survey (USC&G), Washington, D.C.

United States Army Corp of Engineers (USACE) (1881-1915), Annual Report of the Chief of Engineers, US Army, to the Secretary of War. Government Printing Office, Washington, DC

United States Army Corp of Engineers (USACE) (1963), Water Surface Profiles, Floods – 1876, 1894, 1933, 1946, 1948, 1950 and 1956, U.S. Army Corp of Engineers, Portland District

United States Army Corp of Engineers (USACE) (2010), Lower Columbia River Digital Terrain Model, USACE, Portland, OR

United States Coast & Geodetic Survey (1877), Columbia River tide logs, National Archives at College Park, MD, College Park, MD

United States Geological Survey (2005), Topographic Map Symbols, United States Geological Survey, Reston, VA

United States Geological Survey (2012), Daily Discharge, Hydrological Unit 17010105 at Wasco County, OR, Retrieved from http://waterdata.usgs.gov

US Geological Survey (2014), Water-Data Report 2013, Hydrological Unit 17010105 Willamette River at Portland, OR, pp. 3, Retrieved from http://waterdata.usgs.gov

US Weather Bureau (1878-1888), Discharge estimated from the Willamette River in Salem, OR, National Weather Service Archives at Portland, OR, Portland, OR

US Weather Bureau (1879-1898), Water level records from the Willamette River in Portland, OR, City of Portland Archives at Portland, OR, Portland, OR

Valle-Levinson, A. (Ed.) (2010), *Contemporary Issues in Estuarine Physics*, 315 pp., Cambridge University Press, Cambridge, UK

Weinheimer, J. (2002) Draft: Kalama River Subbasin Summary, Columbia Basin Fish and Wildlife Authority, pp. 44

Information about LIDAR is available at http://oceanservice.noaa.gov/facts/lidar.html

8 Appendices

8.1 Appendix A – 19th Century Columbia River Tides

Fort Stevens, OR 1868
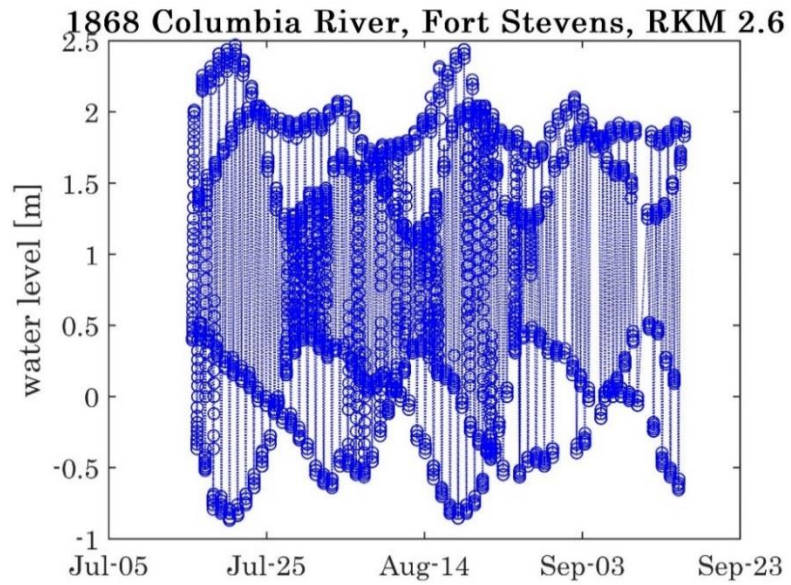
Figure 8-1: Columbia River water level, Fort Stevens Jul 15 – Sep 15, 1868

Oak Point, WA 1877

Figure 8-2: Columbia River water level, Oak Point, WA Sep 12 – Oct 15, 1877
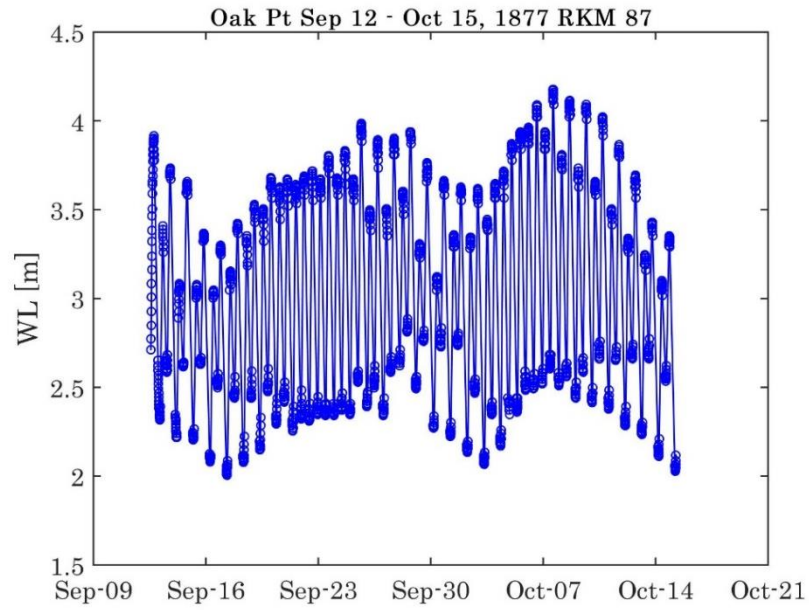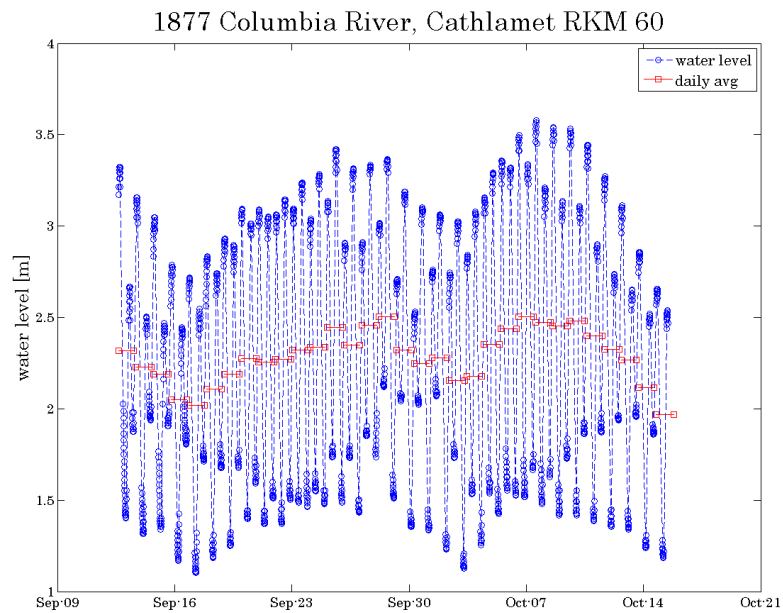
Cathlamet, WA 1877

Figure 8-3: Columbia River water level, Cathlamet,WA September 12 – October 15, 1877
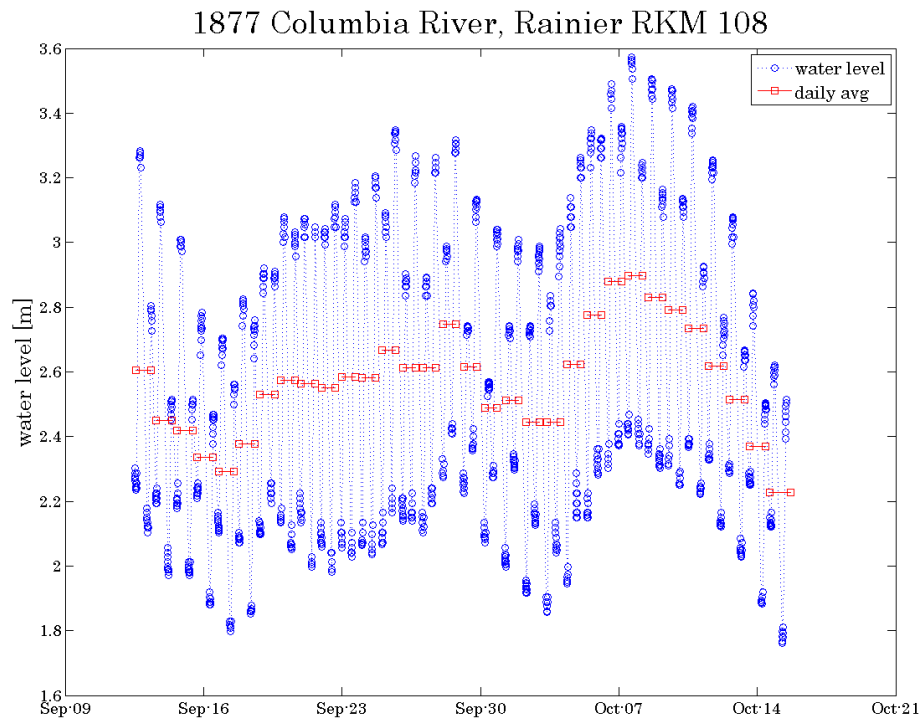
Rainier, WA 1877

Figure 8-4: Columbia River water level, Rainier, OR Sep 12 – Oct 15, 1877
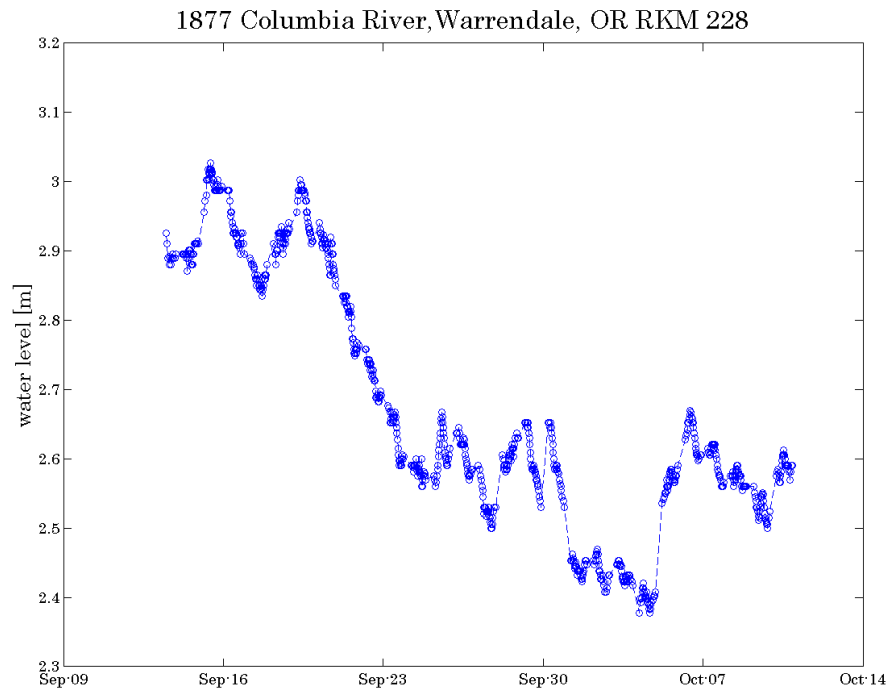
Warrendale, OR 1877

Figure 8-5: Columbia River water level, Warrendale, OR September 12 – October 15, 1877

8.2   Appendix B – Harmonic Analysis of Tides

Fort Stevens, OR Jul 15 – Sep 15, 1877

```
file name: FS1868_RC1_1
date: 03-May-2016
nobs = 2851,  ngood = 2851,  record length (days) = 118.79
start time: 15-Jul-1868 14:20:00
rayleigh criterion = 1.1
Greenwich phase computed with nodal corrections applied to amplitude \n
and phase relative to center time

x0= 0.863, x trend= 0

var(x)= 0.82608   var(xp)= 0.82577   var(xres)= 0.0080968
percent var predicted/var original= 100.0
     tidal amplitude and phase with 95
```

tide	freq	amp	amp_err	pha	pha_err	data.snr
*MM	0.0015122	0.0339872	0.0042339	314.55	8.17	64
*MSF	0.0028219	0.0209510	0.0047537	12.01	14.01	19
*ALP1	0.0343966	0.0129439	0.0049419	252.24	25.58	6.9
*2Q1	0.0357064	0.0258447	0.0057781	221.41	12.41	20
*Q1	0.0372185	0.0399656	0.0054018	96.37	7.29	55
*O1	0.0387307	0.2764844	0.0061913	122.86	1.15	2e+03
NO1	0.0402686	0.0032017	0.0049478	62.60	103.55	0.42
*K1	0.0417807	0.3827900	0.0048997	132.84	0.81	6.1e+03
*J1	0.0432929	0.0380806	0.0058668	160.57	7.42	42
*OO1	0.0448308	0.0358768	0.0084229	192.36	13.70	18
UPS1	0.0463430	0.0076506	0.0076513	280.52	63.25	1
*EPS2	0.0761773	0.0117895	0.0065413	40.83	40.99	3.2
*MU2	0.0776895	0.0454380	0.0081441	2.61	10.76	31
*N2	0.0789992	0.2062542	0.0082044	340.33	2.53	6.3e+02
*M2	0.0805114	0.9064456	0.0093545	6.17	0.46	9.4e+03
*L2	0.0820236	0.0567116	0.0075110	31.74	7.78	57
*S2	0.0833333	0.2144936	0.0090719	44.40	2.51	5.6e+02
*ETA2	0.0850736	0.0199503	0.0122190	186.94	32.79	2.7
*MO3	0.1192421	0.0419849	0.0080849	131.32	12.62	27
*M3	0.1207671	0.0362065	0.0068844	2.47	11.97	28
MK3	0.1222921	0.0092407	0.0068884	243.17	51.17	1.8
SK3	0.1251141	0.0064820	0.0070389	313.39	74.55	0.85
*MN4	0.1595106	0.0206331	0.0071736	9.33	18.24	8.3
*M4	0.1610228	0.0532323	0.0078008	16.29	7.53	47
*SN4	0.1623326	0.0221480	0.0070492	206.93	19.32	9.9
*MS4	0.1638447	0.0286918	0.0076310	29.58	15.39	14
*S4	0.1666667	0.0180772	0.0076764	11.10	25.11	5.5
*2MK5	0.2028035	0.0225277	0.0101470	247.86	28.87	4.9
*2SK5	0.2084474	0.0178460	0.0119404	130.96	34.73	2.2
2MN6	0.2400221	0.0067576	0.0091563	252.60	92.27	0.54
*M6	0.2415342	0.0268348	0.0115648	138.74	23.86	5.4
*2MS6	0.2443561	0.0188180	0.0097705	193.93	31.37	3.7
2SM6	0.2471781	0.0009586	0.0074372	110.58	233.67	0.017
3MK7	0.2833149	0.0028314	0.0044741	5.90	101.46	0.4

136

```
   M8   0.3220456   0.0015102   0.0028728   148.92   114.84      0.28
```
Phases are referenced to local time

Astoria Jul 31 – Aug 31, 1877

```
file name: HA_Ast1874_loflo_1.0.txt
date: 17-Nov-2013
nobs = 761,  ngood = 761,  record length (days) = 31.71
start time: 31-Jul-1874 00:15:18
rayleigh criterion = 1.0
Greenwich phase computed with nodal corrections applied to amplitude \n
and phase relative to center time

x0= 3.68e-15, x trend= 0

var(x)= 0.60067   var(xp)= 0.60134   var(xres)= 0.0028485
percent var predicted/var original= 100.1
     tidal amplitude and phase with 95
tide  freq (1/hr)  amp (m)     amp_err      pha     pha_err    data.snr
*MSF  0.0028219   0.0541804   0.0058943   346.05     7.10        84
 2Q1  0.0357064   0.0046649   0.0048008    74.74    70.11       0.94
*Q1   0.0372185   0.0469069   0.0060850   262.91     6.74        59
*O1   0.0387307   0.2507899   0.0057378   253.87     1.25    1.9e+03
*NO1  0.0402686   0.0270519   0.0041018   247.31     9.23        43
*K1   0.0417807   0.3910071   0.0064510   282.31     0.85    3.7e+03
*J1   0.0432929   0.0178822   0.0060337   280.44    17.58       8.8
*OO1  0.0448308   0.0192419   0.0036472   317.62    10.09        28
 UPS1 0.0463430   0.0016614   0.0026626    20.81   123.37       0.39
*N2   0.0789992   0.1630473   0.0070105   273.65     2.39    5.4e+02
*M2   0.0805114   0.9189521   0.0065952   285.31     0.44    1.9e+04
*S2   0.0833333   0.2663436   0.0060751   333.53     1.45    1.9e+03
*ETA2 0.0850736   0.0101665   0.0047545    71.77    25.16       4.6
*MO3  0.1192421   0.0297401   0.0025928   108.27     4.51    1.3e+02
*M3   0.1207671   0.0073564   0.0030417   173.04    20.06       5.8
*MK3  0.1222921   0.0258507   0.0024449   154.30     5.72    1.1e+02
*SK3  0.1251141   0.0136718   0.0026393   177.44    10.36        27
*MN4  0.1595106   0.0143419   0.0047138   129.51    17.39       9.3
*M4   0.1610228   0.0285730   0.0040328   143.65     8.74        50
*MS4  0.1638447   0.0166651   0.0038147   168.94    15.27        19
 S4   0.1666667   0.0043521   0.0037954   209.23    44.68       1.3
*2MK5 0.2028035   0.0141217   0.0006822   227.98     2.55    4.3e+02
*2SK5 0.2084474   0.0020461   0.0005613    84.66    17.67        13
*2MN6 0.2400221   0.0061315   0.0042280   202.02    36.07       2.1
*M6   0.2415342   0.0133854   0.0038329   213.09    18.09        12
*2MS6 0.2443561   0.0119426   0.0039567   261.43    16.83       9.1
*2SM6 0.2471781   0.0048569   0.0032896   320.48    42.91       2.2
 3MK7 0.2833149   0.0017425   0.0029694   352.27   109.15      0.34
 M8   0.3220456   0.0010604   0.0064680   321.93   214.92     0.027

*Constituents are optimized
```

Phases are referenced to local time

Cathlamet, WA Sep 12 – Oct 15, 1877

```
file name: caha06.txt
date: 04-May-2016
nobs = 1461,  ngood = 1461,  record length (days) = 60.88
start time: 12-Sep-1877 16:10:00
rayleigh criterion = 0.8
Greenwich phase computed with nodal corrections applied to amplitude \n
and phase relative to center time

var(x)= 0.54426   var(xp)= 0.5278   var(xres)= 0.016441
percent var predicted/var original= 97.0
     tidal amplitude and phase with 95
tide   freq        amp       amp_err      pha      pha_err      data.snr
*MSF  0.0028219   0.1325906   0.0480776    40.95    23.84        7.6
*O1   0.0387307   0.1200807   0.0437739   158.32    25.30        7.5
*K1   0.0417807   0.2105073   0.0543319   172.35    12.40         15
*N2   0.0789992   0.1355840   0.0277451    38.90    11.61         24
*M2   0.0805114   0.7135871   0.0287985    76.01     2.18     6.1e+02
*S2   0.0833333   0.2025162   0.0257706    84.50     7.77         62
*M4   0.1610228   0.1132671   0.0269491    56.60    13.64         18
```
Phases are referenced to local time

Oak Point, WA Sep 12 – Oct 15, 1877

```
file name: opha10.txt
date: 20-Apr-2016
nobs = 691,  ngood = 691,  record length (days) = 28.79
start time: 12-Sep-1877 14:00:00
rayleigh criterion = 0.9
Greenwich phase computed with nodal corrections applied to amplitude \n
and phase relative to center time

var(x)= 0.35909   var(xp)= 0.35428   var(xres)= 0.0055688
percent var predicted/var original= 98.7
     tidal amplitude and phase with 95
tide    freq       amp         amp_err      pha    pha_err   data.snr
*MSF  0.0028219  0.2126880   0.0136865    65.24     3.14   2.4e+02
*O1   0.0387307  0.1017734   0.0104109   177.95     7.03       96
*K1   0.0417807  0.2138556   0.0129600   182.08     3.10   2.7e+02
*M2   0.0805114  0.6140019   0.0136645   100.31     1.32     2e+03
*S2   0.0833333  0.1468144   0.0120371   116.29     5.38   1.5e+02
*M3   0.1207671  0.0868303   0.0120518    81.04     7.31       52
*SK3  0.1251141  0.0347008   0.0089080   250.16    15.30       15
*M4   0.1610228  0.0559682   0.0135777   184.79    12.58       17
*MS4  0.1638447  0.0490314   0.0121734   107.31    15.28       16
*S4   0.1666667  0.0379737   0.0126497   118.48    19.01        9
*2MK5 0.2028035  0.0626755   0.0411801   147.47    35.29      2.3
 2SK5 0.2084474  0.0226245   0.0320104   277.40    91.94      0.5
*M6   0.2415342  0.0566060   0.0173043    84.28    16.44       11
*2MS6 0.2443561  0.0461086   0.0152856   203.02    18.81      9.1
*2SM6 0.2471781  0.0273089   0.0141713   172.65    29.49      3.7
*3MK7 0.2833149  0.0308337   0.0133627   333.12    24.86      5.3
*M8   0.3220456  0.0526249   0.0202037   193.13    21.19      6.8
```
Phases are referenced to local time

Rainier, OR Sep 12 – Oct 15, 1877

```
file name: raha08.txt
date: 04-May-2016
nobs = 540,  ngood = 539,  record length (days) = 22.46
start time: 19-Sep-1877 14:00:00
rayleigh criterion = 0.9
Greenwich phase computed with nodal corrections applied to amplitude \n
and phase relative to center time

var(x)= 0.21262   var(xp)= 0.20343   var(xres)= 0.0089664
percent var predicted/var original= 95.7
     tidal amplitude and phase with 95
tide   freq       amp        amp_err     pha      pha_err    data.snr
*MSF  0.0028219  0.0718145  0.0273061    85.88    19.98       6.9
*O1   0.0387307  0.0930381  0.0238832   208.05    14.54        15
*K1   0.0417807  0.1629837  0.0233208   218.30     9.33        49
*N2   0.0789992  0.1107840  0.0271751    73.72    14.77        17
*M2   0.0805114  0.4961478  0.0259589   127.22     3.00    3.7e+02
*S2   0.0833333  0.1693349  0.0259946   145.89     8.84        42
*M4   0.1610228  0.0655036  0.0115325   130.03     9.27        32
*S4   0.1666667  0.0178269  0.0105150   178.42    30.66       2.9
```
Phases are referenced to local time

Vancouver, WA Sep 12 – Oct 15, 1877

```
file name: vaha09.txt
date: 04-May-2016
nobs = 841,  ngood = 841,  record length (days) = 35.04
start time: 12-Sep-1877 10:25:00
rayleigh criterion = 0.9
Greenwich phase computed with nodal corrections applied to amplitude \n
and phase relative to center time

x0= 3.75, x trend= 0

var(x)= 0.018074   var(xp)= 0.014845   var(xres)= 0.0032218
percent var predicted/var original= 82.1
     tidal amplitude and phase with 95
tide   freq       amp        amp_err     pha      pha_err   data.snr
 MSF  0.0028219  0.0124600  0.0117712   113.07    53.92       1.1
*O1   0.0387307  0.0415357  0.0111936   275.20    15.87        14
*K1   0.0417807  0.0516717  0.0124659   274.48    12.73        17
*M2   0.0805114  0.1115512  0.0136794   217.64     7.22        66
*S2   0.0833333  0.0592258  0.0124238   248.82    12.31        23
*MK3  0.1222921  0.0207283  0.0053770     8.39    14.29        15
 M4   0.1610228  0.0103982  0.0121056   247.95    78.72      0.74
```
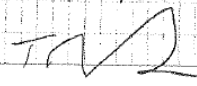Phases are referenced to local time

8.3 Appendix C – Survey Notes of the 1894 Floodmark

*survey notes by Tom Szymoniak of Portland State University

8.4   Appendix D – Additions to Historic Digital Elevation Model

Mouth of the Columbia River to Skamokawa, WA – (RKM 0 – 55)

The final Historic DEM is comprised of the original WET DEM along with points to model the floodplain and coastal ocean. The final Historic DEM is extended beyond the WET DEM to accommodate the 1894 Columbia River Flood (Sec 4.1 and Figure 4-20). In this stretch the required depth is governed by the inundation profiles at Skamokawa (RKM 55). It was also necessary to account for the bathymetry of the islands in the river in channel such as Russian Island and Minaker Island. The ocean boundary is also extended outward from the Oregon and Washington coastline to a point beyond where water level fluctuations due to the Columbia River Plume are minimized. The USC&GS surveys in this section of the river were conducted between 1867 and 1868.
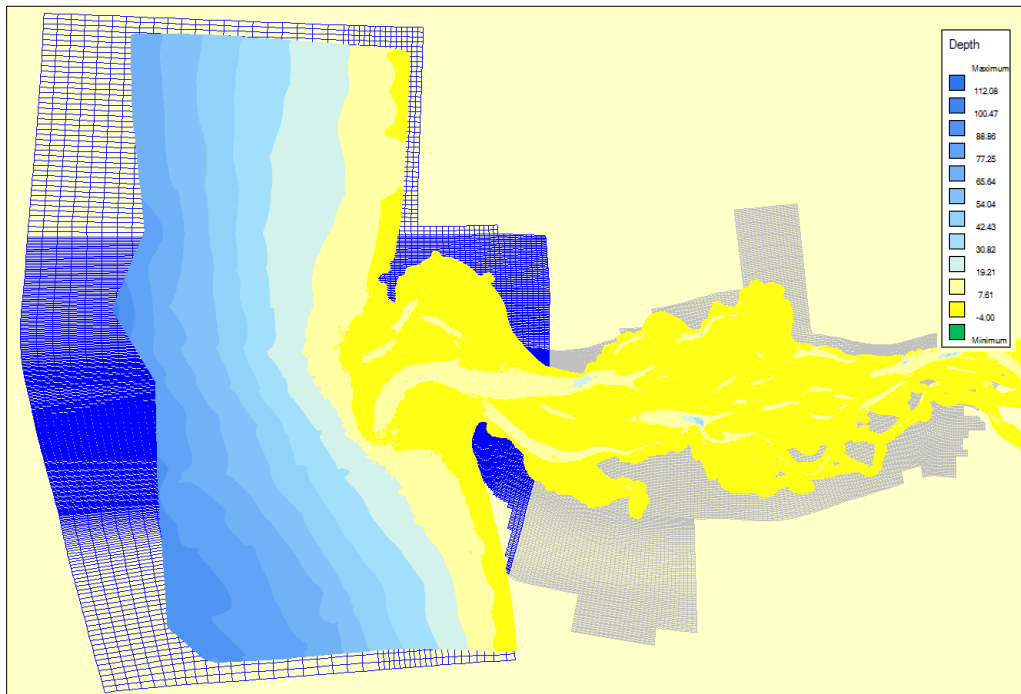

Figure 8-6: Historic DEM interpolated to 30m resolution from the sea to river transect at Skamokawa, WA.
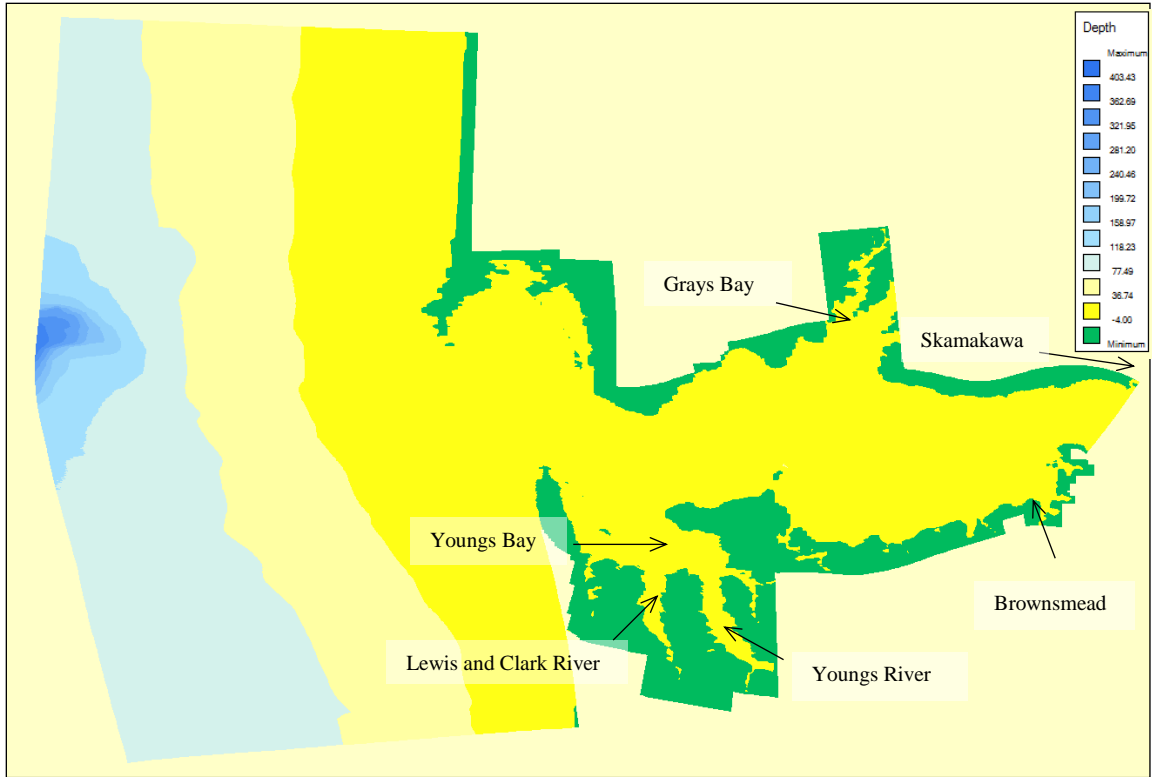
Figure 8-7: Final Historic DEM from sea boundary to river transect at Skamokawa, WA

Skamokawa, WA to Saint Helens, OR – (RKM 55 -141)

The interpolated WET DEM for the stretch of the river is shown in Figure 7-8. The final Historic DEM is extended to accommodate bathymetry up to 8m above NAVD88 by incorporating modern LiDAR and survey data. Puget Island, Beaver Island and Deer Island, along with the floodplains around Beaver Station in Oregon, Woodland, WA and Longview WA are also included in the final bathymetry (Figure 7-9). The USC&GS surveys in this section of the river were conducted between 1875 and 1884.
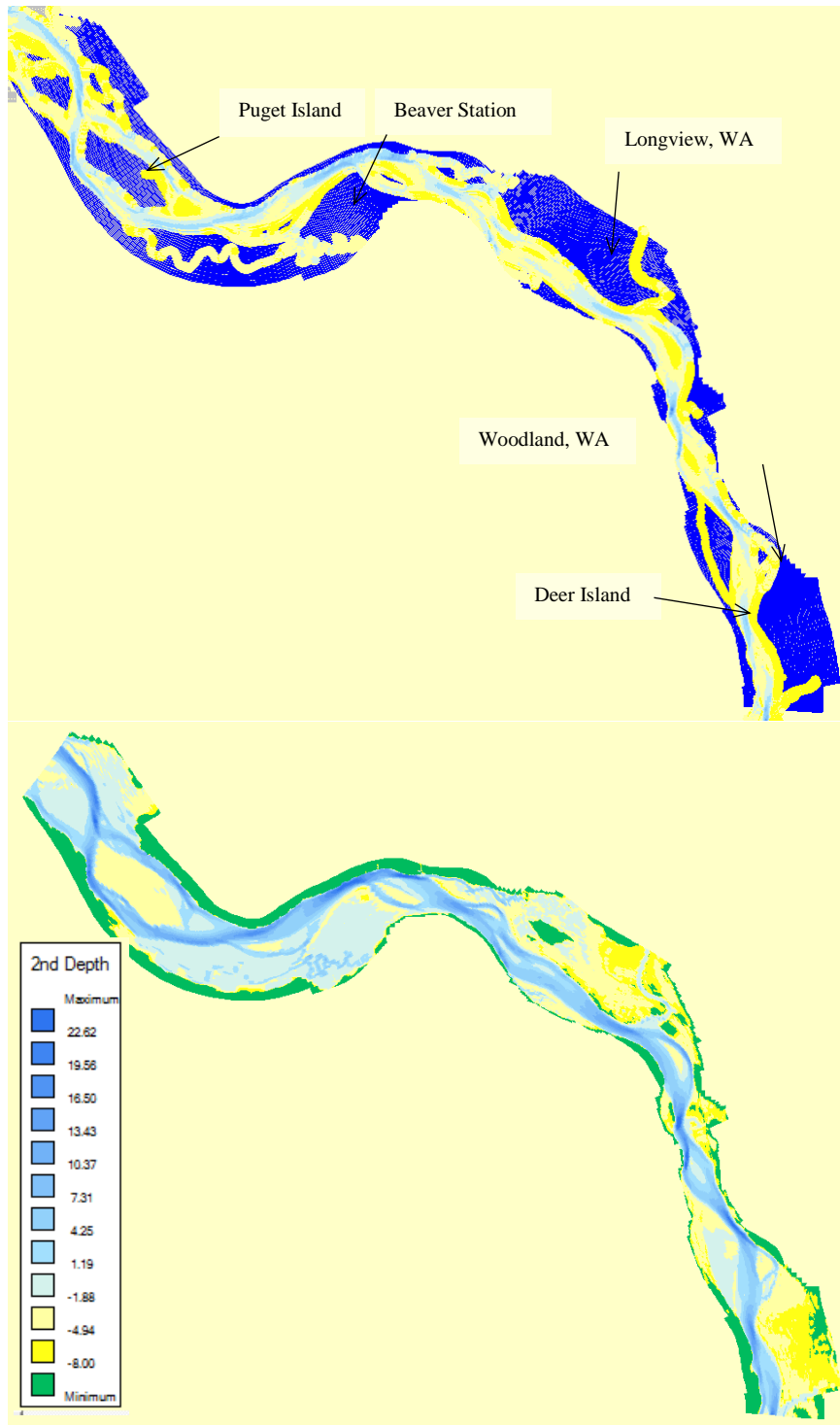
Figure 8-8: (top) WET DEM interpolated to 30m resolution from transect at Skamokawa, WA to transect at Saint Helen's, OR.

Figure 8-9: (bottom) Final Historic DEM from transect at Skamokawa, WA to transect at Saint Helen's, OR.

145

Saint Helens, OR to Vancouver, WA – (RKM 141 – 170)

The following is a detail of the Historic DEM for the stretch between transects at Saint Helens, OR and Vancouver, WA. This stretch of the river includes Sauvie Island on the west bank of the Columbia River and a stretch of flood plain running from Bachelor Island to just south of Vancouver Lake on the east bank. Hayden Island and the floodplain south of the Columbia River in North Portland must also be accounted for in the Historic DEM.

Figure 7-10 is a contour plot of the WET DEM in this section of the model. Figure 7-11 is a contour plot of the final Historic DEM in this section of the model. Several islands and lakes have been added to the model by incorporating modern LiDAR data. A large section of the Multnomah Channel forming the western boundary of Sauvie Island is added to the DEM. Additionally, floodplain up to 12m above NAVD88 has been added to the model. The USC&GS surveys in this section of the river were conducted between 1886 and 1901.
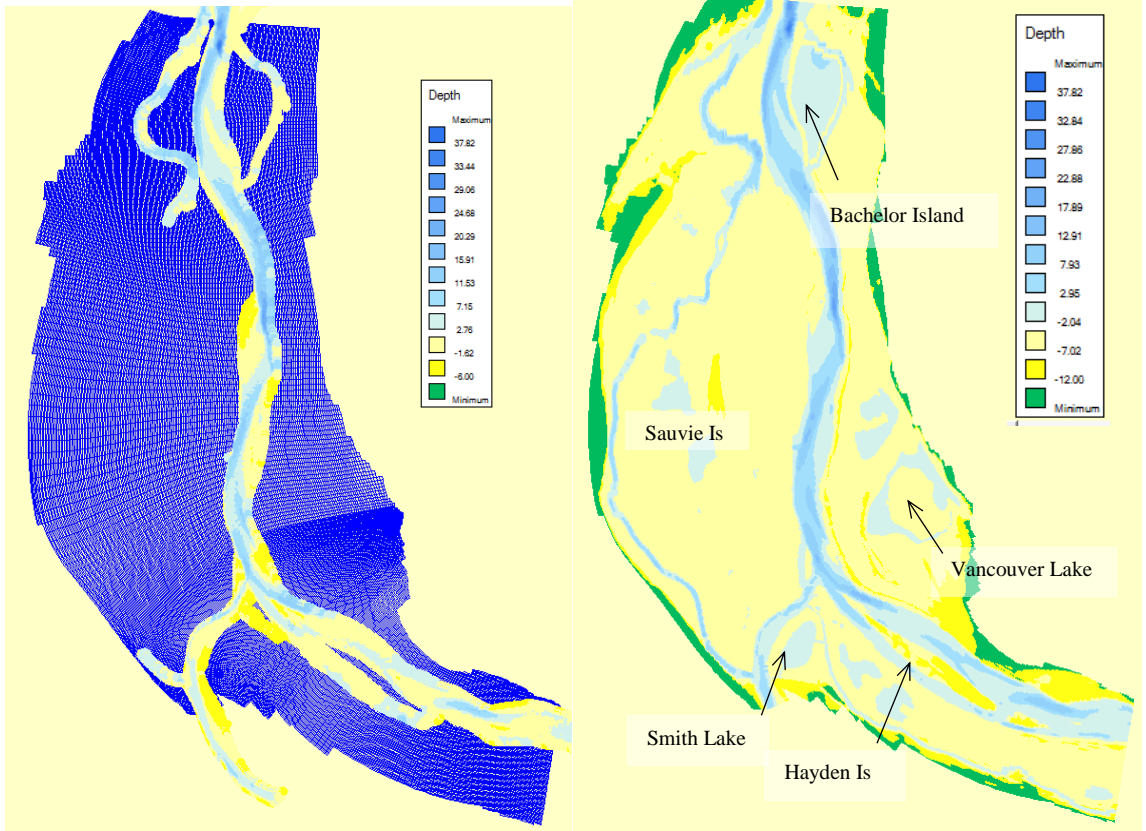
Figure 8-10: (left) WET team DEM interpolated to 30m resolution from transect at Saint Helen's, OR to transect at Vancouver, WA.

Figure 8-11: (right) Final Historic DEM from transect at Saint Helen's, OR to transect Vancouver, WA.

147

Lemon Island to Bonneville, OR – (RKM 176 – 234)

Figure 7-12 shows the Historic DEM. Figure 7-13 is contour plot of the final Historic DEM in this section of the model. The final Historic DEM extends to 16m above NAVD88. Government Island, Lady Island and the western half of Skamania Island were also added. The eastern edge of the model contains the discharge boundary for the Columbia River. The USC&GS surveys in this section of the river were conducted in 1901.
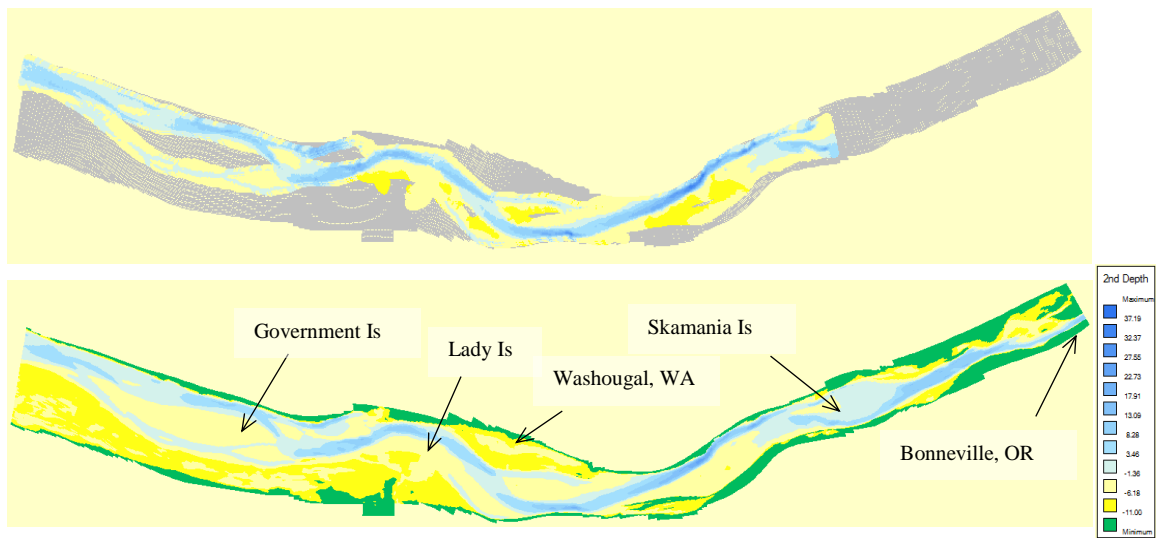

Figure 8-12: (top) WET team DEM interpolated to 30m resolution from transect at Vancouver, WA to Skamania Island.

Figure 8-13: (bottom) Final Historic DEM from Vancouver, WA to Bonneville, OR.

Lower Willamette River North Portland to Oregon City (RKM 10-41)

Figure 7-14 shows the final Historic DEM for the stretch of the Willamette River from North Portland to Oregon City. The red dashed line in the figure indicates the extent of the WET DEM. The remaining bathymetry south of this line was interpolated from modern LiDAR data. I adjusted the added modern bathymetry manually so that it would approximate the late 19th century bathymetry of the Willamette River. A comparison of modern bathymetry and historical bathymetry from navigation maps found at the Oregon Historical Society in Portland [*Rockwell et al.*, 1888 & *McEndoe and* Thomson, 1911], reveals significant changes in mean channel depth and configuration in the Willamette River over the past century. In the past Swan Island was completely surrounded by water and the main channel of the Willamette River ran to the east side of Swan Island. This section of the model is designed to be able model a 12m [NAVD88] inundation event. This is the approximate peak height of 1894 Columbia River Flood [*USWB*, 2012] based on historical records and a survey of a floodmark (Appendix 7.3).
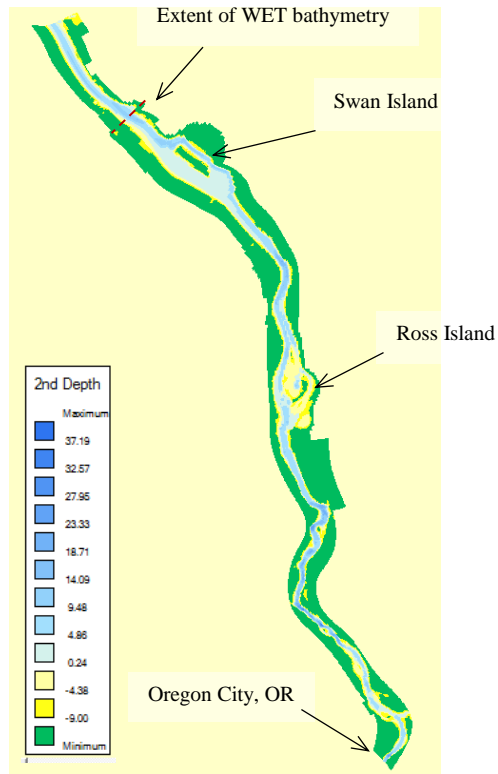
Figure 8-14: Final Historic DEM from Portland to Oregon City (Lower Willamette River).

8.5 Appendix E- Chézy Roughness - Modern Model

C - Lower
depth < -4
Chezy = 5

-1> depth > = --4
Chezy =63

2> depth >= -1
Chezy = 66

depth >=2
Chezzy = 69

A-Sea
depth < -3
Chezy = 25

0 > depth >= -3
Chezy = 93

depth >= 3
Chezy = 96

B - Estuary
depth < -3
Chezy = 25

0> depth >= -3
Chezy = 90

3> depth >= 0
Chezy = 93

depth >= 3
Chezy = 96

D
depth < -5
Chezy =5

-2 > depth >= -5
Chezy =61

depth >= 1
Chezy = 59

E
depth < 06
Chezy =5

-3>depth >= -6
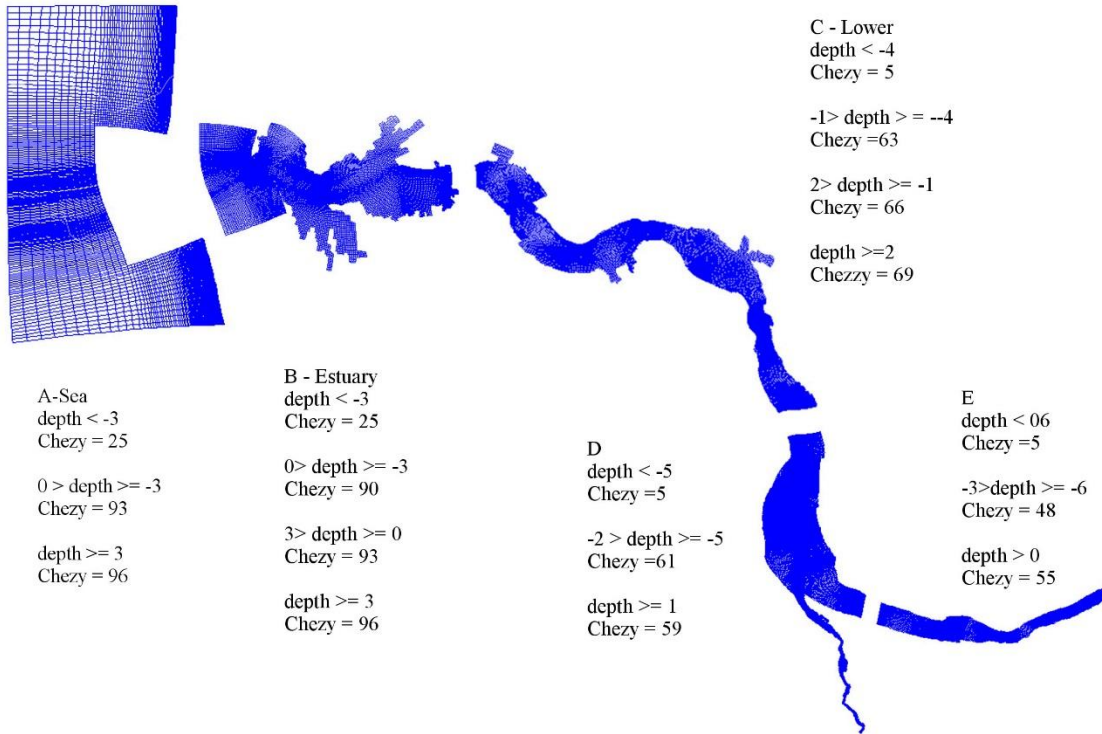Chezy = 48

depth > 0
Chezy = 55

Figure 8-15: Bed roughness of the Modern Model. Depth is in meters, positive downwards.